

124p

NASW-75

137632
F-9

137632
F-9

(Type 3a)

R

FACILITY FORM 602

N64-29562

(ACCESSION NUMBER)

124

(PAGES)

CR-58670

(NASA CR OR TMX OR AD NUMBER)

(THRU)

1

(CODE)

24

(CATEGORY)

EXPLORER 10 PLASMA MEASUREMENTS

by

A. Bonetti, H.S. Bridge, A.J. Lazarus,

B. Rossi and F. Scherb

Physics Department and Laboratory for Nuclear Science
Massachusetts Institute of Technology
Cambridge, Massachusetts

OTS PRICE

XEROX

\$

MICROFILM

\$

1611 ph

EXPLORER 10 PLASMA MEASUREMENTS

by

A. Bonetti,¹ H.S. Bridge, A.J. Lazarus,

B. Rossi and F. Scherb

Physics Department and Laboratory for Nuclear Science²
Massachusetts Institute of Technology
Cambridge, Massachusetts

1 Presently at the Istituto di Fisica,
Universita Degli Studi di Bari, Bari, Italy.

2 This work was supported in part by the National Aeronautics
and Space Administration and the United States Atomic Energy
Commission.

ABSTRACT

Plasma measurements were made with a detector aboard the Explorer 10 satellite, launched on a highly elongated elliptical trajectory with the line of apsides about 33° to the anti-solar direction. Magnetic field measurements were also carried out on Explorer 10 by the Goddard Space Flight Center of NASA.

29562

A plasma moving with a velocity of about 300 km sec^{-1} was first observed when the satellite reached a distance of about 22 earth radii. During the remainder of the observations (which terminated about 40 hours later, at a distance of 42 earth radii) periods in which substantial plasma fluxes were recorded alternated with shorter periods in which the plasma flux was below or just above the detection limit. There was a striking correlation between the plasma flux and the magnetic field: in the absence of plasma the magnetic field direction was nearly radial from the earth, while in the presence of plasma, the field was irregular and generally formed large angles with the earth-satellite direction.

The plasma probe did not provide accurate information on the direction of the plasma flow, but placed the direction within a "window" of about $20^\circ \times 80^\circ$. This window includes the direction pointing radially away from the sun.

The flux densities of the positive ions (presumably protons) corresponding to the observed currents were of the order of a few times $10^8 \text{ cm}^{-2} \text{ sec}^{-1}$. They fluctuated over a range of about a factor of two during the periods when plasma was observed.

auth.

I INTRODUCTION

The purpose of this paper is to present the results of plasma measurements performed by Explorer 10 (1961 Kappa) in the near-by interplanetary space and to discuss them in relation to the magnetic field measurements made aboard the same vehicle. A full report on the latter measurements has appeared recently (Heppner, Ness, Searce, and Skillman, 1963). In what follows, we shall refer to this paper as HNSS. Preliminary reports on both experiments have been presented at various scientific meetings (Bridge, Dilworth, Lazarus, Lyon, Rossi, and Scherb, 1962; Heppner, Ness, Skillman and Searce, 1962 a, 1962 b; Rossi, 1961, 1962; Bridge, 1962; Bonetti, Bridge, Lazarus, Lyon, Rossi and Scherb 1962 a, 1962 b).

At the time when the instrumentation for Explorer 10 was being planned, there were no direct observations of interplanetary plasma and the only indications for its existence came from arguments based on various kinds of indirect evidence. Such evidence included the behavior of comet tails, the scattering of solar light from the distant solar corona and the zodiacal cloud, the occultation of point-like radio sources passing in the general vicinity of the sun, correlations between solar phenomena and geophysical effects, and cosmic-ray observations indicating the existence of an interplanetary magnetic field which was difficult to explain in the absence of a plasma.

For a review of evidence based on the observations mentioned here, the reader may consult, for example, a paper by Rossi (1962).

While it was generally accepted that at least the inner part of the solar system should be filled with a dilute plasma, presumably of solar origin and consisting mainly of fully ionized hydrogen, the estimates concerning the density of this plasma varied over a very wide range, from a few particles to several thousand particles per cm^3 . Similar uncertainties existed with regard to the magnitude and direction of the plasma velocity, to its temperature, etc. Thus, the over-riding requirement in the design of our instrument was that it should be capable of providing meaningful results under a great variety of possible situations. This requirement, together with severe limitations in weight, power, and telemetering capability, made it necessary to sacrifice accuracy for reliability and dynamic range.

While the preparations for Explorer 10 were under way, Soviet scientists flew plasma probes on a number of space vehicles, specifically Lunik 1 (launched in January, 1959), Lunik 2 (launched in September, 1959), Lunik 3 (launched in October, 1959) and Venusik (launched in February, 1961). These probes could^{be} operated so as to detect either positive ions of all energies, or electrons with energies above 200 ev. Their construction consisted essentially of a collector plate with two grids in front of it. The inner grid carried a negative potential

intended to suppress photoelectric current from the collector; the outer grid was given different positive or negative potentials with respect to the body of the satellite in order to obtain some information on the energy of the plasma ions. The observations made during these flights were published partly before, partly after the flight of Explorer 10 (Gringauz, Bezrukikh, Ozerov and Rybchinskii, 1960; Gringauz, Kurt, Moroz and Shklovskii, 1960 a, 1960 b; Gringauz, 1961; Gringauz, Bezrukikh, Balandina, Ozerov and Rybchinskii, 1962). Most directly pertinent to our problem are the following points:

(a) Lunik 2 was fired away from the sun. Radio contact with this vehicle was maintained from take-off to a distance of about 30 earth radii (R_e), and then again from $39 R_e$ to impact on the moon. In the early part of the flight (up to about $4 R_e$) positive-ion currents were observed, indicating the presence of a stationary plasma, swept into the probes by the motion of the vehicle. No positive-ion currents above background were detected from $4 R_e$ to $30 R_e$. From $39 R_e$ to the end of the flight, the probes indicated a flux of positive ions with a density of about 2×10^8 particles $\text{cm}^{-2} \text{sec}^{-1}$. Measurements made with different voltages on the outer grid, showed that the energy of these ions was greater than 15 ev, but did not allow a more precise determination. No information about the direction of the ion flux was obtained.

(b) Lunik 3 was launched in the general direction of the sun. An observation made at about $20 R_e$ revealed a flux density of about 4×10^8 positive ions $\text{cm}^{-2} \text{sec}^{-1}$; the ions appeared to have energies considerably greater than 20 ev. Other readings, .

taken at larger distances, did not reveal any detectable ion flux.

(c) Venusik was launched in the general direction of the sun. On at least one occasion, when the vehicle was at a distance of $297 R_e$, definite evidence for a positive ion flux was obtained; the density of this flux was about 10^9 particles $\text{cm}^{-2} \text{sec}^{-1}$.

It should be noted that, even though the suppressor grid eliminated "direct" photoelectric currents from the collector, "inverse" photoelectric currents (see section II-B) were still present. In most of the measurements, these currents seem to have placed a lower limit of the order of $10^8 \text{ cm}^{-2} \text{sec}^{-1}$ to the detectable flux density of positive plasma ions.

II INSTRUMENTATION

A. Particle Fluxes in a Moving Plasma.

The primary purpose of the plasma measurements performed by Explorer 10 was to provide data on the density of the plasma, on the direction of its bulk motion and on the magnitude of its bulk velocity, V_0 . The bulk velocity is here defined as the velocity (relative to the satellite) of the frame of reference in which the total momentum of the ions and electrons contained in a volume element of the plasma vanishes. It was also hoped that some information would be obtained concerning the random velocities of the plasma particles in this frame of reference. We shall refer to these velocities as "thermal" velocities, without thereby implying that the plasma fulfilled the conditions required for the definition of a temperature (Maxwellian velocity distribution

for each kind of particle, equipartition of energy between the various components).

In general, the ^{shape of the} signal from the plasma probe is determined by the directional distribution and the energy spectrum of the charged particles in the moving plasma. Let us consider one of the components of the plasma, e.g., the electrons or the positive ions. If the "thermal" velocities of the particles in question are very small compared with the bulk velocity V_0 , then the particles form a practically parallel beam having a single energy E_0 given by $E_0 = 1/2 mV_0^2$. If the "thermal" velocities are very large compared with V_0 , then the particles have an energy spectrum which practically depends only on their "temperature", and a directional distribution which is practically unrelated to the direction of motion of the plasma as a whole. If the "thermal" velocities are small, but not negligible compared with the bulk velocity, then the particle beam, while no longer parallel, is still strongly collimated in the direction of \vec{V}_0 . Likewise, the beam, while no longer monoenergetic, has an energy spectrum strongly peaked near the energy $E_0 = 1/2 mV_0^2$. More precisely, the mean angular spread of the beam will be of the order of

$$\Delta \Phi = \pm v_{\perp} / V_0, \quad (1)$$

where v_{\perp} is the average magnitude of the "thermal" velocities perpendicular to the bulk motion. Similarly, the mean fractional energy spread will be of the order of

$$\Delta E/E_0 = [(V_0 \pm v_{||})^2 - V_0^2] / V_0^2 \simeq \pm 2 v_{||} / V_0, \quad (2)$$

where v_{11} is the average magnitude of the "thermal" velocities parallel to the bulk motion. If the distribution of "thermal" velocities is isotropic, then $v_1 = v_{11}$, and Eqs. 1 and 2 establish a connection between the angular spread and the energy spread of the observed plasma particles.

If there were equipartition of energy between electrons and positive ions, then the "thermal" velocities of the two kinds of particles would be inversely proportional to the square root of their masses (e.g., protons would be moving 43 times more slowly than electrons). Although, as noted above, there is no reason to believe that such an equipartition is actually achieved, it is still reasonable to assume that the "thermal" velocities of the heavy positive ions are much smaller than those of the electrons. Thus, we might expect that the bulk motion of the plasma is much more clearly recognizable in the directional distribution and in the energy distribution of the positive ions than in the corresponding distributions of the electrons.

Actually, it turns out that measurements on the electron component would not provide reliable information on the bulk motion of the plasma, even if the "thermal" velocities of the electrons were small compared with the bulk velocity V_0 . This is because the kinetic energy of electrons corresponding to reasonable values of V_0 is of the order of several ev at most (2.5 ev for $V_0 = 1000 \text{ km sec}^{-1}$) and because the unknown electric charge of the satellite introduces serious difficulties

in the interpretation of flux measurements at these very low energies (see section IV-A below).

Another reason why measurements of electrons are of less direct value than measurements of positive ions is that, presumably, the satellite is surrounded by a cloud of photo-electrons ejected from its surface by the solar radiation. These electrons may not easily be distinguished from those belonging to the plasma.

It is clear, therefore, that the quantity of most immediate interest for our purposes is the flux of positive ions rather than the flux of electrons.

B. Description of the Plasma Probe.

The instrument used aboard Explorer 10 to measure the flux of positive ions has already been described in some detail in previous publications (Bridge, Dilworth, Rossi, Scherb and Lyon, 1960; Bridge, Lazarus, Lyon, Rossi and Scherb, 1962). It is a device which separates the positive ions from the electrons in the plasma beam entering the instrument and measures directly the current I carried by the positive ions. If the ions are singly charged, this current is given by:

$$I = (\text{elementary charge} \times \text{ion flux}), \quad (3)$$

where the ion flux is the total number of ions that arrive upon the collecting electrode per second.

During the planning of our experiment, we were concerned about background currents produced by the photoelectric effect. Estimates available at that time (Hinteregger, Damon and Hall, 1959) indicated that ultraviolet rays incident on a metal plate

facing the sun would produce a photocurrent of the order of 10^{-8} amp cm^{-2} . This current was near the upper limit of the expected plasma currents; unless suppressed to a very large extent, it would have probably made it impossible to detect a plasma flowing from the direction of the sun.

The probe, whose schematic design appears in Fig. 1, consisted of a metal cup containing several plane grids (G_1, G_2, G_3, G_4) and a plane collector plate (CP). The cup was mounted in a hole on the outer wall of the satellite, in such a way that grid G_1 (which closed the cup) was part of the satellite's skin. Grids G_1 and G_3 were directly attached to the body of the vehicle, whose potential we shall take as zero. The collector plate CP was also connected, through a resistor, to the body of the vehicle. Grid G_4 was kept at a constant negative voltage of 130 volts.

In order to understand the operation of the probe, suppose first that grid G_2 is at zero potential, and consider what happens when a neutral plasma flows into the probe. The plasma electrons cannot traverse G_4 unless they have energies greater than 130 ev. Therefore, they flow to another grid or to the walls of the cup. The positive ions, on the other hand, go through G_4 and strike the collector, producing a current I as given by Eq. 3.

The negative potential of G_4 not only stops the plasma electrons but also prevents the escape of photoelectrons emitted by the collector CP when it is exposed to sunlight. Thus, G_4 suppresses the so-called "direct photoelectric current"

which otherwise would add to the plasma current (in addition, it suppresses secondary electron emission due to the impact of charged particles on CP). However, sunlight reflected by the collector onto the rear surface of G_4 does produce a photoelectric current, usually referred to as "reverse photoelectric current", which subtracts from the plasma current (as already noted, this current appears to have been a serious background effect in the measurements made by means of the Soviet probes).

Suppose next that, keeping the other grids at the fixed voltages specified above, we apply to G_2 a voltage that varies rapidly and periodically between zero and a positive value sufficiently high to stop the positive ions. The positive ion flux is periodically interrupted, whereas the inverse photoelectric current is not affected in any way. Thus, the collector current will contain a d.c. component which depends both on the positive ion flux and on the inverse photoelectric current, and an a.c. component which depends only on the positive ion flux. By sorting out the a.c. component of the collector current we can now measure the positive ion flux without interference from photoelectric currents.

Any capacitive coupling between the modulating grid G_2 and the collector plate CP would cause a spurious signal to appear on CP. Grid G_3 (made of close-spaced bronze mesh) was added to reduce this effect to a negligible value. This grid also prevented modulation of the inverse photoelectric current between CP and G_4 .

We have neglected so far a possible contribution of electrons with sufficiently high energy to overcome the retarding potential of G_4 . The positive pulsating voltage of G_2 will not stop these electrons; however, it may slightly change the number of electrons reaching the collector CP because the transmission properties of the grid system may depend on the electric field distribution between the grids. Thus, the electron flux on the collector may be slightly modulated and it will then contribute to the observed a.c. component of the collector current in proportion to the degree of modulation. This question was investigated experimentally and the results are described below.

The use of a pulsating positive voltage to modulate the positive ions not only eliminates unwanted background effects, but also affords the possibility of measuring the energy of the ions. In fact, it is clear that if singly-charged ions with energy equal to E ev are incident perpendicularly upon the probe, the minimum amplitude of the pulsating voltage needed for their modulation is $V_m = E$. In other words, the a.c. current produced by a modulating voltage V_m is a measure of the total flux of singly charged ions with energy $E < V_m$. If, on the other hand, the beam is incident at an angle ϕ with respect to the normal to the probe, the pulsating voltage necessary to modulate ions of energy E is

$$V_m = E \cos^2 \phi . \quad (4)$$

In our probe the collector CP had an area of 121 cm^2 , and the combined transparency of all the grids was 23 percent (the shield grid G_3 by itself had a transparency of 36 percent).

Thus, the effective area of collection for normal incidence was 28 cm^2 .

For oblique incidence, the effective area of collection A is a decreasing function of the angle ϕ between the ion beam and the normal to the cup. We computed the dependence of A on ϕ from the geometry of the probe and the estimated variation of the grid transparencies. The result of this computation is shown in Fig. 2 (dotted curve). It is seen that the probe was completely insensitive to ions incident at angles greater than 63° to its normal.

The modulating voltage was applied in the form of a square wave with a frequency of 1400 cycles per second. Six different amplitudes were used; i.e., 5, 20, 80, 250, 800 and 2300 volts. (Since it was inconvenient to obtain pulsating voltages varying over such a wide range from a single supply, we used, in place of G_2 , two separate modulating grids connected to two separate supplies, one providing the lower three modulating voltages and the other one providing the higher three modulating voltages.).

A block diagram of the electronic system appears in Fig. 1. The collector CP was capacity coupled to a wide-band a.c. pre-amplifier which had an input impedance of 15,000 ohms. This was followed by a narrow-band filter tuned to the modulation frequency, by a compression (non-linear) amplifier with a dynamic range of about 5,000, and by a rectifier. The rectified signal, in the range from 0 to 5 volts, was applied to the input of the telemetering system.

The lower limit of the measurable a.c. current (determined by the amplifier noise) was about 2×10^{-11} amp. The upper limit (determined by saturation of the amplifier) was about 10^{-7} amp. Thus, for perpendicular incidence, the minimum detectable flux density (flux per unit area) was about 4×10^6 singly charged particles $\text{cm}^{-2} \text{sec}^{-1}$; the maximum measurable flux density was about 2×10^{10} particles $\text{cm}^{-2} \text{sec}^{-1}$.

The collector CP was also directly coupled to a d.c. amplifier through a 1- megohm resistor. The useful range of this amplifier was from about 10^{-7} amp to 5×10^{-7} amp.

C. The Explorer 10 Configuration.

Fig. 3 shows the structure of Explorer 10 and the location of the various instruments aboard this satellite.

The instruments used for measurements of the magnetic field included a rubidium vapor magnetometer and two flux-gate magnetometers (see HNSS).

The satellite spun around its axis of symmetry (see Fig. 3) with a rotation period of 548 milliseconds. A sun-earth-moon aspect sensor, instrumented by the Goddard Space Flight Center, provided information on the orientation of the spin axis and on the instantaneous angular position of the various instruments with respect to a plane passing through the spin axis and the sun.

The normal to the plasma probe was perpendicular to the spin axis. Thus, during each rotation it swept out a plane which we may call the "equatorial" plane of the satellite. As explained above, the probe was only sensitive to ions incident

at angles smaller than 63° above or below this plane.

If the "thermal" velocities of the ions are not large compared with the bulk velocity V_0 , the current recorded by the probe varies periodically with the rotation of the satellite. One should expect that it reaches a maximum at the time when the angle δ between the normal to the probe \vec{n} and the vector $-\vec{V}_0$ has its minimum value; i.e., when the probe looks as closely as possible into the plasma stream. In order to express δ as a function of time, it is convenient to introduce the angles defined in Fig. 4, i.e. the angle α between $-\vec{V}_0$ and the equatorial plane of the satellite, and the angle β between \vec{n} and the projection of $-\vec{V}_0$ onto this plane. As the satellite rotates, α remains constant, β increases uniformly with time, and the instantaneous value of δ is given by:

$$\cos \delta = \cos \alpha \cos \beta \quad . \quad (5)$$

The shape of the current signals from the probe (collector current I vs. β) depends on the degree of collimation of the ion beam and on the value of the angle α . As an example, let us consider the case of a parallel beam. If $\alpha = 0^\circ$, then $\delta = \beta$ and the computed signal is illustrated by the dotted curve in Fig. 2. Using this curve and Eq. 5, one can easily compute the expected height and shape of the signals produced by parallel beams incident at any angle α between 0° and 63° .

We have considered thus far a situation in which the modulating voltage V_m is higher than the kinetic energy E of

the ions; in this case, full modulation occurs at all angles of incidence. However, if $V_m < E$, modulation occurs only when the angle of incidence is greater than the angle defined by Eq. 4 (provided ϕ is smaller than 63° - the maximum angle of acceptance of the probe). Thus, for $\cos^2 63^\circ < V_m / E < \cos^2 \alpha$, the current signal obtained during the rotation of the satellite will have a characteristically "horned" shape such as illustrated in Fig. 5 for the case of $\alpha = 0^\circ$.

D. Laboratory Tests.

Prior to the flight, we subjected the probe and the associated electronic circuits to extensive laboratory tests, and other tests were made after the flight on a duplicate of the flight unit.

The probe was placed in a vacuum system and exposed to parallel beams of protons of various energies and at various angles of incidence. We thus verified that for each energy and for each angle, there was a sharp lower limit, V_m , for the amplitude of the voltage necessary to modulate the proton beam, and that V_m agreed with the value given by Eq 4. Above this limit, the a.c. signal was found to be independent of the modulating voltage.

It was also verified that even the highest modulating voltages did not produce a detectable signal through capacity coupling of the modulating grid to the collector plate.

In order to determine the importance of photoelectric effects in the cup, we placed in the vacuum system a source of ultraviolet rays whose intensity at the probe was about one third the intensity of solar ultraviolet rays. At the beginning

of the test, a small signal was detected, but it disappeared when the probe had been thoroughly outgassed. We attribute this signal to photoionization of the residual gas.

The probe was exposed to a beam of electrons of sufficient energy to overcome the retarding potential of G_4 . An a.c. signal was observed corresponding to a partial modulation of the electron flux, the degree of modulation depending somewhat on the electron energy and on the modulating voltage. The modulated component was usually one to three percent of the total flux, in no case larger than 5 percent. Thus, the probe, when operated as described, detects only a small fraction of the high-energy electrons that may be present in the plasma.

Using a well-defined narrow beam of electrons, and keeping G_2 at zero potential, we tested the geometrical response of the probe, i.e., the dependence of the effective area of collection A on the angle of incidence θ . The solid curve in Fig. 2 represents the results of these measurements. This curve may be compared with the computed response curve (dotted in Fig. 2), both curves having been normalized to $A = 1$ at normal incidence. While there is no difference in the cut-off angle, the experimental curve is about 10° wider than the computed curve at half height. In what follows, we shall refer to the solid curve in Fig. 2 as the geometric response curve of the probe and we shall use this curve in the analysis of our data.

The geometric response curve and Eq. 5 can be used to compute the effective area of collection A as a function of the angles α and β (see Fig. 4). Curves showing A vs β for various values of α ,

normalized to $A = 1$ for perpendicular incidence, appear in Fig. 6. To bring out more clearly the differences among the shapes of these curves, we have replotted them in Fig. 7 after normalizing each curve to $A = 1$ at $\beta = 0^\circ$.*

* These curves differ somewhat in shape from those shown in Figs. 10 - 14 of our previous communication (Bridge, Dilworth, Lazarus, Lyon, Rossi, and Scherb, 1962) because of a plotting error in the earlier curves.

We also used the narrow electron beam and a deep Faraday well to make an absolute calibration of the probe for normal incidence.

Finally, we tested the effect of the electronic circuits on the signals by putting in pulses of known shape and recording the corresponding output pulses. Some of the results thus obtained are shown in Fig. 8. The input signals are those computed for parallel ion beams incident at different angles to the equatorial plane of the satellite. They are represented by curves identical to those shown in Fig. 7, with the time scale adjusted to the period of rotation of the satellite. There are two main effects produced by the electronic circuits: (1) the pulses are distorted by the non-linear amplifier which tends to increase their width, and (2) the pulses are delayed by about 15 milliseconds (corresponding to $\beta = 10^\circ$) due to the time constant of the rectifier. The non-linear distortion of the pulses increases rapidly with their amplitude, so that large pulses are significantly wider than smaller pulses.

No further significant distortion of the current signals was introduced by the telemetering circuits, or by the data processing equipment on the ground.

III THE FLIGHT

The flight of Explorer 10 is described in detail in HNSS. We recall here its main features.

The satellite was placed into a very elongated elliptical trajectory with an apogee of 46.6 earth radii (R_e). The line of apsides was about 33° to the antisolar direction.

Fig. 9 shows the trajectory in a solar-ecliptic cartesian frame of reference, with one of the coordinate planes parallel to the ecliptic, and another perpendicular to the sun-earth line (which ^{was} practically the same as the sun-satellite line). Fig. 10 shows the projections of the orbit onto the three coordinate planes, and Fig. 11 describes the frame of reference that we shall use to specify directions; the angular coordinates are the ecliptic latitude θ , and the solar ecliptic longitude ϕ (measured eastward from the earth-sun line).

Fig. 12 is a Mercator projection of the celestial sphere drawn using ϕ as abscissa and θ as ordinate. Shown on this map are:

- (a) the spin axis orientation "A" (which was fixed throughout the flight);
- (b) the plane "n" traced by the normal to the probe during the rotation of the vehicle (notice that the sun-vehicle line made an angle of 22° with this plane);

- (c) The plane "p" which contained the spin axis and the direction to the sun;
- (d) The regions (shaded oval areas) for which $\alpha > 63^\circ$. The sensitivity of the probe was a maximum along the plane "n" and dropped gradually to zero at the boundary of these regions.

The satellite was powered by chemical batteries, which provided reliable operation for about 50 hours, during which time the satellite reached a geocentric distance of about $42 R_e$.

Fig. 13 shows the telemetering sequence. One sees that during a telemetering cycle, lasting 148 seconds, 5 seconds were assigned to the plasma probe. These 5-second intervals were subcommutated by an internal program and were used to transmit sequentially the following data:

- (a) a marker signal;
- (b) the output signal of the d.c. amplifier;
- (c) the output signal of the a.c. amplifier as the probe was operating with one of the six modulating voltages.

Thus, a complete plasma probe sequence consisted of eight telemetering cycles and lasted $19^m 44^s$.

Because of the low sensitivity of the d.c. amplifier, no current measurements were obtained in the d.c. mode.

As explained in HNSS, the rubidium vapor magnetometer operated satisfactorily only during the early part of the flight. Thus, the magnetic field measurements that are of interest for a comparison with the plasma measurements at large geocentric distances were obtained with the flux-gate magnetometers. As seen from Fig. 13, the flux-gate

measurements were made immediately before the plasma measurements.

IV GENERAL RESULTS ,

The flight of Explorer 10 may be divided into four periods, characterized by distinctly different conditions of the plasma and the magnetic field.

A. First Period (3-25-1517, $R = 1.0 R_e$, to 3-25-1629, $R = 3.9 R_e$). The first signal from the plasma probe was received at 3-25-1522 (meaning March 25, 15^h 22^m UT), about 5 minutes after liftoff when the satellite was at an altitude of about 200 kilometers (geocentric distance $R = 1.03 R_e$); the modulating voltage was then 20 volts.

From that time until 3-25-1610, when the satellite was at $R = 3.0 R_e$, a plasma current was detected whenever the probe was operated with any one of the six different modulating voltages (except in two cases, occurring at the 2300 volt modulating level, when noise obscured the telemetered signal). During each of the 5-second telemetering intervals, the current varied periodically with the rotation of the satellite, the maximum occurring at the time when the normal to the probe came closest to the direction of motion of the satellite. The current maxima observed with the various modulating voltages, when plotted against geocentric distance, lay close to a smooth curve, indicating that the current was independent of the modulating voltage (from 5 to 2300 volts). The current peaks decreased from a value of about 9×10^{-8} amp at $R = 1.03 R_e$ to a value of about 2×10^{-10} amp at $R = 3.0 R_e$.

The above results can be understood if one assumes that during this part of the flight the satellite was moving through a relatively stationary plasma. Up to $3 R_e$, the velocity of the satellite relative to the earth varied from about 10 to about 5 km sec⁻¹ (the maximum

velocity during the acceleration period was 10.9 km sec^{-1} . Protons at rest with respect to the earth would have kinetic energies of a few tenths of one ev, oxygen or nitrogen ions energies of a few ev, with respect to the satellite. These energies are consistent with the observation that full modulation of the plasma current occurred at the 5 volt level.

The order of magnitude of the current is consistent with the ion densities deduced from whistler data (Smith and Helliwell, 1960). There are, however, several reasons why it is difficult to draw firm quantitative conclusions from the observations made during this period:

- (a) Explorer 10 reached a distance of $3 R_e$ in less than one hour; thus this observation period included less than three complete telemetering sequences.
- (b) It is known that a satellite in orbit acquires a certain electric potential with respect to the medium as a result of (1) the differential velocity of electrons and positive ions in the surrounding plasma, (2) the photoelectric effect due to solar ultra-violet rays and (3) the secondary electron emission due to bombardment of high-energy particles. The first effect tends to make the satellite electrically negative, the two last act in the opposite direction. Presumably, the resulting potential, which might be of the order of a few volts, changes with altitude; during the flight of Explorer 10 it might even have reversed its sign. Such a potential would substantially affect the flux of low-energy positive ions into the probe.
- (c) The probe was not yet completely outgassed. As we had found in the laboratory (see section II-D), incomplete outgassing makes the probe

slightly sensitive to electromagnetic radiation capable of ionizing the residual gas. In fact, toward the end of the first period, small secondary maxima, corresponding to currents of about 10^{-10} amp or less, began to appear at the highest modulating voltages. These maxima occurred when the normal to the plasma probe came closest to the solar direction. We are inclined to ascribe them to photoionization by solar U.V. or X-rays. Presumably, photoionization currents had not been observed in the earlier part of the flight because the plasma currents were strong enough to obscure them.

The magnetic field measured by the instruments aboard Explorer 10 during this period did not deviate much from a reference field defined in HNSS as the "main geomagnetic field" (which is an extrapolation of the field measured near the earth's surface, made under the assumption that the field is entirely produced by sources below the region of observation). However, there was some evidence for a small perturbation such as might be produced by a ring current at about $3 R_e$.

During the last telemetering sequence of the first period, while the vehicle was moving from $3.0 R_e$ to $3.9 R_e$, the plasma current decreased to a value below the detection limit. This rapid disappearance of the plasma current agrees with the observations of the Soviet scientists (see section I). However, present uncertainties concerning the electric potential acquired by space vehicles call for some caution in the interpretation of these results.

B. Second Period (from 3-25-1629, $R = 3.9 R_e$, to 3-26-0408, $R = 20.9 R_e$).

In this period no currents were observed which could be ascribed to the motion of the satellite through a stationary plasma. However,

during the first part of the period the probe continued to give the small signals, due presumably to photoionization of the gas, which had already been observed at the end of the first period. These signals gradually faded away because of the progressive outgassing of the probe. During a 4-hour interval extending from 3-26-0001 ($R = 16.3 R_e$) to 3-26-0408 ($R = 20.9 R_e$) no currents were recorded at any of the modulating voltages.

For our purposes, the most important result of the observations made during the second period is that, when the probe was sufficiently well outgassed, it became practically insensitive to sunlight, which confirms the results of our laboratory tests. In addition, these observations provided a check on possible disturbances of the electronic equipment. The only disturbances detected were some anomalies appearing occasionally in the 2300 volt modulation mode. Such anomalies (which were probably due to the large currents in the circuit supplying power to the modulator) included: (1) an occasional premature termination of the normal 5-second on-time of the probe, and (2) an occasional abnormal shift in the zero level of the output signal. This shift in level may have obscured small plasma currents (corresponding to less than 1.5×10^{-10} amp; (see section V-C)*

* In this connection, we note that even under normal undisturbed conditions, the zero level was slightly shifted when the probe was operated at the 2300 volt modulation level; we attribute this shift to insufficient electrical isolation of the amplifier from the modulator circuits.

The anomalies noted above persisted throughout the flight; in a number of cases they made it impossible to obtain readings at the 2300 volt modulation level.

The measurements of the magnetic field during the second period (see HN55) revealed a field that deviated more and more from the "main geomagnetic field" until, toward the end of the period, the field lines became nearly radial from the earth. The magnitude of the field decreased gradually, but much more slowly than the "main field". However, near the end of the period (i.e., beginning at 3-26-0250, $R = 19.5 R_e$) the field, which had been for some time near 25γ , began to increase gradually. After one hour, it reached a value of about 32γ (these field strengths may be compared with a value of 4.5γ for the extrapolated "main field").

C. Third Period (from 3-26-0408, $R = 20.9 R_e$, to 3-27-1437, $R = 41.3 R_e$).

Beginning at 3-26-0408, when the satellite was at a geocentric distance $R = 20.9 R_e$, small plasma currents ($< 2 \times 10^{-10}$ amp) were observed intermittently. Then at 3-26-0603 ($R = 22.7 R_e$) much stronger and more persistent signals appeared.

Though the plasma currents observed earlier during the first period were fully modulated even at ^{the} 5 volt level, substantial modulation now occurred only at the three highest voltage levels (250, 800 and 2300 volts), with an occasional small signal at the 80 volt level. This means that the positive ions of the plasma had energies of the order of several hundred ev.

Since Explorer 10 was about 23 earth radii away from the earth, it is reasonable to assume that the observed plasma, whether of terrestrial or solar origin, consisted mainly of ionized hydrogen, with perhaps a small admixture of ionized helium. In discussing

our experimental results, we shall assume that the positive ions detected by the probe were protons. Under this assumption, the ion velocities corresponding to the observed energies were of the order of several hundred km sec⁻¹.

The plasma current varied periodically, going through a sharp maximum during each rotation of the satellite, then falling below the detection limit for more than half of the rotation period (Fig. 14). Thus the positive ions formed a reasonably well-collimated beam. In other words, the "thermal" velocities of these ions were substantially smaller than the bulk velocity of the plasma.

After correcting for the time response of the electronic system (see section II-D), it was found that the current peaks occurred at about the time when the angle between the normal to the probe and the direction of the sun was a minimum. As already mentioned, this minimum angle was about 22°. Making a generous allowance for the experimental errors, we conclude that the vector \vec{V}_0 describing the bulk velocity of the plasma was within 10° to the plane passing through the spin axis of the satellite and containing the sun-earth direction (plane "p" of Fig. 12).

Since the sensitivity of the probe was zero for $\alpha > 63^\circ$, the vector \vec{V}_0 was certainly at an angle smaller than 63° to the equatorial plane of the satellite.

Additional information on the value of the angle α is contained in the shape of the current signals. The possibility of an angular spread in the positive ion beam is a complicating factor in the interpretation of the observed shapes, so that a very detailed analysis is

needed to extract from the experimental data all of the potentially available information. Such an analysis has not yet been completed; however, preliminary results place an upper limit of about 40° to the value of α . Thus, the possible directions of the "plasma wind" are restricted to a "window" bounded by the cones corresponding to $\alpha = \pm 40^\circ$ and by the planes at $\pm 10^\circ$ to the plane "p" (see Fig. 12). Notice that the antisolar direction is well within this window. Notice also that for $\alpha = 40^\circ$ the effective area of collection of the probe is 3.7 times smaller than for $\alpha = 0^\circ$ (see Fig. 2).

The situation described above prevailed for about 75 percent of the time during the period considered here. However, on several occasions, and for time intervals of the order of hours, the plasma current fell to a value below (or occasionally barely above) the noise level and then later reappeared in full strength (i.e., with a value more than 10 times the noise level). The portions of the trajectory where substantial plasma currents were recorded are marked by the heavy lines in Fig. 10. ¶ During the third period, the magnetic field, as described in HNSS, underwent sharp transitions from a situation where it was nearly radial from the earth (as it had been at the end of the second period) to a situation where it was at a large angle to the earth-satellite line. The changes in the plasma current mentioned above showed a striking correlation with these changes in the field direction. Substantial plasma currents consistently appeared whenever the field changed from radial to non-radial, and disappeared whenever the field reverted to the radial configuration.

D. Fourth Period (From 3-27-1437, $R = 41.3 R_e$, to 3-27-1800, $R = 42.3 R_e$).

This period was characterized by magnetic disturbances, which included the sudden commencement of a magnetic storm observed on the earth

at 3-27-1503. At about the same time, there was a substantial increase both in the plasma flux and in the magnetic field strength measured by Explorer 10. These higher intensities persisted, with some fluctuations, until the end of the observations; i.e., for about 3.5 hours. During the first two hours of the fourth period, there was also a considerable increase in the mean energy of the plasma protons. Later, however, the mean energy appeared to return to the prestorm value. At about 3-27-1800, the zero-levels shifted, due to exhaustion of the chemical batteries, and the data obtained after this time were no longer reliable.

V. DETAILED ANALYSIS OF THE EXPERIMENTAL DATA.

For the reasons explained in section IV, we have not attempted to carry out a detailed analysis of the data obtained in the vicinity of the earth, but have concentrated our attention on the plasma measurements made in the more distant regions.

The graphs in Fig. 16 provide an over-all view of these measurements and afford a comparison with the magnetometer data obtained by the Goddard group. The vertical bars in the bottom part of this figure represent the "nominal" flux densities corresponding to the maxima of the signals recorded at the various modulation levels. By "nominal" flux densities, we mean the numbers of positive, singly-charged ions per cm^2 per sec, computed from the observed currents assuming normal incidence upon the probe. Above this graph are graphs giving the magnitude B of the magnetic field, and the angles ϕ and θ which specify its direction

(see Fig. 11). These data were kindly provided us by Dr. Heppner prior to their publication and are identical with those appearing in HNSS.

A. Third Period - Correlation Between Plasma and Magnetic Field

The correlation between magnitude of the plasma current and direction of the magnetic field is clearly visible in the graphs of Fig. 16. We shall now examine it in more detail.

Inspection of Fig. 16 shows that during the third period, the current signals obtained at the 800 and 2300 volt modulation levels were, on the average, nearly equal. Thus, full or almost full modulation of the plasma protons was achieved at both these levels, so that we may take the heights of the corresponding current signals as a measure of the total "nominal" flux density of plasma protons.

The histogram in Fig. 17 gives the frequency distribution of the flux densities observed during the third period, based on all available readings at the 800 and 2300 volt levels.

It is clear from this graph that the observed flux densities fall into two distinct groups; a narrow group, including those cases where the flux density was below or barely above the detection limit ($4 \times 10^6 \text{ cm}^{-2} \text{ sec}^{-1}$), and a broad group peaked somewhat above $10^8 \text{ cm}^{-2} \text{ sec}^{-1}$. We shall refer to the observations corresponding to the two groups as weak and strong plasma signals respectively. Because of the small number of intermediate cases, the distinction between weak and strong signals does not depend critically on the choice of the flux density used for the separation of the two groups. In what follows, we shall

set this limiting flux density at $5 \times 10^7 \text{ cm}^{-2} \text{ sec}^{-1}$.

As already noted, each plasma measurement ~~was~~ preceded, within a few seconds, by measurements of the magnetic field made by means of the flux-gate magnetometers. In Fig. 18, we have plotted the directions of the magnetic field measured before each of the available plasma readings at the 800 volt and 2300 volt levels. Open circles refer to magnetic fields associated with strong plasma fluxes and solid dots refer to magnetic fields associated with weak plasma fluxes. During the time of observation, the representative point of the vector pointing from the earth to the satellite moved along the short line segment $E_1 E_2$. One sees that practically all the solid dots fall within a restricted area around this segment (enclosed by the line "a" in Fig. 18). The very few exceptions correspond to measurements taken when plasma and magnetic conditions were changing rapidly, or when the plasma signal was close to the limiting value of $5 \times 10^7 \text{ cm}^{-2} \text{ sec}^{-1}$. On the other hand, practically all the open circles fall outside this area. They are distributed over a wide region, but not at random throughout the map, clustering mainly in the area to the south of the ecliptic plane, between -30° and $+110^\circ$ ecliptic longitude.

These results point to the conclusion that during the third period, Explorer 10 encountered alternately two distinct physical situations. The first, which shall be called situation A, was characterized by weak plasma fluxes, often below the detection limit, and by nearly radial magnetic fields. The second, which shall be called situation B, was characterized by strong plasma fluxes, and by non-radial fields. Note that the field directions corresponding

to situation A fill the region denoted as "region A" in Fig. 23 of HNSS, while the field directions corresponding to situation B fall within regions "B" and "C" of the same figure.

While measurements of the magnetic field were made during every telemetering cycle (i.e., every $2^m 28^s$), significant plasma data were obtained only during the 250, 800, and 2300 volt modulation periods or roughly $3/8$ of the time during which the plasma probe was turned on. On the other hand, the essentially one-to-one correspondence between the magnetic field and the plasma fluxes, established by all near-simultaneous observations of these two quantities, enables us to use the magnetic field measurements to identify the times at which transitions between situation A and situation B occurred more precisely than we could do by means of the less frequent plasma signals.

As noted also in HNSS, it was usually found that the conditions typical of situation A or B persisted through many observations; then, quite suddenly, often within the $2^m 28^s$ separating two subsequent magnetic measurements, a switch to the other situation occurred. We shall call these changes "simple" transitions. Occasionally, however, it appears that situations A and B alternated rapidly during time intervals extending through several magnetic field and plasma measurements. We shall call these "complex" transitions.

The time intervals in the third period during which situations A and B prevailed, and the types of transitions between them, are shown in Table 1. Details of the measurements made in the vicinity of the transitions appear in Table 2. Listed in Tables 3 and 4 are the

average magnitudes and the average directions of the magnetic field observed during the various intervals of type A and type B respectively. The average directions of the magnetic field are also shown graphically in Fig. 19, where solid dots correspond to situations of type A and open circles to situations of type B. The number by each experimental point specifies the time interval to which the point refers, according to the listing in Table 1.

Tables 3 and 4 show that the magnetic field was usually weaker in the presence of plasma (situation B) than in the absence, or near-absence of plasma (situation A). However, the strength of the magnetic field did not correlate with plasma conditions quite as strikingly as did the direction of the field.

We call attention to the fact that, in contrast with the steady behavior of the magnetic field characteristic of situation A, the field in situation B underwent substantial changes during each time interval (the bars crossing at the point No. 2 in Fig. 19 are an indication of the spread in the direction of the magnetic field observed in the corresponding time interval). However, the changes were usually gradual and not quite as large as those occurring from one time interval to another. One exception was the long interval No. 10 during which substantial changes of the magnetic field (as well as of the plasma flux) were observed. For this reason, interval No. 10 is divided into four sub-intervals in Tables 1 and 4 and in Fig. 19.*

* This subdivision, while based on the behavior of the plasma flow and the magnetic field, is admittedly somewhat arbitrary.

B. Third Period - Properties of the Plasma Observed in Situation of Type B.

From an experiment of the type considered here, one would wish, ideally, to determine the energy spectrum and the total flux of protons

per unit area per unit solid angle in any given direction at any given instant of time. Actually, our instrument was not designed to achieve anything approaching this ambitious aim. However, the experimental data contain information of a somewhat more specific nature than the qualitative results presented in section IV-C.

(1) Plasma Flux Densities

Because of the frequent electronic disturbances which interfered with the measurements at the 2300 volt modulation level, we chose to use the measurements at the 800 volt level to evaluate the total flux density of plasma protons. As we shall discuss later in more detail, it is possible that a small fraction of the plasma protons did not undergo modulation at this level. We believe, however, that the error introduced by this lack of complete modulation is negligible within the accuracy claimed for the absolute values of the plasma current in the present experiment. The flux densities measured at the 800 volt level, which are shown in Fig. 16, are replotted on a condensed time scale in Fig. 20. It can be seen that these flux densities exhibit both short-time fluctuations and long-time changes; moreover, the long-time changes have a larger amplitude than the short-time fluctuations. Therefore, it is meaningful to compare the time averages of the flux densities observed during the individual time intervals of type B. These averages appear in Table 4 under the heading $\bar{\phi}(800)$.

(2) Dependence of the Plasma Current on the Modulating Voltage

The main source of information on the energy spectrum of the plasma protons lies in the relative amplitudes of the current signals

observed with the different modulating voltages. However, because of the time fluctuations in the plasma flux, it is not possible to draw firm conclusions from a comparison of consecutive measurements at different modulation levels. A more promising approach is to compare the averages of such measurements for each of the time intervals. This is done in the last three columns of Table 4, where we list the ratios of the average nominal flux densities observed at the 80, 250, and 2300 volt levels, $\bar{\phi}(80)$, $\bar{\phi}(250)$, and $\bar{\phi}(2300)$, to that observed at the 800 volt level, $\bar{\phi}(800)$.

As a comment on these data, we note the following: The current signals at the 80 volt level were often below the detection limit, particularly during those time intervals when the ^{total} flux density was low. The pairs of figures appearing under $\bar{\phi}(80) / \bar{\phi}(800)$ represent lower and upper limits for this ratio, computed respectively under the assumptions that the flux density corresponding to a signal below the noise level was (a) zero, or (b) equal to the minimum detectable value ($4 \times 10^6 \text{ cm}^{-2} \text{ sec}^{-1}$). We see that during some of the time intervals $\bar{\phi}(80) / \bar{\phi}(800)$ was of the order of one or two percent; during other time intervals $\bar{\phi}(80) / \bar{\phi}(800)$ might have had any value from zero to several percent.

The values of $\bar{\phi}(250) / \bar{\phi}(800)$ listed in Table 4 vary from 5 percent to 15 percent. The values of $\bar{\phi}(2300) / \bar{\phi}(800)$ oscillate around unity, from a minimum of 81 percent to a maximum of 109 percent.

There are two possible interpretations for the variability of these ratios. The first is that it is due to short-time fluctuations in the

total proton flux whose effects are not entirely eliminated by the averaging process. The second is that it is due, at least in part, to changes in the energy spectrum of the protons.

If we accept the first interpretation and assume, accordingly, that the proton spectrum was the same during all time intervals listed in Table 4, we do not need to consider these various time intervals separately, but we may take for $\bar{\phi}(250)$, $\bar{\phi}(800)$ and $\bar{\phi}(2300)$ the averages of the measurements made at each modulating voltage during all such time intervals. As for the computation of $\bar{\phi}(80)$, it is more advantageous to consider only those time intervals when the total flux density was sufficiently high to yield significant data at the 80-volt modulation level (intervals No. 2, 4, 6, 10c). The results obtained in this manner are listed in the first row of Table 5.

At any one instant of time, the ratio $\bar{\phi}(2300) / \bar{\phi}(800)$ must be greater than or equal to unity because there cannot be more protons with energies below 800 ev than protons with energy below 2300 ev. The ratio of the over-all averages of $\bar{\phi}(2300)$ and $\bar{\phi}(800)$ is actually close to unity. According to the interpretation discussed here, the reason why $\bar{\phi}(2300) / \bar{\phi}(800)$ is less than unity for the averages taken over some of the individual intervals must be found in the short-time fluctuations of the flux.

There are, however, strong arguments against this interpretation.

In the first place, the changes of the ratio $\bar{\phi}(250) / \bar{\phi}(800)$ for the individual time intervals were, percentagewise, much greater than those of the ratio $\bar{\phi}(2300) / \bar{\phi}(800)$. If both changes were due to fluctuations of the total proton flux, they should be approximately equal in relative magnitude.

In the second place, there appears to be a definite correlation between the values of $\bar{\phi}(250) / \bar{\phi}(800)$ and the values of $\bar{\phi}(2300) / \bar{\phi}(800)$ relative to the same time intervals. For example, in all four cases where $\bar{\phi}(250) / \bar{\phi}(800) > .10$, we find that $\bar{\phi}(2300) / \bar{\phi}(800) > 1.0$, whereas in five out of seven cases where $\bar{\phi}(250) / \bar{\phi}(800) < .10$, we find that $\bar{\phi}(2300) / \bar{\phi}(800) \leq .95$. Thus, the experimental data support the interpretation that the proton spectrum did indeed change from one time interval to another, and we shall now analyze our results under this assumption.

Since the accuracy of the data does not warrant a more detailed treatment, we shall group together, for the purpose of analysis, all time intervals for which $\bar{\phi}(250) / \bar{\phi}(800) \geq .10$ (No. 2, 4, 6, 10b 10c) and all time intervals for which $\bar{\phi}(250) / \bar{\phi}(800) < .10$ (No. 8, 10a, 10d, 12, 14, 16). The ratios between the average flux densities computed separately for these two groups appear in the second and third rows of Table 5. We see that $\bar{\phi}(2300) / \bar{\phi}(800)$ has a value of 1.04 for the first group and a value of 0.92 for the second group. As already pointed out, the "true" value of this quantity cannot be smaller than unity. To explain the value 0.92 as a statistical result due to short-time fluctuations in the proton flux would not be consistent with the point of view adopted here. On the other hand, it is possible that we may have slightly misjudged the effective gain of the compression amplifier when the probe was operated at the 2300 volt level, because as already noted, the zero line was somewhat displaced in this mode of operation. We can estimate a lower limit for the

instrumental error by assuming that $\bar{\phi}(2300) / \bar{\phi}(800)$ was actually unity for the time intervals of the second group. This lower limit amounts to 8 percent; therefore, the minimum value of the correction factor is 1.08. With this correction factor, the value of $\bar{\phi}(2300) / \bar{\phi}(800)$ for the time intervals of the first group becomes 1.13.

(3) The Proton Energy Spectrum

If we neglect the angular spread of the plasma protons and assume that the particles formed a parallel beam, we can relate the flux densities observed at the various modulating voltages directly to the energy spectrum of the protons. The uncertainty in the value of the angle α which the proton beam formed with the equatorial plane of the satellite introduces an uncertainty in the value of the energy because the minimum voltage needed to modulate protons of energy E is $V_m = E \cos^2 \alpha$. In what follows, we shall call the quantity $E \cos^2 \alpha$ the "nominal" proton energy.

Fig. 21 shows ^{the} values of $\bar{\phi}(80)$, $\bar{\phi}(250)$, $\bar{\phi}(800)$ and $\bar{\phi}(2300)$ for the two groups of time intervals (see Table 5), normalized to unity at 2300 volts. According to our assumptions, these values represent the fractions of protons in the total flux whose nominal energies are less than 80, 250, 800 and 2300 ev respectively. We see that, during the time intervals of the first group, a very small fraction of the protons have nominal energies lower than 80 ev and a somewhat larger fraction have nominal energies greater than 2300 ev. During the time intervals of the second group, the spectrum appears to be narrower, but is less well defined; the data in fact are consistent with a complete absence of protons with energies less than

80 ev or more than 800 ev, but they do not rule out the possibility that a few percent of the protons may have energies beyond these limits.

The energy spread of the plasma protons may be interpreted in terms of a "thermal" agitation of these particles in the frame of reference of the moving plasma. For the sake of orientation, let us compare the experimental results with the energy spectra computed under the assumption that the "thermal" velocities obey a Maxwellian distribution, corresponding to a certain temperature T , and let us simplify the calculations by neglecting the components of the thermal velocities perpendicular to the direction of bulk motion. (This simplification is consistent with the assumption of a parallel proton beam and is partially justified by the fact that the perpendicular components of the thermal velocities have only a second-order effect on the resultant velocity of the protons, while the parallel components have a first-order effect.) The kinetic energy of the individual protons ($E = mV^2/2$), the proton energy corresponding to the bulk motion ($E_0 = mV_0^2/2$), and the mean thermal energy in one dimension ($kT/2$) appear only through their ratios in the results of this computation. Since the experimental spectra are given in terms of the "nominal" energy, $V_m = E \cos^2 \alpha$, comparison with the theoretical curves yields information on the "nominal" energy of bulk motion, $E_0 \cos^2 \alpha$, and on the

"nominal" temperature, $T \cos^2 \alpha$. The results of this comparison are shown in Fig. 21. One sees that the experimental points for the first group of time intervals fit satisfactorily the theoretical curve corresponding to $E_0 \cos^2 \alpha = 420$ ev and to $T \cos^2 \alpha = 6 \times 10^5$ °K. Considering the uncertainties of the measurements and the crude character of our analysis, we assign an uncertainty of ± 15 percent for the value of $E_0 \cos^2 \alpha$ and a range of values from 4×10^5 °K to 1×10^6 °K for the nominal temperature.

Less definite conclusions can be reached concerning the conditions of the plasma during the time intervals of the second group, except that the spectrum appears to be narrower, and, therefore, the nominal temperature appears to be lower than that of the plasma observed during the time intervals of the first group. The nominal energy of bulk motion, on the other hand, is probably not very different from that estimated above. (The tentative spectrum shown in Fig. 21 corresponds to $E_0 \cos^2 \alpha = 420$ ev and $T \cos^2 \alpha = 2.6 \times 10^5$ °K; this temperature represents an approximate upper limit for the range of temperatures which could be used to obtain reasonable agreement between the experimental data and the theoretical model.)

Another source of information on the proton energy spectrum may be found in the shapes of the current signals. Throughout the third period of the flight, the signals at the 2300 volt and at the 800 volt modulation levels had round tops, while those

at the 250 volt level had flat tops (see Figs. 14 a, b). This is consistent with the tentative spectra shown in Fig. 21, according to which the flux density of protons with nominal energy less than E increases rapidly near $E = 250$ ev, increases slowly near $E = 800$ ev and has already reached saturation before $E = 2300$ ev. (As the rotation angle β increases, the effective area of collection decreases but the energy of the protons which can be modulated by a given modulating voltage increases; if the spectrum is sufficiently steep, the consequent increase in modulated flux compensates for the decrease in collection area, giving rise to a current which is nearly independent of β over a certain range.)

The properties of the plasma and of the associated magnetic field, as they emerge from the present discussion, are summarized in Table 6. Note that while the experimental data appear to be consistent with the assumption of a Maxwellian distribution for the random velocities of the protons, they certainly do not prove that this assumption represents more than a crude approximation. Thus, the temperatures in Table 6 are simply an indication of the mean energy of random motion of the protons in the frame of reference of the moving plasma.

(4) Average Direction and Angular Spread of the Proton Beam.

Since the plasma was fully modulated at the 2300 volt level, the shapes of the current signals obtained at this level are independent of the proton energy spectrum; they depend only on the angle α formed by the bulk velocity vector \vec{V}_0 with the equatorial plane of the satellite, and on the angular spread of the proton beam. The position of their maxima,

on the other hand, determines the angle which the plane passing through the spin axis and the vector \vec{V}_0 forms with the plane through the spin axis and the solar direction (plane "p" in Fig. 12). We shall call this angle β_0 .

Figs. 22a and 22b illustrate the procedure used for the analysis of the observed pulses. The scale on the horizontal axis indicates times in milliseconds measured from the instant when the normal to the cup was closest to the solar direction. The dots in each figure represent superposed measurements of individual current signals obtained during two different telemetering cycles. The solid curves represent the geometrical response of the probe for parallel beams with $\alpha = 0^\circ$ and $\alpha = 40^\circ$, respectively, corrected for the distortion due to the electronic circuits (see Fig. 8). The vertical scales for these curves and their horizontal positions were adjusted so as to obtain the best fit with the maxima of the experimental current signals. The times at which these maxima occur are shown in the figures as t_m . Considering the 15 ms delay introduced by the electronic circuits, the values of t_m shown in Figs. 22a and 22b correspond, respectively, to $\beta_0 = -7^\circ$ and $\beta_0 = 0^\circ$ (negative angles indicate directions to the south-east of the plane "p"). Analysis of the various current signals recorded at the 2300 volt level gives values of β_0 which cluster around 0° , with a dispersion of a few degrees. We were unable to determine whether this dispersion is due to actual fluctuations in the direction of the plasma flow or is due entirely to experimental errors. In this

connection, we note that the timing signal from the optical aspect sensor had an uncertainty of about 4 ms, corresponding to an uncertainty of about 2.5° in β_0 , and that a somewhat larger uncertainty is involved in the determination of t_m . In any case, we can safely state that whenever plasma was observed during the third period of the Explorer 10 flight, the angle β_0 was smaller than 10° in absolute value.

The current signals shown in Figs. 22a and 22b are slightly wider than the curve representing the response of the probe to a parallel beam of particles incident at $\alpha = 0^\circ$. The difference is even greater for $\alpha > 0^\circ$. We shall make a crude estimate of the angular spread of the proton beam needed to account for the observed widening by assuming that both the response curve of the probe and the angular distribution of the protons may be approximated by gaussian functions, with root mean square angles equal to $\Delta\theta$ and $\Delta\phi$ respectively. The observed current signal should then be a gaussian function with a root mean square angle $\Delta\theta_e$ given by:

$$(\Delta\theta_e)^2 = (\Delta\theta)^2 + (\Delta\phi)^2.$$

Comparing the observed signals with the response curve for $\alpha = 0^\circ$ (corrected for the distortion of the pulses due to the non-linearity of the electronic circuits), and considering that, for a gaussian distribution, the root mean square angle equals the half-width at 0.6 maximum height, we find from Fig. 22a, a value of $(\Delta\phi)^2$ between .02 and .10, and from Fig. 22b a value of $(\Delta\phi)^2$ between .03 and .12.

If we interpret the angular spread in terms of a "thermal" agitation of the protons in the frame of reference of the moving plasma, we have:

$$(\Delta\phi)^2 = kT/2E_0.$$

Using the above values of $(\Delta\phi)^2$ and a kinetic energy of bulk motion $E_0 = 420$ ev, we obtain "temperature" estimates ranging roughly from 2×10^5 °K to 1×10^6 °K in the case of Fig. 21a and from 3×10^5 °K to 1×10^6 °K in the case of Fig. 21b.

These results appear to be more or less typical of all current signals obtained at the 2300 volt level. Thus, we conclude that the range of possible "temperatures" deduced from the width of the current signals is not in disagreement with that deduced from the proton energy spectrum. Of course, it should be noted that both temperature determinations are very crude. Also there is no "a priori" reason why the two "temperatures" should be identical since the root mean square velocities of agitation parallel and perpendicular to \vec{V}_0 may well differ from one another.

C. Third Period - Currents Observed in Situations of Type A.

The currents observed at times when the radial configuration of the magnetic field was indicative of a type A situation corresponded always to nominal flux densities smaller than 5×10^7 cm⁻²sec⁻¹. However, these currents were occasionally distinctly above the noise level. They were modulated by the

rotation of the satellite, with the maximum at the time when the normal to the probe was closest to the direction of the sun (as in the case of the currents observed in situations of type B). In many instances, they appeared only at the 2300 volt modulation level; in some cases, they appeared also at the 800 volt and at the 250 volt levels, once even at the 80 volt level. Modulation at the latter voltages was observed more frequently toward the end of the flight. The origin of these small currents cannot be established with certainty.

D. Observations during the Fourth Period.

During the fourth period, the following sequences of events took place.

Between 3-27-1440 and 3-27-1452, the magnetic field changed direction abruptly (from about $\phi = 0^\circ$, $\theta = -60^\circ$ to about $\phi = 90^\circ$, $\theta = 0^\circ$) and then returned just as abruptly to approximately the original direction. The next two plasma measurements at the 800 volt and 2300 volt levels indicate that a substantial increase in the mean proton energy had occurred ($\bar{\phi}(2300) \simeq 2 \bar{\phi}(800)$, flat-topped signal at the 800 volt level), while the total flux density had not changed appreciably.

At about 3-27-1500, the magnitude of the magnetic field at the satellite (which had been for some time in the neighborhood of 13γ) began to increase and reached a maximum of about 25γ

at 3-27-1640, after which time it decreased slightly, oscillating around a value of about 20 γ .

At 3-27-1503, when the satellite was at a geocentric distance of $41.4 R_e$, the sudden commencement of a magnetic storm was recorded on the earth. In the next six telemetering sequences, (i.e., until 3-27-1655) the signals at the 2300 volt level (when available) were about twice the size of those at the 800 volt level. Moreover, the latter had a distinct "horned" shape which had not been observed previously (see Fig. 15), while the signals at the 2300 volt level still had a round top. There was also a large increase in the total proton flux.

For the remainder of the observation period (i.e., until 3-27-1800, when the satellite was at $42.3 R_e$) the proton flux remained at a level about double that observed prior to the sudden commencement. However, there was no longer any marked difference between $\bar{\phi}$ (2300) and $\bar{\phi}$ (800), and the signals at the 800 volt level again had a rounded top.

The above results show that during the first two hours after the sudden commencement about half of the plasma protons had nominal energies above 800 ev. However, the round tops of the signals at the 2300 volt level indicate that the proton spectrum did not extend much beyond 2300 ev. Thus the kinetic energy of bulk motion was of the order of 1000 ev; however, the shape of the proton spectrum does not appear to be consistent with a Maxwellian distribution of the proton velocities in the frame of reference of the moving plasma.

Throughout the fourth period, the positions of the maxima were not appreciably different from those observed during the

preceding third period. Thus, there was no evidence for any change in the direction of the plasma flow.

VI INTERPRETATION

There is little doubt that the fast-moving plasma encountered by Explorer 10 during the third and fourth periods of its flight did not originate from the earth, but was a feature of interplanetary space (however, it is likely, as we shall see, that the presence of the earth might have materially modified the plasma flow in the region explored by the satellite).

It is also difficult to avoid the conclusion that the reason why no fast-moving plasma had been detected in the previous periods is that the geomagnetic field acts as an obstacle to the plasma flow, creating around the earth a "cavity" which the interplanetary plasma cannot penetrate (though the cavity may contain a quasi-stationary plasma representing an extension of the earth's atmosphere). The first appearance of the plasma at the beginning of the third period means that, at that time, Explorer 10 had traversed the boundary of the geomagnetic cavity.

A. Theoretical Considerations

The interaction of a moving plasma with the earth's magnetic field was first studied theoretically by Chapman and Ferraro (1931, 1932, 1933). The problem was taken up again by Ferraro (1952, 1960) whose work led to the prediction of a geomagnetic cavity of the general shape shown in Fig. 23a. Its characteristic features are a blunt "nose" pointing toward the oncoming wind, and a long "tail" stretching in the downwind direction (see also Johnson, 1960; more recent developments of the theory are described in a paper by Davis and Beard, 1962, which also contains

a good bibliography of the subject).

This theoretical model is based on a set of highly idealized assumptions, of which the most important are: (1) absence of plasma within the geomagnetic cavity, (2) absence of magnetic field in the moving interplanetary plasma, and (3) absence of random motions of the plasma particles in the rest frame of reference of the plasma ("perfectly cold" plasma).

During the last few years, it has become increasingly clear that none of these assumptions correspond to reality. Thus, before the flight of Explorer 10, even the qualitative validity of the theoretical conclusions was questionable.

On the other hand, the findings of Explorer 10 showed that the theoretical model was correct in predicting a sharp boundary between the geomagnetic cavity and the surrounding interplanetary plasma. Moreover, another important feature of the theoretical model, i.e., the strong forward-backward asymmetry of the cavity with respect to the direction of the plasma flow, was also experimentally confirmed; while Explorer 10 crossed the geomagnetic boundary at a distance of about 22 earth radii in the anti-solar region, Explorer 12, moving in the subsolar region, crossed the boundary at about 10 earth radii (see section B below). It is thus reasonable to explore the possibility of interpreting the experimental results on the basis of the theoretical model suitably modified to make it compatible with the properties of the "real" interplanetary plasma.

The irreversible flow, indicated by the asymmetric shape of

the geomagnetic cavity, implies dissipative processes such as are likely to occur prominently if the plasma approaches the earth at supersonic speed.

In the idealized theoretical model, the plasma flow is indeed "infinitely" supersonic because in a "perfectly cold" plasma with no magnetic field, the velocity of propagation of small low-frequency disturbances ("sound" waves as well as Alfvén waves) is zero.*

* A collisionless plasma does not propagate ordinary sound waves. However, some of the possible wave modes have propagation velocities that are close to the velocity of sound, defined in the ordinary manner.

In the actual interplanetary plasma, on the other hand, both the "sound" velocity and the Alfvén velocity have finite values, and we must examine the experimental data to determine whether these velocities are actually smaller than the bulk velocity.

In this connection, we note that the properties of the plasma wind observed by Explorer 10 may differ substantially from those of the "distant wind". In fact, it is well known that a supersonic flow cannot be stopped suddenly by an obstacle (in our case, by the geomagnetic cavity), but must first be modified in such a way that, in the region ahead of the stagnation point, the velocity of the flow becomes subsonic. In the case of ordinary fluids, the conversion occurs through a stationary shock front (or bow wave) that forms ahead and around the obstacle. It is reasonable to assume that a similar shock front exists in the interplanetary plasma around the geomagnetic cavity (see Fig. 23b).

Since collisions do not play any appreciable role in the exceedingly dilute interplanetary plasma, the dissipation processes that occur in the passage of the plasma across the shock front must be due to a mechanism different from that operative in ordinary fluids, a mechanism which is not yet well understood. In any case, it is certainly true that between the shock front and the geomagnetic cavity, plasma and magnetic conditions are different from those beyond the front, where no effect of the earth's magnetic field can be felt. In particular, the plasma in this region will not only move with a smaller speed and in a direction different from that of the distant wind, but it will also have a higher "temperature" and carry a stronger magnetic field. For these reasons, the "Mach numbers" of the local wind relative to both "sound" waves and Alfvén waves will be smaller than the corresponding Mach numbers of the distant wind.

With this in mind, let us consider the Explorer 10 results. The velocity of bulk motion of the plasma was found to be substantially larger than the mean "thermal" velocity of agitation of the plasma protons. Since the "thermal" velocity is close to the "sound" velocity, we conclude that the velocity of bulk motion was larger than the "sound" velocity.

From Table 6, we see that the ratio of the kinetic energy density of bulk motion to the magnetic energy density was greater than unity. Since this ratio equals the square of the ratio of the bulk velocity to the Alfvén velocity, we conclude

that the bulk velocity was also larger than the Alfvén velocity.

The observed plasma wind was thus supersonic with respect to both "sound" waves and Alfvén waves; for the reasons explained above, this conclusion applies a fortiori to the distant wind.

Note that a bow wave does not appear in the theoretical model because in the limit of an infinitely large Mach number the bow wave becomes coincident with the boundary of the geomagnetic cavity.

B. Experimental Data Relating to the Geomagnetic Cavity and the Bow Wave.

Besides Explorer 10, several other space vehicles have provided information that can be used to specify some of the parameters characteristic of the interaction region between the interplanetary plasma and the geomagnetic field.

Pioneer 1 (launched October 11, 1958) and Pioneer 5 (launched March 11, 1960) both went in the general direction of the sun. They did not carry plasma probes, but they did carry rotating-coil magnetometers which measured, intermittently, the component of the magnetic field perpendicular to their spin axes.

Up to a geocentric distance of about $13 R_e$, the observations of Pioneer 1 indicated a magnetic field which was not very different from that of a dipole; however, in the neighborhood of $13 R_e$, the field was decreasing more slowly than a dipole field. Between $13 R_e$ and $14 R_e$, the field became highly disturbed and decreased in strength from about 25γ to less than 10γ (Sonett, Smith and Sims, 1960; Sonett, Judge, Sims, and Kelso, 1960).

The observations of Pioneer 5 (Coleman, Sonett, Judge, and

Smith, 1960) indicated a quiet magnetic field out to $10 R_e$. Then between $10 R_e$ and $14 R_e$, the field became highly disturbed. Between $14 R_e$ and $15 R_e$ the situation changed again, and after $15 R_e$ the field became much quieter and decreased in strength, dropping to a value of about 5γ at $20 R_e$.

Explorer 12 (which was launched August 15, 1961, on an elliptical orbit with an apogee of about $13 R_e$) carried a plasma probe, three flux-gate magnetometers and various high-energy particle detectors. Its measurements refer to the subsolar region. The magnetometers showed that, in this region, the field was regular and had a structure consistent (in strength and direction) with that of a "compressed" dipole field up to a certain distance, beyond which it became highly irregular and its direction changed drastically (by about 180°). The distance at which the transitions occurred varied between $8 R_e$ and $12 R_e$ (Cahill, 1962; Cahill and Amazeen, 1962).

The plasma probe aboard Explorer 12 did not supply data pertinent to this discussion. However, the high-energy particle detectors showed that the region populated by trapped particles terminated near the point where the magnetic transition occurred (Rosser, O'Brien, Van Allen, Frank and Laughlin, 1962).

The combined results of Pioneer 1, Pioneer 5, and Explorer 12 support the theoretical model described in Section A. Moreover, they show that the boundary of the geomagnetic cavity (separating the magnetically disturbed region from the magnetically "quiet"

region populated by trapped particles) lies, in the subsolar region, between $8 R_e$ and $12 R_e$. They also indicate the presence of a second surface of discontinuity at $14 R_e$ or $15 R_e$, which presumably represents the bow wave, separating the magnetically disturbed region around the geomagnetic cavity from the unperturbed interplanetary field.

Fig. 24 summarizes in graphical form the data mentioned above. This figure was taken from the report presented by one of us at a recent Symposium of IRE-PGNS (Bridge, 1962). A similar picture was presented by Cahill at the same symposium.

C. A Tentative Model for the Geomagnetical Cavity.

Making use of the above results, we now attempt to draw a tentative and schematic model for the geomagnetic cavity as it existed at the time when Explorer 10 crossed the boundary and first detected the plasma wind. For this purpose, we still need to supplement the experimental data with a few hypotheses.

In the first place, we assume that the distant plasma wind comes directly from the sun. Then in an earth-bound frame of reference, the plasma wind outside the bow wave arrives at an angle of about 6° to the sun-earth direction in the plane of the ecliptic, because of the orbital velocity of the earth.

We assume next that the geomagnetic cavity has axial symmetry around a line parallel to the distant wind and passing through the center of the earth. Moreover, we assume that the boundary of the cavity can be approximated by a spherical cap

joining smoothly to a conical surface.

Finally, we take for the radius of the spherical cap a value of $10 R_e$, which is the average distance at which Explorer 12 detected the termination of the geomagnetic cavity in the sub-solar region.

The above assumptions, together with the observed position at which Explorer 10 first encountered the plasma wind, determine the boundary of the geomagnetic cavity; the conical surface of this boundary has a half-angle at the vertex of about 20° (see Bridge, Lazarus, Lyon and Scherb, 1962; Bonetti, Olbert, Rossi and Siscoe, 1962).

The assumed shape of the geomagnetic boundary (a spherical cap joining to a conical "tail") is obviously an oversimplification. Indeed, since the earth's magnetic field is not axially symmetric with respect to the direction of the distant wind, there is no reason to believe that the geomagnetic cavity has axial symmetry. We have also neglected here the complex phenomena that are likely to occur in the vicinity of those singular points of the boundary surface where the magnetic field vanishes (see, for example, Dungey, 1958). Moreover, the choice of $10 R_e$ for the geocentric distance of the geomagnetic boundary in the subsolar region is, to some extent, arbitrary. This distance could easily have been 20 percent larger or smaller; correspondingly, the half-angle of the conical "tail" could have been smaller or

greater than 20° . Finally, one must remember that, as demonstrated by the Explorer 12 results, the boundary of the geomagnetic cavity changes with time. Therefore, our specific model refers only to the geomagnetic cavity at one particular instant of time, i.e., the time when Explorer 10 left the cavity.

Undoubtedly, the present model will be refined and revised as more experimental data become available. We believe, however, that its general features will not change drastically, and we feel justified in using it as a basis for the interpretation of our data.

D. Alternate Appearances and Disappearances of the Plasma.

An important feature of the Explorer 10 observations is the alternate appearance and disappearance of the plasma during the third period of its flight (transitions from situation A to situation B and vice versa). There are, in principle, two interpretations of these occurrences. The first is that the interplanetary plasma has a "stratified" structure, in which tubes of force which are essentially empty alternate with tubes of force containing substantial amounts of plasma. The second is that, during the third period of its flight, Explorer 10 found itself alternately inside and outside the geomagnetic cavity.*

* We dismiss here, as unlikely, the possibility that during intervals of type A the direction of the plasma flow was within the solid angle where the plasma probe was insensitive ($\alpha > 63^{\circ}$, see Fig. 12).

After examining in detail the results of the magnetic field measurements, we are convinced (as discussed below) that the second interpretation is the correct one (Rossi, 1962; other authors such as Piddington, 1962, have reached the same conclusion independently). These measurements, in fact, strongly suggest that the field corresponding to situations of type A was to some extent modified by the presence of the earth, whereas the field corresponding to situations of type B was not.

In the first place, the field observed in the absence of plasma (situation A), was found to point almost directly away from the earth. This is the expected direction of field lines originating from the earth and contained in the elongated "tail" of the geomagnetic cavity. Only by pure accident would one find field lines with this particular orientation in a region of space where the field arises from sources totally unrelated to the earth.

In the second place, the data summarized in Tables 3 and 4 show that the strength of the magnetic field observed during the intervals of type A decreased with increasing geocentric distance, whereas no such consistent trend is detectable in the magnetic field measured during intervals of type B. These observations are easily understood if we assume that the field typical of situation A is the geomagnetic field modified by the plasma wind, and that the field typical of situation B is of non-terrestrial origin. On the other hand, if we assumed that

the field typical of situation A is also unrelated to the earth, the observed decrease with increasing geocentric distance would be entirely accidental.

A much more detailed and critical analysis of these questions appears in HNSS, to which we refer the reader for further information.*

* H. Elliot, in a private communication (October, 1961), first pointed out that the strength of the magnetic field detected by Explorer 10 prior to the sudden commencement decreased with increasing geocentric distance. He used this observation as evidence that the field was of terrestrial origin (although modified by the interplanetary plasma). When the distinction between "situation A" and "situation B" was clearly established, it became evident that Elliot's argument was valid for situations of the first type but not for situations of the second type. The careful analysis of the magnetic measurements carried out by J. Heppner and his collaborators (see HNSS) has now added considerable strength to the conclusion that the field observed in situations of type A was of terrestrial origin.

The above interpretation of the alternate appearances and disappearances of the plasma is consistent with our model of the geomagnetic cavity. To illustrate this point, Fig. 25 shows the intersection of this cavity with the plane of the satellite's trajectory. One sees that Explorer 10 kept close to the assumed boundary after leaving the geomagnetic cavity. While we

do not claim that the situation depicted in Fig. 25 represents more than a crude approximation, we feel justified in assuming that Explorer 10, during the remainder of its flight, was never very far from the boundary as it existed at the time of the first crossing. It is thus very likely that fluctuations in the position of the boundary brought the satellite alternately inside and outside the geomagnetic cavity. Such fluctuations are to be expected, since the position of the boundary depends on the dynamic pressure of the plasma wind and the Explorer 10 data obtained outside the cavity reveal appreciable changes in the plasma flux.

It is possible, also, that the boundary surface might be somewhat "wavy", thus allowing several successive traversals even without any temporal changes in the position of the surface.

In connection with the present discussion, it is of interest to recall that on March 26, at 0250 UT, while the satellite was still within the geomagnetic cavity, the magnetic field began to increase in strength without changing direction (see section IV-B). Presumably, this increase was due to a compression of the geomagnetic cavity, caused by an increase in the plasma flux. Possibly, when the plasma wind was first detected a few hours later, the geomagnetic boundary was still moving inward at a speed greater than the outward speed of the satellite. If so, it would be more appropriate to say that the geomagnetic boundary had moved

past the satellite, rather than to say that the satellite itself had crossed a relatively stationary boundary.

E. Properties of the Plasma Detected by Explorer 10 During the Magnetically Quiet Third Period.

If Explorer 10 never got very far from the geomagnetic boundary, the local wind detected by the plasma probe must have been practically tangent to this boundary. If, moreover, the boundary was axially symmetric, the wind direction would lie in the plane passing through the axis of the cavity and the point of observation.

Let us assume that at all times when Explorer 10 detected a plasma wind, the geomagnetic cavity had the shape shown in Fig. 25. We then find that at the point where the satellite's trajectory first crossed the geomagnetic boundary, the plasma wind must have had the direction shown by point L_1 in Fig. 25. We also find that, despite the motion of the satellite, the wind direction changed very little during the remainder of the flight, the representative point moving only from L_1 to L_2 . Points L_1 and L_2 are well within the "window" that contains the wind directions compatible with our observations. Thus, the proposed model of the cavity is consistent with these observations.

The directions corresponding to points L_1 and L_2 lie practically in the equatorial plane of the satellite (represented by the line "n" in Fig. 26). Therefore, the angle α for the local wind is practically zero. Of course the exact value of α thus determined is not significant because the assumed shape

of the geomagnetic cavity does not represent more than a crude approximation. However, it would seem that for all reasonable directions of the local wind which are consistent with a distant wind coming directly from the sun, α should lie between 0° and 20° (notice that $\alpha = 20^\circ$ corresponds to a nearly cylindrical, rather than conical, "tail" of the geomagnetic cavity).

For angles smaller than 20° , the differences between "nominal" and actual values of the flux and the energy are within the limits of our experimental uncertainties. Thus, we may use the figures listed in Table 6 as a reasonable estimate for the properties of the plasma observed during the third period of the flight.

We wish to note again that, in all likelihood, Explorer 10 never went out of the stationary shock front which has been assumed to surround the geomagnetic cavity. Presumably, the mechanical and magnetic properties of the plasma undergo a change across the shock front; thus, the experimental data of Explorer 10 may not represent accurately the properties of the interplanetary plasma at large distances from the earth.

F. Explorer 10 Observations at the Time of the Sudden Commencement

As noted in HNSS, a class 3 flare appeared on the east limb of the sun about 29 hours before the sudden commencement observed on the earth and the almost simultaneous increase in plasma flux and magnetic field strength recorded by the instruments aboard Explorer 10. If this flare was indeed responsible for these effects, the mean velocity of propagation of the disturbance in interplanetary space was about 1400 km sec^{-1} .

Presumably, the disturbance consisted of a shock wave produced by the solar outburst and travelling over the "normal" solar wind. Immediately behind the shock front, one should expect to find a plasma moving with a bulk velocity smaller than that of the shock front itself (which corresponds to a proton energy of about 11 kev). The protons detected by the plasma probe had energies below 2300 ev, corresponding to a velocity of less than 640 km sec^{-1} . The shape of the current signals is not consistent with the assumption that the probe was detecting the low-energy tail of a broad distribution peaked at an energy greater than 2300 ev.

Thus, the bulk velocity of the plasma appears to differ from the computed mean velocity of propagation of the shock front by at least a factor of two. However, one must consider (1) that the velocity of the shock front, near the earth might have been smaller than its mean velocity, (2) that passage through the bow wave might have decreased the bulk velocity of the plasma. It is also possible, of course, that the observed magnetic field and plasma flux increases were not caused by the flare referred to above.

G. Configuration of the Magnetic Field Lines

In the theoretical model of the cavity produced by the interaction of a moving interplanetary plasma with the geomagnetic field, all of the magnetic field lines originating from the earth return to the earth. This is a consequence of the assumption that the interplanetary plasma does not carry any magnetic field. Even though it is now known that a magnetic field exists in

interplanetary space, one might be inclined to believe that the earth's magnetic field is still confined to the geomagnetic cavity. According to this picture, the lines of force of the interplanetary field would spread out in the vicinity of the earth so as to envelope the geomagnetic cavity and remain disconnected from the field lines originating in the earth. The magnetic field vectors on the inner and outer side of the geomagnetic boundary would then be tangent to this surface (without necessarily being parallel to each other).

The general pattern of the experimental data provided by Explorer 10 does not appear to support this view. In fact, along those sections of the trajectory which were outside the cavity, the average magnetic field formed large angles with the boundary, being often approximately perpendicular to it. Inside the cavity, the average magnetic field (which was nearly radial from the earth) also formed a finite angle with the boundary of the cavity. Thus, it would seem that the field lines originating from the earth do not remain confined to the geomagnetic cavity but connect to the field lines of interplanetary space through the boundary of the cavity.*

* As noted in HNSS, some uncertainty exists in the direction of the Explorer 10 spin axis; the extreme values for its ecliptic longitude are 59.5° and 63° , and the extreme values for its ecliptic latitude are -30° and -46.5° . However, these uncertainties do not affect significantly the conclusions stated here concerning the magnetic field directions.

Since the interplanetary plasma flows past the geomagnetic cavity at great speed, while the cavity itself contains a nearly stationary plasma, it seems difficult to reconcile such a magnetic configuration with the generally accepted belief that the magnetic field lines are frozen into the plasma.

In view of this difficulty, it is advisable to exercise great caution in the interpretation of the experimental results.

One possibility is that the geomagnetic cavity is separated from the interplanetary plasma by a boundary layer of finite thickness, and that within this layer violent dissipative processes occur which effectively de-couple the field lines of the interplanetary plasma from those contained in the geomagnetic cavity. The transitions which we have defined as "complex" (see section V-A) appear to suggest, in fact, the presence of a boundary layer of considerable thickness. However, most of the transitions were not complex. Moreover, it is possible that the rapid changes of magnetic field and plasma flux occurring during the complex transitions may have been due to fluctuations of a thin geomagnetic boundary. The fact that, even during such transitions, the correlation between plasma flux and magnetic field direction persisted, supports the latter point of view. In any case, the character of the fluctuations in the magnetic field observed during the complex transitions does not suggest the kind of turbulence that one would associate with strongly dissipative processes. Thus, there is little experimental evidence to support the view that dissipation of energy within a boundary layer of finite thickness may provide a way out of the difficulties.

Another possibility is that the field lines, both inside and outside the geomagnetic cavity, approach the boundary at a finite angle and then turn sharply so as to become parallel to this boundary.

To test such a possibility, we examined in detail the behavior of the magnetic field in the vicinity of the various transitions which, according to our interpretation, represent traversals of the geomagnetic boundary (see Table 2). We found no evidence that the magnetic field tended to become parallel to such a boundary at the times when any one of the 13 simple transitions occurred, and only a few of the observations made during the two complex transitions might be compatible with magnetic fields parallel to the boundary. A typical example of the changes in the direction of B corresponding to a simple transition is illustrated in Fig. 27.

It would be premature, perhaps, to draw any firm conclusion from the above results, in view of the fact that the magnetic field was not measured continuously, but only at intervals of $2^{m}28^s$. One must also consider the uncertainties introduced by the arbitrary assumptions on which our tentative model of the geomagnetic cavity is based (see section VI-C). Of these assumptions, the one which affects the predicted orientation of the geomagnetic boundary most critically is the hypothesis that the plasma wind flows radially away from the sun. One might inquire if, by abandoning this assumption, one can construct a reasonable model for the geomagnetic cavity such that its boundary is parallel to the magnetic fields observed near the transitions. It turns out that this is possible, provided one assumes that the distant wind comes from a direction near the plane of the ecliptic at about 45° west of the sun (see Bonetti, Bridge, Lazarus, Lyon, Rossi, and Scherb, 1962a). The direction of the "local" wind corresponding to this model falls within the "window" containing the allowed directions of the observed plasma flow. However, this model appears

unrealistic on the following grounds: First, it is difficult to imagine a mechanism that would account for the wind coming from that particular direction. Second, considering the intersection of the geomagnetic cavity produced by this wind with the orbital plane of Explorer 10, we now find that the satellite, after crossing the boundary at $22 R_e$, moved rapidly away from it. Thus, it is no longer possible to explain the alternate disappearances and reappearances of the plasma by expansions and contractions of the geomagnetic boundary, unless these oscillations had a very large amplitude.

In conclusion, we wish to stress the fact that questions of basic importance are still unresolved by present experimental information on the interplanetary plasma and the geomagnetic boundary. It is essential that further experiments be undertaken, designed to provide a detailed description of conditions existing in the immediate vicinity of the geomagnetic boundary and within the boundary layer itself, through continuous recording of magnetic fields and plasma fluxes.

ACKNOWLEDGEMENTS

The Project Manager for Explorer 10 was Dr. J. P. Heppner of the Goddard Space Flight Center; his group was also responsible for the magnetic field measurements reported in HNSS. We would like to acknowledge particularly the essential contribution of this group to the success of our own experiment. In addition, the cooperation and collaboration of NASA personnel too numerous to mention individually contributed to the experiment reported in this paper.

We recall gratefully the important part played by Dr. Constance Occhialini and Mr. Ervin F. Lyon in the preparation of the experiment and in the early analysis of its results. We are greatly indebted to Dr. S. Olbert for many suggestions and critical discussions concerning the interpretation of the experimental data.

REFERENCES

Bonetti, A., S. Olbert, B. Rossi and G. Siscoe, Problems concerning the interaction of the interplanetary plasma with the geomagnetic field, paper presented at the Symposium on Recent Results in Space Physics, American Geophysical Union, Washington, April 25-28, 1962.

Bonetti, A., H. S. Bridge, A. J. Lazarus, E. F. Lyon, B. Rossi and F. Scherb, Explorer 10 plasma measurements, paper presented at the Third International Space Science Symposium (COSPAR), Washington D.C., 1962a, to be published in Space Research III by North-Holland Publishing Co.

Bonetti, A., H.S. Bridge, A.J. Lazarus, E. F. Lyon, B. Rossi and F. Scherb, Results of Explorer 10 plasma measurements, Proceedings of the Fifth Inter-American Seminar on Cosmic Rays, La Paz, July, 1962b.

Bridge, H.S., Interplanetary plasma, paper presented at the International Symposium on Space Phenomena and Measurements, Annual Meeting of IRE-PGNS, Detroit, October 16, 1962.

Bridge, H.S., C. Dilworth, B. Rossi, F. Scherb and E.F. Lyon, An instrument for the investigation of interplanetary plasma, J. Geophys. Research 65, 3053, 1960.

Bridge, H.S., C. Dilworth, A.J. Lazarus, E.F. Lyon, B. Rossi and F. Scherb, Direct observations of the interplanetary plasma, J. Phys. Soc. of Japan, 17, Suppl. A-II, 553, 1962.

Bridge, H.S., A.J. Lazarus, E.F. Lyon, B. Rossi and F. Scherb, Plasma probe instrumentation on Explorer 10, paper presented at the Third International Space Science Symposium (COSPAR), Washington, D.C., 1962, to be published in Space Research III by North-Holland Publishing Co.

Bridge, H.S., A.J. Lazarus, E.F. Lyon and F. Scherb, Plasma measurements on Explorer 10, paper presented at the Symposium on Recent Results in Space Physics, American Geophysical Union, Washington, April 25-28, 1962.

Cahill, L., paper presented at the Annual Meeting of the American Geophys. Union, Washington, April, 1962.

Cahill, L.J., and P.G. Amazeen, The boundary of the geomagnetic field, preprint.

Chapman, S., and V.C.A. Ferraro, A new theory on magnetic storms, Terrestrial Magnetism and Atmospheric Elec., 35, 77-97, 171-186, 1931.

Chapman, S., and V.C.A. Ferraro, A new theory on magnetic storms, *Terrestrial Magnetism and Atmospheric Elec.*, 37, 147-156, 421-429, 1932.

Chapman, S. and V.C.A. Ferraro, A new theory on magnetic storms, *Terrestrial Magnetism and Atmospheric Elec.*, 38, 79, 1933.

Coleman, P.J., C.P. Sonett, D.L. Judge, and E.J. Smith, Some preliminary results of the Pioneer 5 magnetometer experiment, *J. Geophys. Research*, 65, 1856, 1960.

Davis, L., and D.B. Beard, A correction to the approximate condition for locating the boundary between a magnetic field and a plasma, *J. Geophys. Research* 67, 4505, 1962.

Dungey, J.W., *Cosmic Electrodynamics*, p. 98 and f.f., Cambridge University Press, London, 1958.

Ferraro, V.C.A., On the theory of the first phase of a geomagnetic storm, *J. Geophys. Research*, 57, 15, 1952.

Ferraro, V.C.A., An approximate method of estimating the size and shape of the stationary hollow carved out in a neutral ionized stream of corpuscles impinging on the geomagnetic field, *J. Geophys. Research*, 65, 3951, 1960.

Gringauz, K.I., Investigation of interplanetary plasma and planetary ionospheres by means of charged particles traps on space rockets, paper presented at the Twelfth International Astronautical Congress, Washington, D.C., October, 1961.

Gringauz, K.I., V.V. Bezrukikh, S.M. Balandina, V.D. Ozerov, and R.E. Rybchinskii, Direct Observations of solar plasma streams at a distance of $\sim 1,900,000$ km from the earth on February 17, 1961, and simultaneous observations of the geomagnetic field, paper presented at the Third International Space Science Symposium (COSPAR), Washington, D.C., 1962, to be published in *Space Research III* by North-Holland Publishing Co.

Gringauz, K.I., V.V. Bezrukikh, V.D. Ozerov and R.E. Rybchinskii, A study of interplanetary ionized gas, energetic electrons and solar corpuscular radiation using three-electrode charged particle traps on the second Soviet Cosmic Rocket, *Doklady Akad. Nauk SSSR*, 131, 1301, 1960, and L. V. Kurnosova, *Artificial Earth Satellites*, No. 6, page 122.

Gringauz, K. I., V. G. Kurt, V. I. Moroz and I. S. Shklovskii, Ionized gas and fast electrons in the neighborhood of the earth and in interplanetary space, *Doklady, Akad. Nauk SSSR*, 132, 1062, 1960a, and L.V. Kurnosova, *Artificial Earth Satellites*, No. 6, page 130.

Gringauz, K.I., V. G. Kurt, V. I. Moroz, and I. S. Shklovskii, Results of observations of charged particles observed out to $R = 100,000$ km, with the aid of charged-particle traps on Soviet space rockets, translated from *Astronomicheskii Zhurnal*, 37, 716, 1960b.

Heppner, J.P., N.F. Ness, T.L. Skillman and C.S. Searce, Magnetic field measurements with the Explorer 10 satellite, *J. Phys. Soc. of Japan*, 17, Suppl. A-II, 546, 1962a.

Heppner, J.P. N.F. Ness, T.L. Skillman, C.S. Searce, Explorer 10 magnetic field results, paper presented at the Third International Space Science Symposium (COSPAR), Washington, D.C., 1962b, to be published in *Space Research III* by North-Holland Publishing Co.

Heppner, J.P., N.F. Ness, C.S. Searce and T.L. Skillman, Explorer 10 magnetic field measurements, *J. Geophys. Research*, 68, 1, 1963.

Hinteregger, H. E., K. R. Damon, and L. A. Hall, *J. Geophys. Research*, 64, 961, 1959.

Johnson, F. S., The gross character of the geomagnetic field in the solar wind, *J. Geophys. Research*, 65, 3049, 1960.

Rosser, W.G.V., B.J. O'Brien, J.A. Van Allen, L.A. Frank and C.D. Laughlin, Electrons in the earth's outer radiation zone, *J. Geophys. Research*, 67, 4533, 1962.

Rossi, B., The interplanetary plasma, paper presented at the January, 1961 meeting of the American Physical Society, New York (unpublished).

Rossi, B., Interplanetary plasma, paper presented at the Third International Space Science Symposium, Washington D.C., 1962 (COSPAR), to be published in *Space Research III* by North-Holland Publishing Co.

Smith, R.L., and R. A. Helliwell, Electron densities to 5 earth radii deduced from nose whistlers, *J. Geophys. Research*, 65, 2583, 1960.

Sonett, C.P., E.J. Smith and A.R. Sims, Survey of the distant geomagnetic field: Pioneer 1 and Explorer 6, proceedings of the First International Space Science Symposium, Nice, 1960, p. 921, North-Holland Publishing Co., Amsterdam.

Sonett, C.P., D.L. Judge, A.R. Sims, and J. M. Kelso, A radial rocket survey of the distant geomagnetic field, *J. Geophys. Research*, 65, 55, 1960

Table 1.








Time intervals during the third period of the flight when measurements of the magnetic field and plasma fluxes indicated situations of type A or type B. Geocentric distance is the distance of the satellite from the center of the earth (in earth radii). Lateral distance is the distance from the sun-earth line. During interval No. 10, which was considerably longer than the others, plasma and magnetic conditions underwent substantial changes. Therefore, this interval has been divided into four sub-intervals for the purpose of analysis. The transitions between intervals 1 and 2 and between intervals 4 and 5 are of the "complex" type. All other transitions are of the "simple" type.




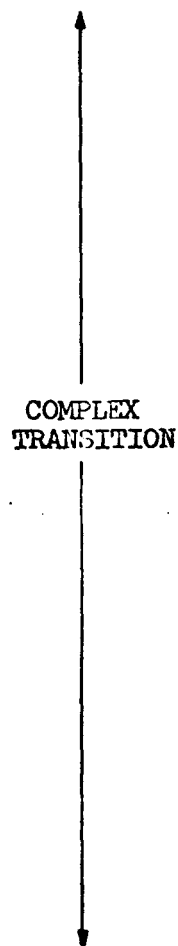
The telemetry cycles, times and distances indicated in the table correspond to the first sequence of measurements (optical aspect, magnetic field, plasma flux) made in the respective intervals.

Interval No.	Telemetry Cycle	Time	Geocentric Distance (Re)	Lateral Distance (Re)	Situation
----- 1	318	26/0410	21.0	16.7	-----
----- Complex Transition	352	0534	22.2	17.3	A
----- 2	364	0603	22.6	17.6	-----
----- 3	409	0754	24.2	18.5	B
----- 4	414	0805	24.4	18.6	A
----- Complex Transition	450	0935	25.7	19.3	B
----- 5	471 ^r	1026	26.5 ¹	19.6	-----
----- 6	512	1207	27.7	20.3	A
----- 7	544	1326	28.7	20.8	B
----- 8	578	1450	29.7	21.3	A
----- 9	622	1639	30.9	21.9	B
----- 10a	662	1817	32.0	22.4	A
----- 10b	734	2115	33.7	23.6	B
----- 10c	814	27/0032	35.3	24.3	B
----- 10d	854	0211	36.1	24.8	B
----- 11	952	0613	38.0	25.1	B
----- 12	965	0645	38.2	25.3	A
----- 13	1000	0811	38.8	25.5	B
----- 14	1050	1014	39.6	25.7	A
----- 15	1081	1131	40.1	26.0	B
----- 16	1118	1300	40.6	26.2	A
-----	1157	1438	41.3	26.4	B


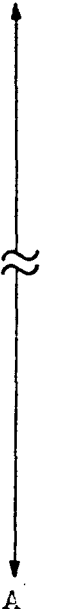


Table 2.




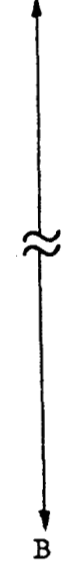
. Details of measurements of magnetic field and plasma in the vicinity of transitions. The numbers in the first column specify the telemetering cycle; measurements referring to subsequent cycles are separated by $2^m 28^s$. B is the absolute magnitude of the magnetic field vector (in units of 10^{-5} gauss, or gammas); ϕ and θ are the two angles (solar ecliptic longitude and ecliptic latitude) which describe the direction of this vector. The nominal flux densities listed correspond to the currents measured at the 80, 250, 800 and 2300 volt modulation levels. These measurements occupy four of the eight telemetering cycles which form a complete sequence (see Fig. 13). Question marks indicate measurements missing because of electronic disturbances. From 26/0534 to 26/0603, and then again from 26/0935 to 26/1026 more frequent changes from situation A to situation B and vice versa took place than during the rest of the flight. We chose to describe these occurrences as "complex transitions" rather than as a sequence of short time intervals of type A and B, although it is not clear that the distinction is physically significant. Notice the isolated occurrence of situation A during one telemetering cycle (No. 419) of time interval No. 4.



Telemetry Cycle	Interval	Magnetic Field			Plasma				Situation
		B (gammas)	ϕ (degrees)	θ (degrees)	Nominal Flux Density ($10^7 \text{ cm}^{-2} \text{ sec}^{-1}$)				
					$\Phi(80)$	$\Phi(250)$	$\Phi(800)$	$\Phi(2300)$	
346		31	150	-35	0	-	-	-	A
347		31	150	-36	-	.4	-	-	
348		31	156	-30	-	-	.5	-	
349		32	155	-32.5	-	-	-	0	
350		33	157	-37	-	-	-	-	
351		32	156	-32.5	-	-	-	-	
352		12	46	-22.5	-	-	-	-	B
353		20	137	-21	-	-	-	-	A
354		14	65	-19.5	.4	-	-	-	B
355		13.5	115	-55	-	3.0	-	-	B
356		32.5	152	-28.5	-	-	0	-	A
357		32	152	-28.5	-	-	-	?	A
358		32	151	-26	-	-	-	-	A
359		26	130	+14	-	-	-	-	B
360		10	59	-44	-	-	-	-	B
361		28.5	89	+31.5	-	-	-	-	B
362		30	152	-28	0	-	-	-	A
363		31	151	-34	-	0	-	-	A
364		14	-33	-49	-	-	30	-	B
365		8	43	-60.5	-	-	-	26	
366		10.5	16	+11	-	-	-	-	
367		13	21	-44	-	-	-	-	
368		11	29	-41	-	-	-	-	
369		13.5	3	-25.5	-	-	-	-	
404		14	29	-34	-	-	28	-	
405		14	20	-38	-	-	-	22.5	
406		15	-10	-41	-	-	-	-	
407		13	9	-61	-	-	-	-	
408		12	50	-30	-	-	-	-	
409		29	159	-30	-	-	-	-	A
410		28.5	160	-34	0	-	-	-	
411		18.5	140	-40.5	-	1.0	-	-	
412		28.5	162	-33	-	-	1.1	-	
413		28.5	169	-40	-	-	-	.7	




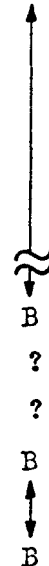
elementary Cycle	Interval	Magnetic Field			Plasma				Situation	
		B (gammas)	ϕ (degrees)	θ (degrees)	Nominal Flux Density ($10^7 \text{ cm}^{-2} \text{ sec}^{-1}$)					
					$\Phi(80)$	$\Phi(250)$	$\Phi(800)$	$\Phi(2300)$		
414	26/0805	15	-1	-46	-	-	-	-	B	
415		14.5	88	-59	-	-	-	-	↑	
416		13.5	13	-1	-	-	-	-		
417		19.5	240	-49	-	-	-	-	↓	
418		13.5	-53	-61	0	-	-	-		
419		24	160	-40	-	2.3	-	-	A	
420		11	2	-56	-	-	32	-	B	
421		11	266	-80	-	-	-	21	↑	
										
443			13.5	-28	-50	-	.7	-	-	↑
444			10.5	-11	-56	-	-	16.8	-	
445			17.5	13	+34	-	-	-	15.4	
446			15.5	-36	-46	-	-	-	-	
447			19.5	-83	-71	-	-	-	-	
448			20	-60	-30.5	-	-	-	-	
449			20	211	-46	-	-	-	-	
450	26/0935	29.5	176	-30	0	-	-	-	A	
451		16.5	150	-30	-	.5	-	-	A	
452		28	170	-33	-	-	0	-	A	
453		14.5	165	-54	-	-	-	22.8	B	
454		24	180	-45	-	-	-	-	A(?)	
455		19	-39	-2.5	-	-	-	-	B	
456		11.5	-29	-34	-	-	-	-	B	
457		18	-36	-52	-	-	-	-	B	
458		8.5	38	-34	0	-	-	-	B	
459		22.5	178	-41	-	0	-	-	A	
460		26.5	175	-33	-	-	0	-	A	
461		26	168	-40	-	-	-	?	A	
462		25.5	169	-40	-	-	-	-	A	
463		11.5	-10	-21	-	-	-	-	B	
464		17.5	-60	-56	-	-	-	-	B	
465		17.5	0	-38.5	-	-	-	-	B	
466		15.5	-50	-33.5	0	-	-	-	B	
467		18	-17	-40	-	.8	-	-	B	
468		20	191	-41.5	-	-	.5	-	A(?)	
469		10	128	-48	-	-	-	?	B	
470		10.5	98	-8.5	-	-	-	-	B	

Telemetry Cycle	Interval	Magnetic Field			Plasma				Situation
		B	ϕ	θ	Nominal Flux Density				
		(gammas)	(degrees)	(degrees)	$(10^7 \text{ cm}^{-2} \text{ sec}^{-1})$				
					$\Phi(80)$	$\Phi(250)$	$\Phi(800)$	$\Phi(2300)$	
471	26/1026	21.5	173	-38	-	-	-	-	A
472	⑤	20.5	161	-32	-	-	-	-	↑
473		24	169	-27.5	-	-	-	-	
474		22.5	165	-38.5	0	-	-	-	
475		22	165	-33	-	0	-	-	
476		24	172	-30	-	-	0	-	
		≈							
506	↓	20.5	161	-38.5	0	-	-	-	↓
507		22.5	162	-41	-	0	-	-	
508		21	158	-44	-	-	0	-	
509		21.5	160	-35	-	-	-	0	
510		23.5	173	-31.5	-	-	-	-	
511		21.5	162	-40.5	-	-	-	-	
512	26/1207	16.5	111	-65	-	-	-	-	B
513	⑥	8.5	184	-75	-	-	-	-	↑
514		9.5	69	-57	0	-	-	-	
515		13	121	-67	-	2.1	-	-	
516		12	-29	-52	-	-	11.4	-	
517		10	?	-45	-	-	-	11.7	
		≈							
538	↓	13.5	109	-40	.4	-	-	-	↓
539		12	100	-64	-	2.3	-	-	
540		11	104	-46	-	-	21	-	
541		10	97	-39.5	-	-	-	17	
542		11	114	-45	-	-	-	-	
543		11	93	-22.5	-	-	-	-	

Telemetry Cycle	Interval	Magnetic Field			Plasma				Situation
		B (gammas)	ϕ (degrees)	θ (degrees)	Nominal Flux Density ($10^7 \text{ cm}^{-2} \text{ sec}^{-1}$)				
					$\Phi(80)$	$\Phi(250)$	$\Phi(800)$	$\Phi(2300)$	
544	26/1326	18.5	164	-44	-	-	-	-	A
545		18	140	-30	-	-	-	-	
546		20	162.5	-35	0	-	-	-	
547		19.5	158	-32.5	-	.67	-	-	
548		21.5	161	-30	-	-	1	-	
549		19.5	167	-27	-	-	-	?	
571		19	151	-43.5	-	0	-	-	
572		18.5	151	-47.5	-	-	0	-	
573		18	143	-39.5	-	-	-	.4	
574		18.5	151.5	-40	-	-	-	-	
575		19	169	-37	-	-	-	-	
576		19	165	-32.5	-	-	-	-	
577		19.5	161	-30	-	-	-	-	A
578	26/1450	16	132.5	-48.5	0	-	-	-	?
579		14	96	+22	-	1.2	-	-	
580		15.5	109	-13.5	-	-	12.7	-	
581		14	100	-7	-	-	-	9.0	
582		14	110	-23	-	-	-	-	
583		16.5	100	-11	-	-	-	-	
584		14.5	57	+6.5	-	-	-	-	
616		18.5	92	-9	-	-	-	-	
617		18.5	92	-9	-	-	-	-	
618		19	92	-8.5	0	-	-	-	
619		16.5	85	-6	-	1	-	-	
620		18	68	-2	-	-	15.7	-	
621		26/1636	15.5	106	-24	-	-	-	3.4

Telemetry Cycle	Interval	<u>Magnetic Field</u>			<u>Plasma</u>				Situa- tion
		B (gammas)	ϕ (degrees)	θ (degrees)	Nominal Flux Density ($10^7 \text{ cm}^{-2} \text{ sec}^{-1}$)				
					$\bar{\Phi}(80)$	$\bar{\Phi}(250)$	$\bar{\Phi}(800)$	$\bar{\Phi}(2300)$	
622	26/1639	19.5	138	-38	-	-	-	-	A
623		20	142	-42.5	-	-	-	-	
624		19	142	-47	-	-	-	-	
625		18.5	144	-45	-	-	-	-	
626		18.5	140	-44.5	0	-	-	-	
627		17.5	141	-41	-	.5	-	-	
656		15.5	143	-30	-	-	-	-	
657		16	160	-32	-	-	-	-	
658		16	143	-33	0	-	-	-	
659		15	163	-57	-	0	-	-	
660		16	130	-38	-	-	0	-	
661		18	143	-43	-	-	-	?	A
662	26/1815	15.5	81	+2	-	-	-	-	B
663		17	70	+7	-	-	-	-	
664		16.5	102	-15.5	-	-	-	-	
665		17.5	88	-9	-	-	-	-	
666		16	90	-11	0	-	-	-	
667		16	98	-13	-	.5	-	-	
946		15	-27	-43	0	-	-	-	
947		14	-31	-46	-	.7	-	-	
948		11.5	-31	-46	-	-	12.4	-	
949		9.5	-48	-39	-	-	-	?	
950		12	-27	-52.5	-	-	-	-	
951		12.5	233	-69	-	-	-	-	B

elemetry Cycle	Interval	Magnetic Field			Plasma				Situa- tion
		B	ϕ	θ	Nominal Flux Density				
		(gammas)	(degrees)	(degrees)	(10 ⁷ cm ⁻² sec ⁻¹)				
					$\Phi(80)$	$\Phi(250)$	$\Phi(800)$	$\Phi(2300)$	
952	27/0613	16	160	-46	-	-	-	-	
953		22	169	-37	-	-	-	-	
954		22	151	-40	0	-	-	-	
955		20.5	166	-37	-	0	-	-	
956		19.5	181	-22	-	-	0	-	
957		21.5	159	-40	-	-	-	.4	
958		22.5	161	-30	-	-	-	-	
959		22.5	167	-35	-	-	-	-	
960		23	170	-27	-	-	-	-	
961		21.5	161	-35	-	-	-	-	
962		24	171	-36	0	-	-	-	
963		23	169	-39	-	0	-	-	
964		17.5	178	-46	-	-	.5	-	
965	27/0645	13	169	-63	-	-	-	14.2	
966		10	77	-63	-	-	-	-	
967		8	45	-50	-	-	-	-	
968		11	8	-54	-	-	-	-	
969		9	9	-40.5	-	-	-	-	
970		8	38	-59	-	-	-	-	
994		11	68	-71	-	-	-	-	
995		9	18	-90	-	1.4	-	-	
996		9.5	50	-81	-	-	15.0	-	
997		11	108	-85	-	-	-	11.1	
998		8.5	46	-60	-	-	-	-	
999		11	140	-60	-	-	-	-	

Telemetry Cycle	Interval	<u>Magnetic Field</u>			<u>Plasma</u> Nominal Flux Density ($10^7 \text{ cm}^{-2} \text{ sec}^{-1}$)				Situa- tion
		B (gammas)	ϕ (degrees)	θ (degrees)	$\Phi(80)$	$\Phi(250)$	$\Phi(800)$	$\Phi(2300)$	
1000	27/0811	19	160	-35	-	-	-	-	A
1001		20	154	-43	-	-	-	-	
1002		21	163	-36	0	-	-	-	
1003		20.5	157	-40	-	0	-	-	
1004		21.5	163	-33	-	-	1	-	
1005		21	166	-34	-	-	-	.7	
1044		16.5	151	-45.5	-	-	0	-	
1045		16.5	153	-44.5	-	-	-	?	
1046		16	151	-44	-	-	-	-	
1047		16	146	-45	-	-	-	-	
1048		15.5	146	-46	-	-	-	-	
1049		15.5	140	-51	-	-	-	-	A
1050	27/1014	11	72	-51	0	-	-	-	B
1051		11	20	-36	-	.4	-	-	
1052		10	-10	-52	-	-	8	-	
1053		10.5	-2	-46	-	-	-	?	
1054		10	30	-47	-	-	-	-	
1055		11	20	-18	-	-	-	-	
1074		10	81	-60	0	-	-	-	
1075		13	126	-35.5	-	.4	-	-	
1076		11	137	-62.5	-	-	5.7	-	
1077		10.5	58	-48.5	-	-	-	4.7	
1078		9.5	69	-51	-	-	-	-	
1079		11.5	106	-16	-	-	-	-	B
1080	27/1128	12.5	134	-53	-	-	-	-	?






Telemetry Cycle	Interval	<u>Magnetic Field</u>			<u>Plasma</u>				Situa- tion	
		B (gammas)	ϕ (degrees)	θ (degrees)	Nominal Flux Density ($10^7 \text{ cm}^{-2} \text{ sec}^{-1}$)					
					$\Phi(80)$	$\Phi(250)$	$\Phi(800)$	$\Phi(2300)$		
1081	27/1131	14	146	-56	-	-	-	-	A	
1082		14	142	-54	0	-	-	-	A	
1083		14	110	-13	-	.5	-	-	?	
1084		14	140	-49	-	-	1.7	-	A	
1085		14	140	-51	-	-	-	3.6		
1086		14	149	-60	-	-	-	-		
1112		17	132	-46	-	-	-	-		
1113		17	132	-42	-	-	-	-		
1114		16.5	133	-45	0	-	-	-		
1115		15.5	133	-48	-	2.1	-	-		
1116		14.5	133	-49	-	-	3.2	-		A
1117		16.5	130	-67	-	-	-	2.7		?
1118	27/1302	4	137	-68.5	-	-	-	-	?	
1119		9.5	-4	?	-	-	-	-	B	
1120		11	-4	-28	-	-	-	-		
1121		12.5	7	-28	-	-	-	-		
1122		12.5	0	-38	0	-	-	-		
1123		11	4	-32.5	-	.4	-	-		
1124		11	-2.5	-31	-	-	7.7	-		
1125		11.5	-1	-32	-	-	-	?	B	

Table 3.

Average magnetic conditions during the time intervals of type A listed in Table 1. \overline{B} is the arithmetic average of the magnetic field strengths measured during each individual interval (in units of 10^{-5} gauss); $\overline{\phi}$ and $\overline{\theta}$ are similar averages for the two angles (solar ecliptic longitude and ecliptic latitude) which describe the direction of the vector \vec{B} .

Interval No.	\bar{B} (gammas)	$\bar{\phi}$ (degrees)	$\bar{\theta}$ (degrees)
1	31	155	-32
3	27	158	-36
5	22	164	-35
7	20	154	-36
9	17	143	-38
11	21	166	-36
13	18	155	-44
15	15	139	-48

Table 4.

Average magnetic and plasma conditions during the time intervals of type B listed in Table 1. \overline{B} , $\overline{\phi}$, and $\overline{\theta}$ have the same meaning as in table 3. $\overline{\Phi}(80)$, $\overline{\Phi}(250)$, $\overline{\Phi}(800)$ and $\overline{\Phi}(2300)$ are the average values of the nominal flux densities at the 80, 250, 800 and 2300 volt modulation levels respectively for each interval. The two sets of figures in the column under $\overline{\Phi}(80) / \overline{\Phi}(800)$ represent minimum and maximum values of this ratio.

Interval No.	Magnetic Field			Plasma			
	\overline{B} (gammas)	$\overline{\theta}$ (degrees)	$\overline{\alpha}$ (degrees)	$\overline{\Phi}$ (800) ($10^7 \text{ cm}^{-2} \text{ sec}^{-1}$)	$\overline{\Phi}$ (80) $\overline{\Phi}$ (800) (percent)	$\overline{\Phi}$ (250) $\overline{\Phi}$ (800) (percent)	$\overline{\Phi}$ (2300) $\overline{\Phi}$ (800) (percent)
2	13	22	-35	24	1.6	12	105
4	15	-24	-44	25	.9-1.6	10	99
6	11	50	-37	17	1.2-2.3	14	105
8	16	100	-9.2	13	0-2.7	7.4	86
10a	16	88	-11	9.8	0-3.7	5.3	92
10b	14	68	-31	10	0-3.5	14	109
10c	12	77	-34	15	1.9-2.8	15	109
10d	13	39	-34	12	0-2.9	7.4	95
12	9.7	39	-60	16	0-2.2	9.4	81
14	10	38	-37	8.0	0-4.4	6.7	102
16	11	1	-42	9.2	0-3.9	6.0	91

Table 5.

Ratios of the average values of $\bar{\Phi}(80)$, $\bar{\Phi}(250)$ and $\bar{\Phi}(2300)$ to the average value of $\bar{\Phi}(800)$ for all time intervals of type B, for those time intervals in which $\bar{\Phi}(250) / \bar{\Phi}(800) \geq .10$ and for those time intervals in which $\bar{\Phi}(250) / \bar{\Phi}(800) < .10$ (corrected values for $\bar{\Phi}(2300) / \bar{\Phi}(800)$ appear in parentheses).

	$\bar{\Phi}$ (80) $\bar{\Phi}$ (800) (percent)	$\bar{\Phi}$ (250) $\bar{\Phi}$ (800) (percent)	$\bar{\Phi}$ (2300) $\bar{\Phi}$ (800) (percent)
Average for all Type B intervals	1.5 - 2.1 *	9.3	97
Average for intervals 2,4,6, 10b, 10c	1 - 2.5	13	104 (113)
Average for intervals 8, 10a, 10d, 12, 14, 16	0 - 3.3	6.9	92 (100)

* Only time intervals 2, 4, 6, 10c are included here.

Table 6.

Average properties of the plasma and the magnetic field observed during time intervals of the first group ($\overline{\Phi}(250) / \overline{\Phi}(800) \geq .10$) and during time intervals of the second group ($\overline{\Phi}(250) / \overline{\Phi}(800) < .10$). The values labelled "minimum" and "maximum" are respectively the smallest and largest of each group of average values (see Table 4). The proton density n is the ratio of the average flux density $\overline{\Phi}$ to the bulk velocity V_0 . All the results given for the plasma were computed for $\alpha = 0^\circ$ and, therefore, represent nominal values of the corresponding quantities.

	Intervals No. 2, 4, 6, 10b, 10c (\bar{I} (250) / \bar{I} (800) $\geq .10$)	Intervals No. 8, 10a, 10d, 12, 14, 16 (\bar{I} (250) / \bar{I} (800) $< .10$)
Average Proton Flux Density, \bar{I} ($10^7 \text{ cm}^{-2} \text{ sec}^{-1}$)	19 (minimum: 10) (maximum: 25)	11 (minimum: 8) (maximum: 16)
Velocity of Bulk Motion, V_o (km sec^{-1})	300 ± 25	300 ± 25
Proton Kinetic Energy, $mV_o^2/2$ (ev)	400 ± 60	400 ± 60
Proton Density, n (cm^{-3})	7 (minimum: 3) (maximum: 8)	4 (minimum: 3) (maximum: 5)
Proton "Temperature", T ($10^5 \text{ }^\circ\text{K}$)	6 (between 4 and 10)	≤ 3
Magnetic Field, B (gammas)	13 (minimum: 11) (maximum: 15)	13 (minimum: 10) (maximum: 16)
Energy Density of Bulk Motion, $nmV_o^2/2$ (ev cm^{-3})	2,800 (minimum: 1,500) (maximum: 3,800)	1,600 (minimum: 1,200) (maximum: 2,600)
Energy Density of "Thermal" Motion, $3nkT/2$ (ev cm^{-3})	(between 200 and 700)	200
Magnetic Energy Density, $B^2/2\mu_o$ (ev cm^{-3})	400 (minimum: 300) (maximum: 600)	400 (minimum: 200) (maximum: 700)

FIGURE CAPTIONS

- Fig. 1. Schematic diagram of the plasma probe and block diagram of the electronic system.
- Fig. 2. Angular response curve of the probe for a parallel beam of particles. The abscissa is the angle δ between the normal to the cup and the direction of the incident beam. The ordinate is the effective area of collection, normalized to unity for perpendicular incidence. The dotted curve is the result of a computation based on the geometry of the cup; the solid curve is the result of a direct measurement made by means of a well collimated electron beam.
- Fig. 3. Explorer 10 (from the paper by Heppner, Ness, Searce and Skillman, 1963).
- Fig. 4. Showing the spin axis of the satellite, the normal to the cup n , the plasma velocity vector \vec{V}_0 , and illustrating the angles α , θ , δ .
- Fig. 5. Computed current signal for a parallel beam of singly charged ions whose energy (in ev) is 1.2 times the modulating voltage. The velocity vector lies in the equatorial plane of the satellite ($\alpha = 0^\circ$). The abscissa is the angle of rotation θ (see Fig. 4) and the ordinate is the magnitude of the current relative to that corresponding to a fully modulated beam incident perpendicularly upon the probe.
- Fig. 6. Response curves of the probe for fully modulated parallel beams of ions forming different angles α with the equatorial plane of the satellite. The ordinate is the effective area of collection A normalized to unity for perpendicular incidence ($\delta = 0^\circ$).
- Fig. 7. Same as Fig. 6, with the effective area of collection normalized to unity at $\theta = 0^\circ$.
- Fig. 8. Distortion due to the non-linearity of the amplifier and the finite time delay of the electronic circuits. The dashed curves correspond to the computed response curves for $\alpha = 0^\circ$, $\alpha = 20^\circ$, $\alpha = 40^\circ$, $\alpha = 60^\circ$ (see Fig. 7).
- Fig. 9. Representation of the Explorer 10 trajectory in a cartesian coordinate system with the origin at the center of the earth, the x-axis toward the sun, the z-axis toward the north ecliptic pole, and, therefore, the x-y plane coincident with the plane of the ecliptic. The distances marked on the coordinate axes are measured in earth radii (R_e). The motion of the earth is in the direction of the negative y-axis.

- Fig. 10 . Projections of the trajectory of Explorer 10 on the x-y plane (the plane of the ecliptic), on the x-z plane and on the y-z plane (see Fig. 9). The line marked "Equator" represents the intersection of the y-z plane with the equatorial plane of the earth. Heavy lines by the curves represent sections of the trajectory where substantial plasma fluxes were observed. "SC" represents the position of Explorer 10 at the time of the sudden commencement. Dots represent positions of the satellite at 8-hr. intervals (25/20 means March 25, 20^h 00^m U.T., etc.).
- Fig. 11. Polar frame of reference used to specify directions. The angle θ is the latitude measured from the plane of the ecliptic, positive toward the north. The angle ϕ is the longitude, measured from the solar direction, positive toward the east.
- Fig. 12. Mercator projection showing the following: the direction A of the spin axis; the plane n traced by the normal to the probe during the rotation of the satellite; the plane p defined by the spin axis and the solar direction; the directions (shaded oval areas) for which the probe was insensitive; the "window" showing directions of the plasma wind consistent with the measurements made beyond 21 R_e .
- Fig. 13. Explorer 10 telemetry sequence.
- Fig. 14. Two samples of the telemetry records obtained during the third period at the 80, 250, 800 and 2300 volt modulation levels. The figure under each modulation voltage indicates the nominal flux corresponding to the peak of the current signal. Vertical lines represent times when the normal to the probe was closest to the direction of the sun; thus the distance between two consecutive vertical lines represents one rotation period. Notice that the signal at the 80 volt level is below the noise level in (a) and slightly above the noise level in (b).
- Fig. 15. Sample of the telemetry records obtained during the fourth period. Notice the "horned" shape of the signal at the 800 volt modulation level, indicating the presence of a substantial number of protons with nominal energies somewhat greater than 800 ev.
- Fig. 16. Plasma and magnetic field measurements during the third and fourth periods of the flight. The magnetic field data were provided to us by Dr. J.P. Heppner prior to their publication (see HNSS). Question marks in the plasma data indicate missing measurements and the short horizontal bars in many of the 2300 volt measurements indicate a shift of the zero level in the amplifier output (see section IV-B). The different intervals listed in Table 1 are indicated by the numbers above the plasma data.

- Fig. 17. Distribution of flux densities observed at the 800 and 2300 volt levels during the third period.
- Fig. 18. Directions of the magnetic field observed immediately before each of the plasma readings at the 800 volt and 2300 volt levels during the third period. Open circles refer to "strong" plasma signals; solid dots refer to "weak" plasma signals.
- Fig. 19. Average directions of the magnetic field observed during the various time intervals of the third period. Solid dots refer to situations of type A; open circles refer to situations of type B. The number by each point specifies the time interval to which the point refers, as listed in Table 1. The two bars crossing at point No.2 represent the spread in the directions of \vec{B} observed during this time interval. The line segment E_1E_2 represents the angular displacement of the earth-satellite line during the time of observation.
- Fig. 20. Plasma measurements at the 800 volt level on a condensed time scale.
- Fig. 21. "Nominal energy" distribution of plasma protons. The experimental points are obtained from Table 5 ("corrected" values for $\frac{I(2300)}{I(800)}$ are used). The curves represent theoretical spectra computed under the assumption of a one-dimensional Maxwellian distribution for the "thermal" velocities with the following parameters:
 (1) $E_0 = 420$ ev, $T = 6.2 \times 10^5$ °K
 (2) $E_0 = 420$ ev, $T = 2.6 \times 10^5$ °K.
- Fig. 22. Comparison between observed current signals and theoretical curves which represent the response of the probe and electronic circuits for a parallel beam of particles with $\alpha = 0^\circ$ and $\alpha = 40^\circ$.
- Fig. 23. (a) Schematic representation of the geomagnetic cavity predicted in the case of a moving, perfectly cold interplanetary plasma with no magnetic field.
 (b) Tentative model for the cavity and the stationary shock front produced by the interaction of the actual plasma wind with the geomagnetic field.
- Fig. 24. Pictorial summary of combined results of Pioneer 1, Pioneer 5, and Explorer 12 concerning the boundary of the geomagnetic cavity and the location of the bow wave.
- Fig. 25. Intersection of the geomagnetic cavity with the plane of the trajectory of Explorer 10. The cavity is assumed to have axial symmetry around the direction of the "distant" wind (which is at 6° to the solar direction in the plane of the ecliptic), and to consist of a spherical cap joining to a conical tail with a half-angle at the vertex of 20° .

Fig. 26. Showing the directions of the "local" wind (L_1 , L_2) at the time when plasma was first detected and at the end of the observing period. Shown also are the directions of the earth-satellite line (E_1 , E_2) at the same times, and the direction of the distant wind (D).

Fig. 27. Directions of the magnetic field observed in the vicinity of the transition occurring during telemetry cycles No. 1044 to 1055 (see Table 2). Points labelled by consecutive numbers indicate successive measurements, made at intervals of $2^m 28^s$. All points corresponding to measurements made before the transition (1 to 6) fall within the small area enclosed by the dotted line. The point E indicates the direction from the earth to the satellite. The solid curve represents the plane tangent to the geomagnetic boundary at the moment of the transition, according to the schematic model of the geomagnetic cavity described in section VI-C. The point labelled "perpendicular" is the direction perpendicular to the tangent plane. There is no evidence from these data that during the transition the direction of the magnetic field came near to the tangent plane.

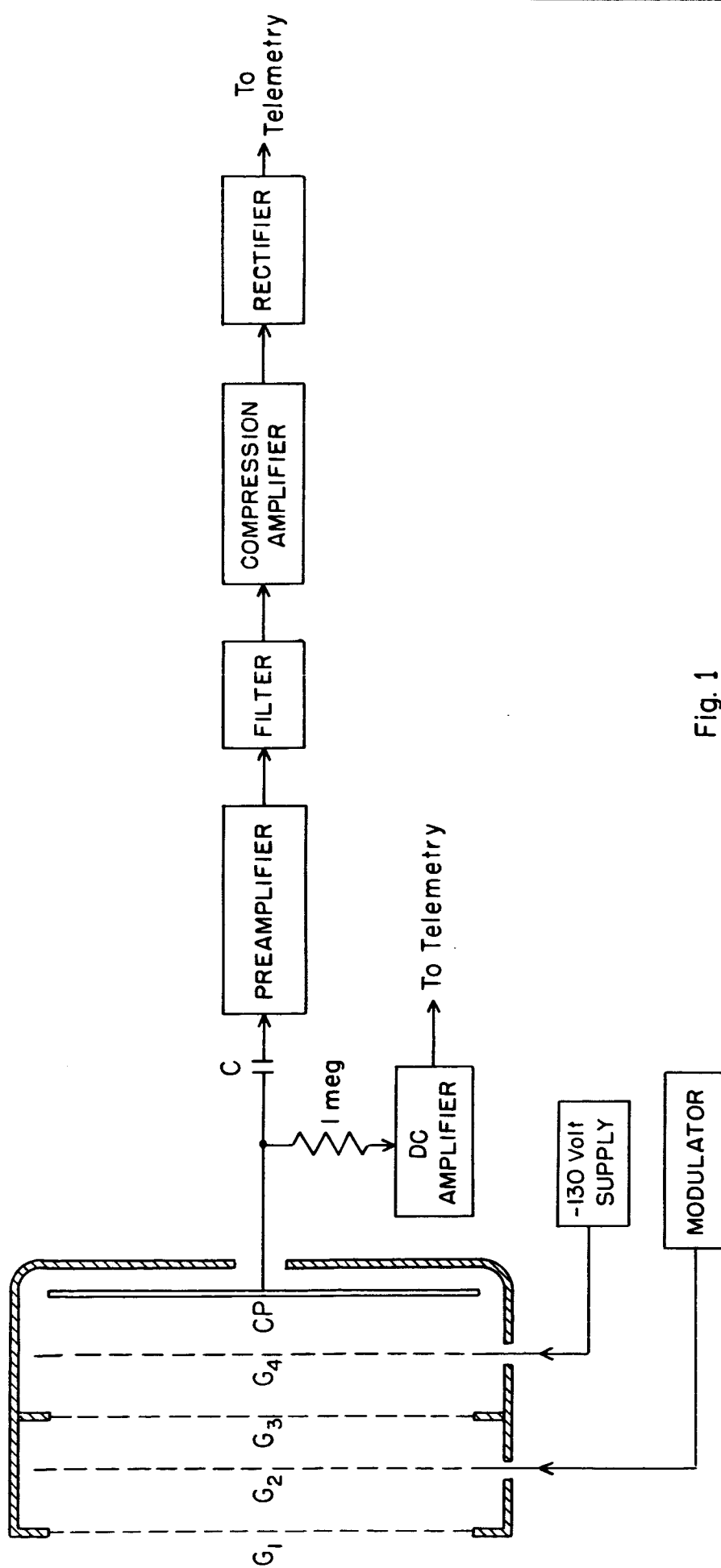


Fig. 1

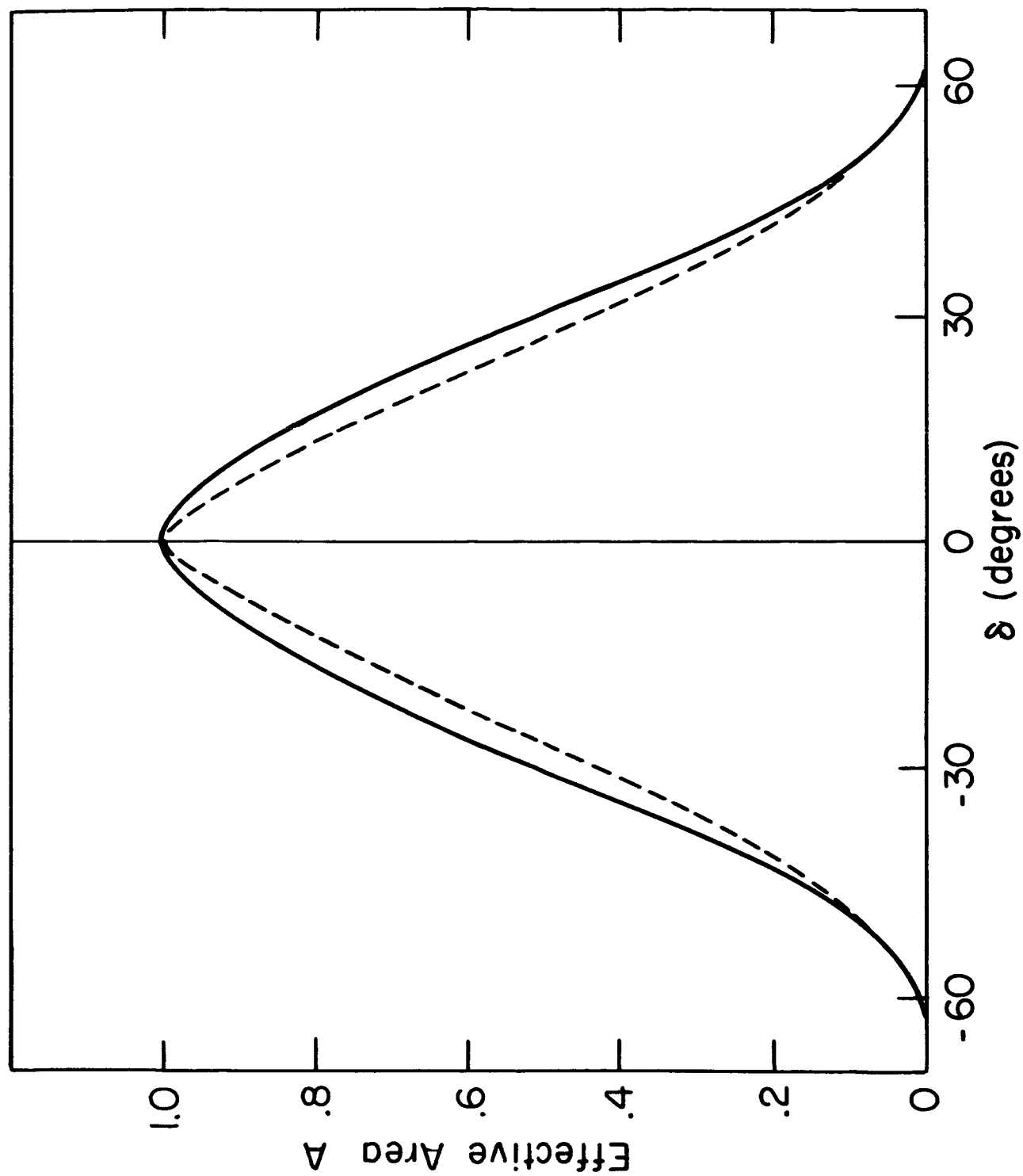


Fig. 2

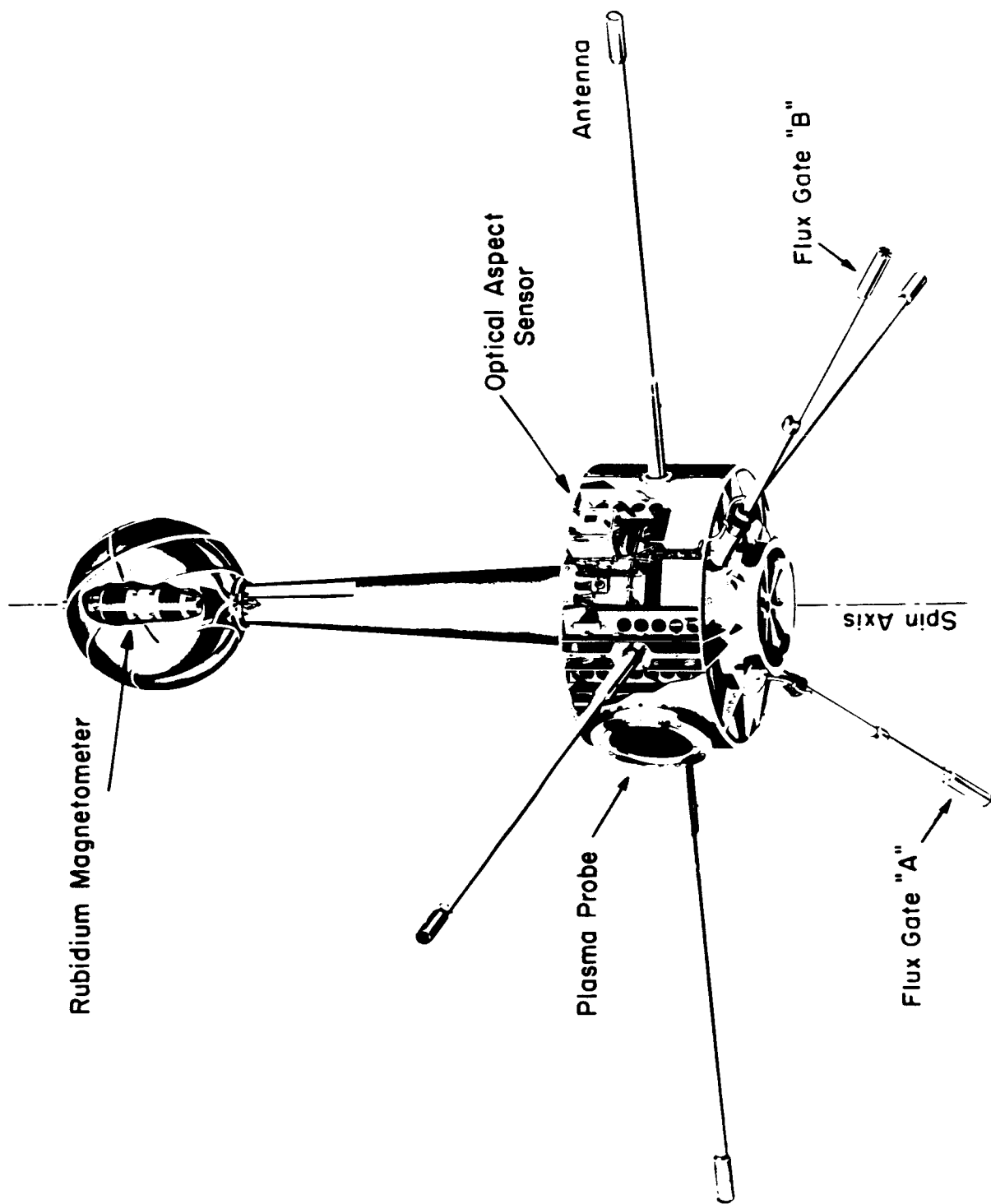


Fig. 3

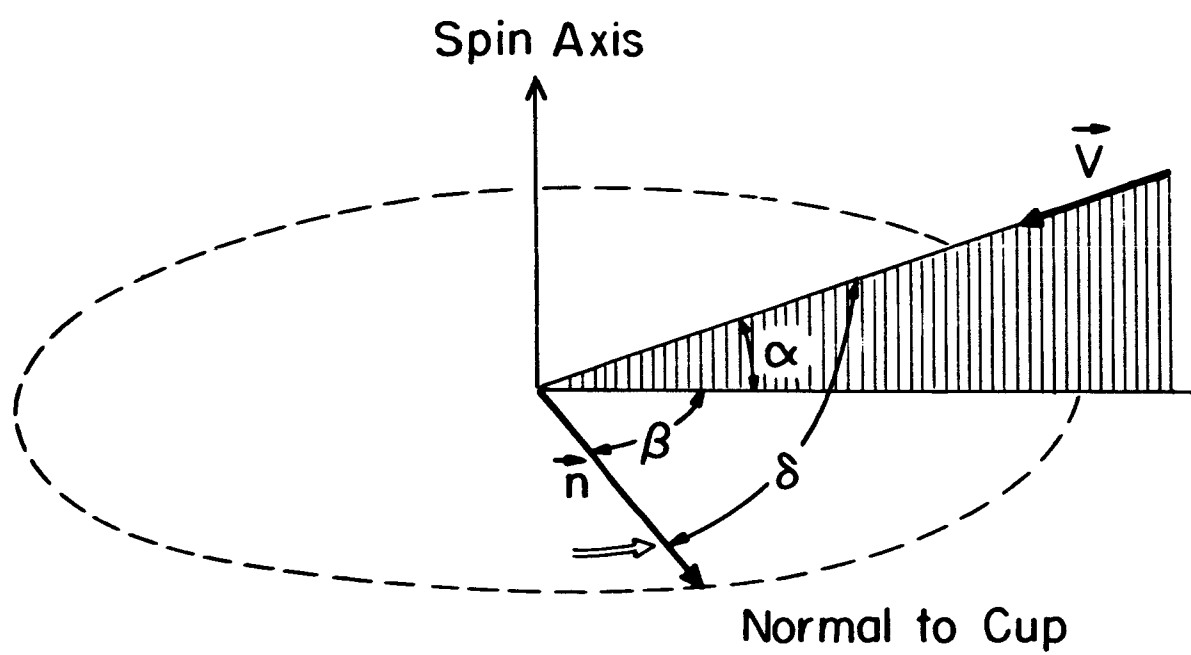


Fig. 4

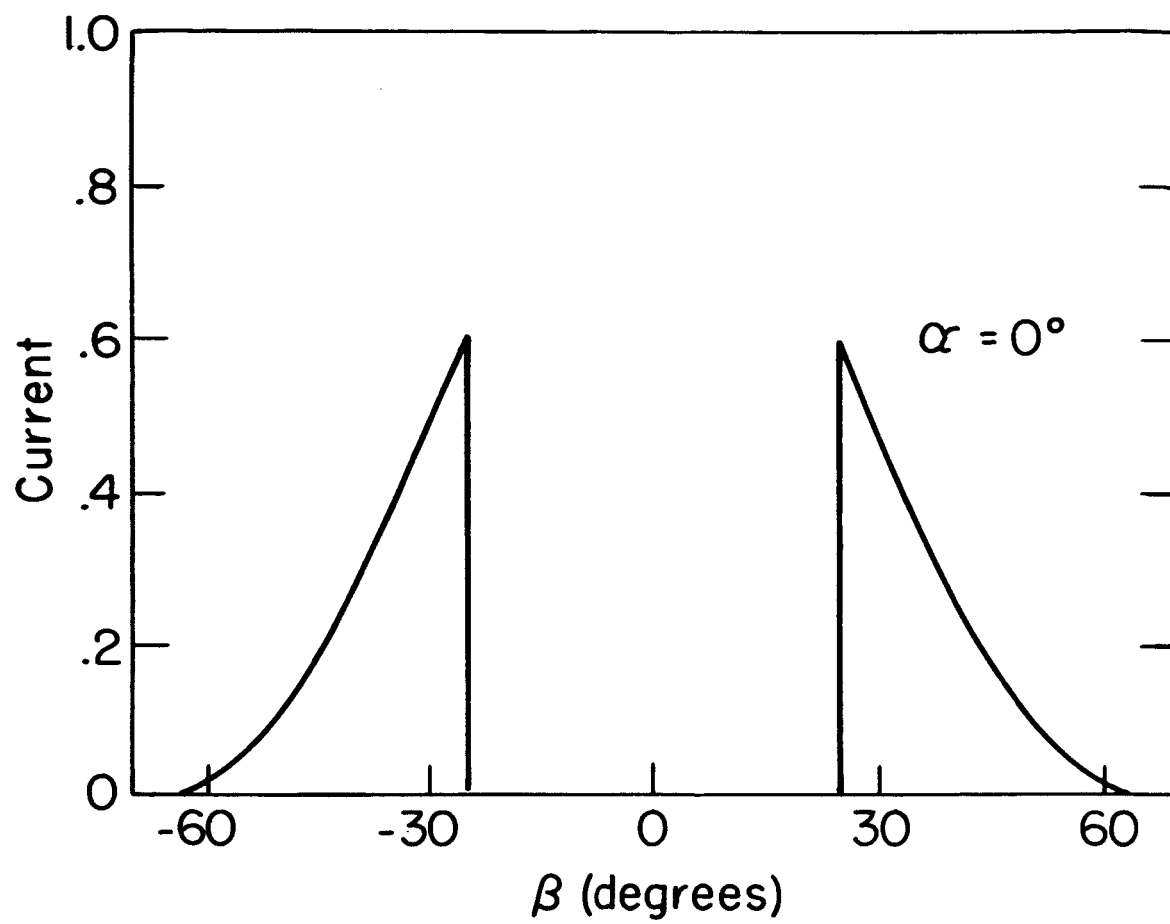


Fig. 5

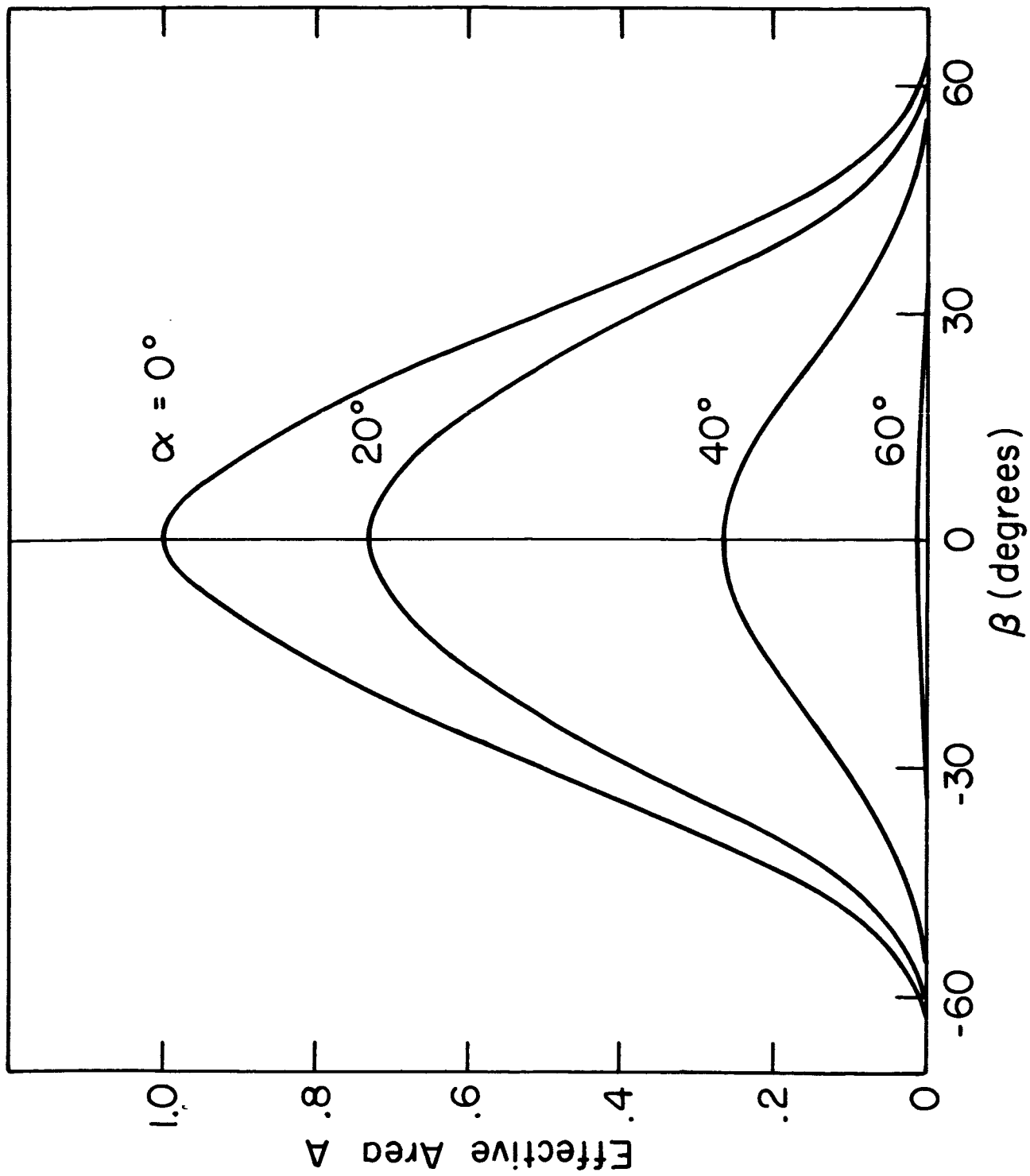


Fig.6

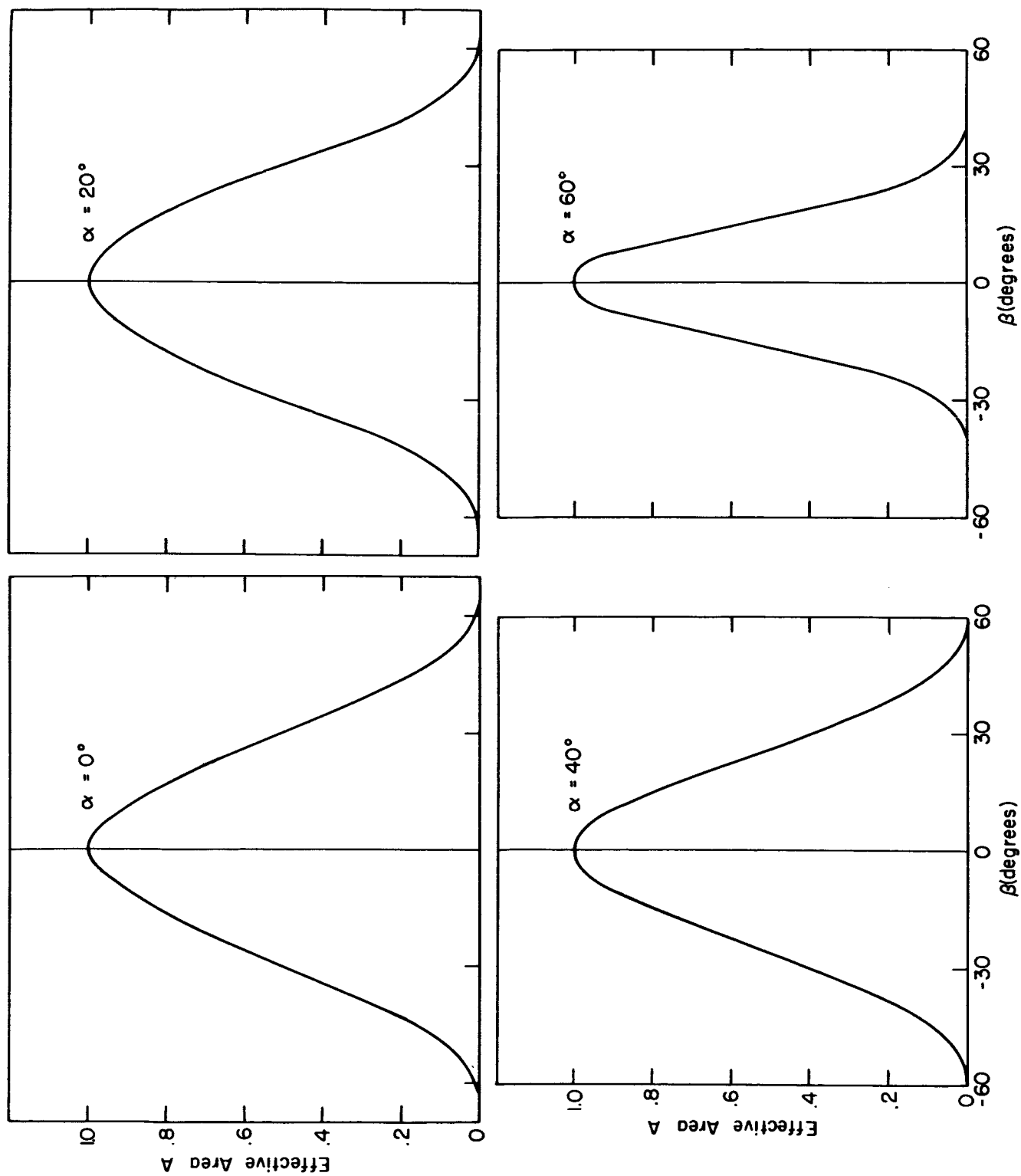


Fig. 7

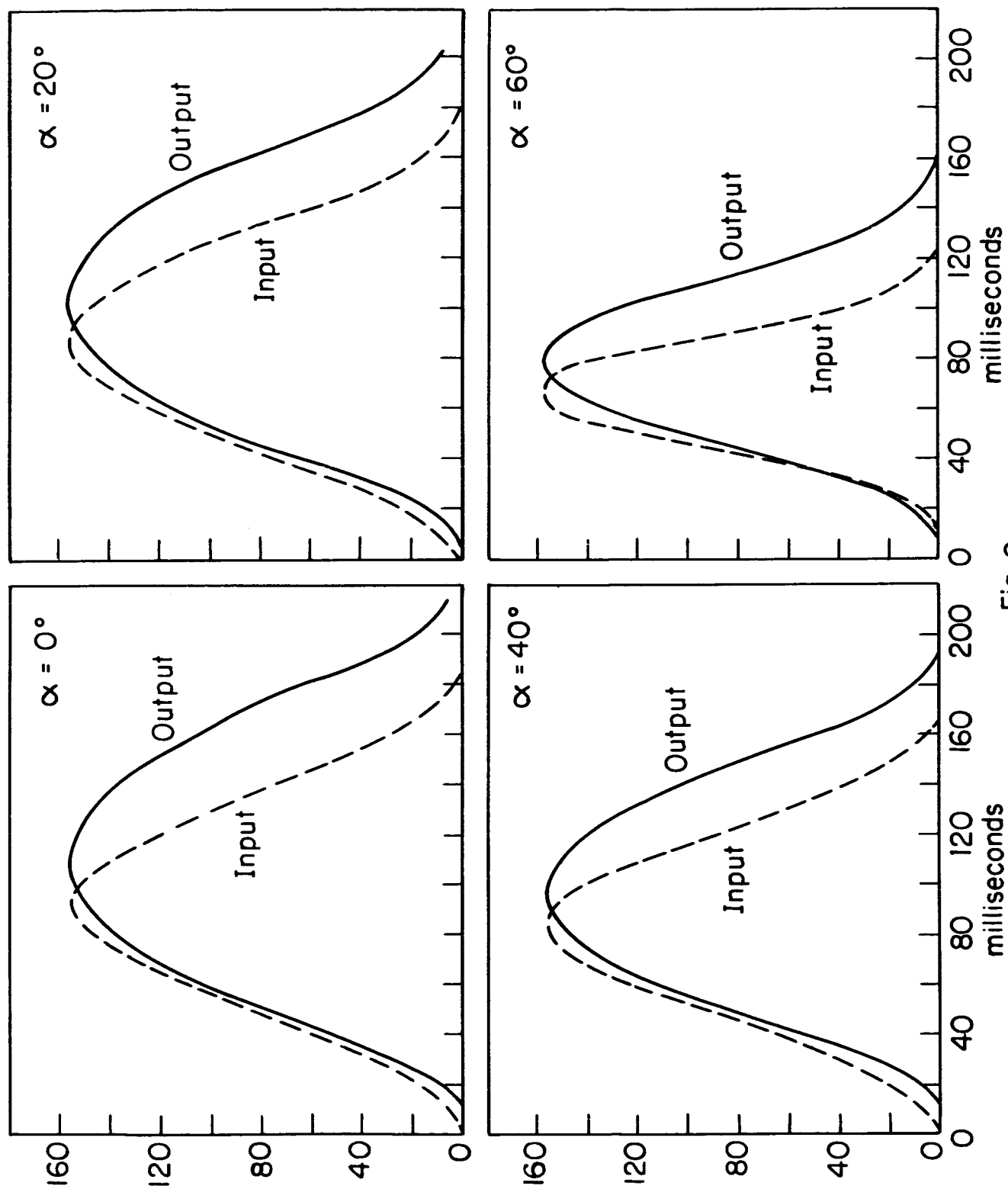


Fig. 8

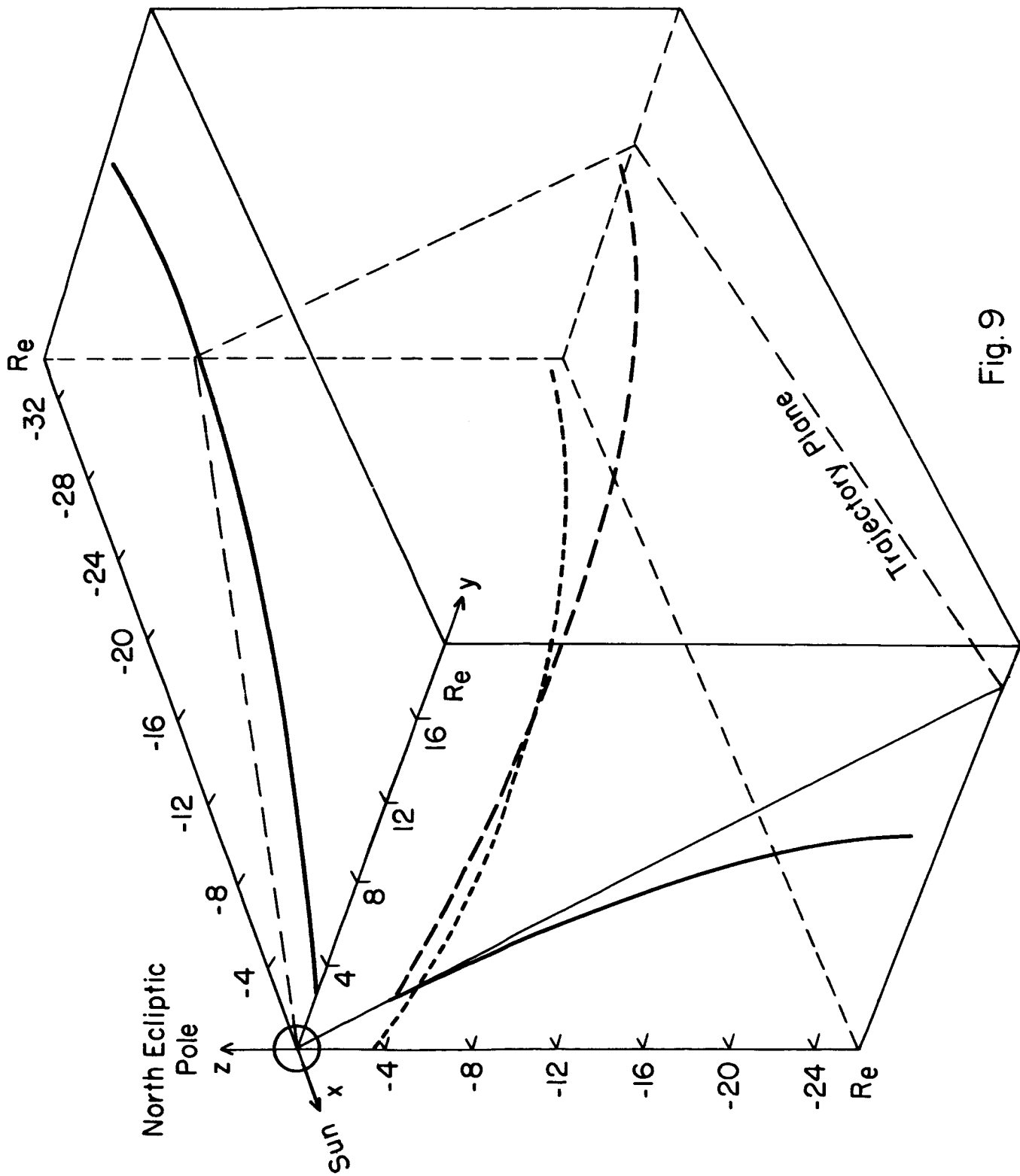


Fig. 9

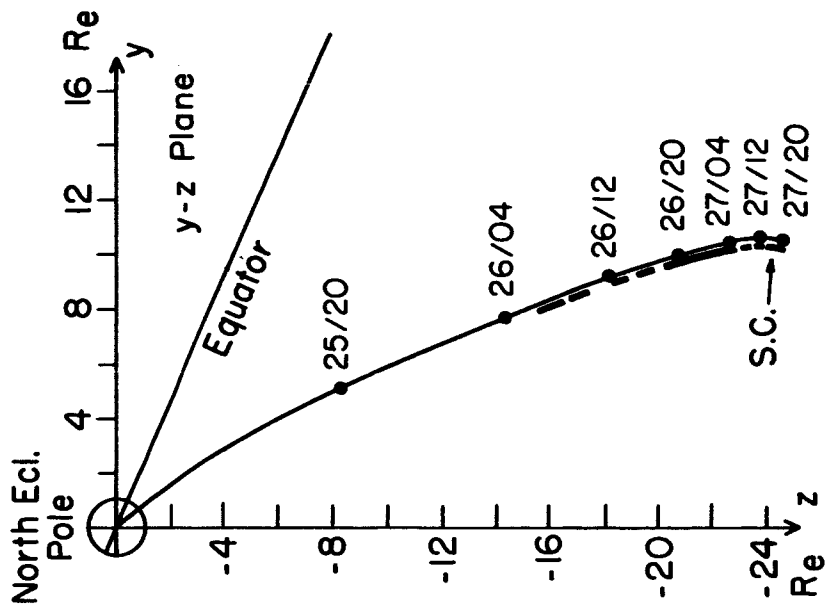
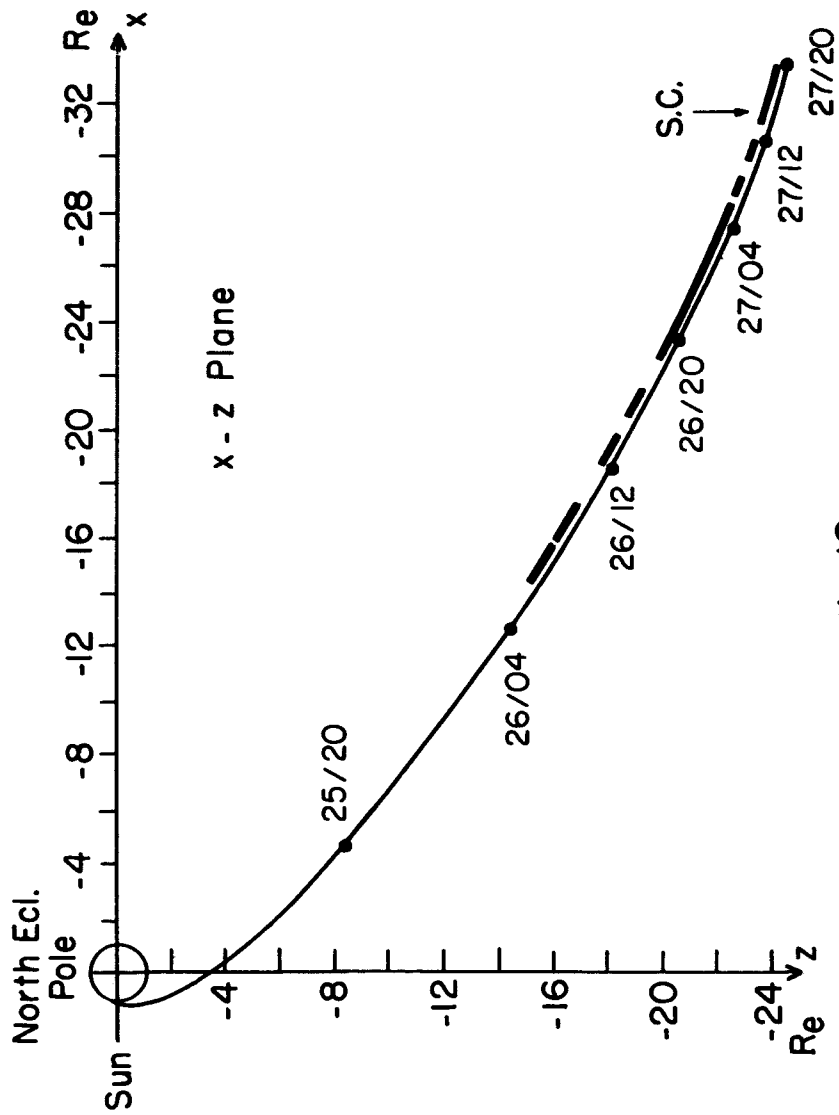
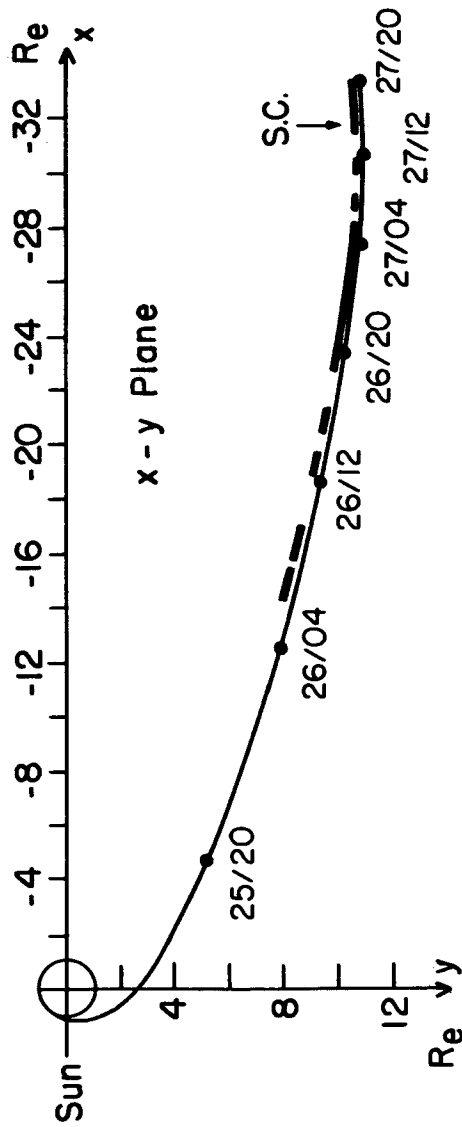


Fig. 10

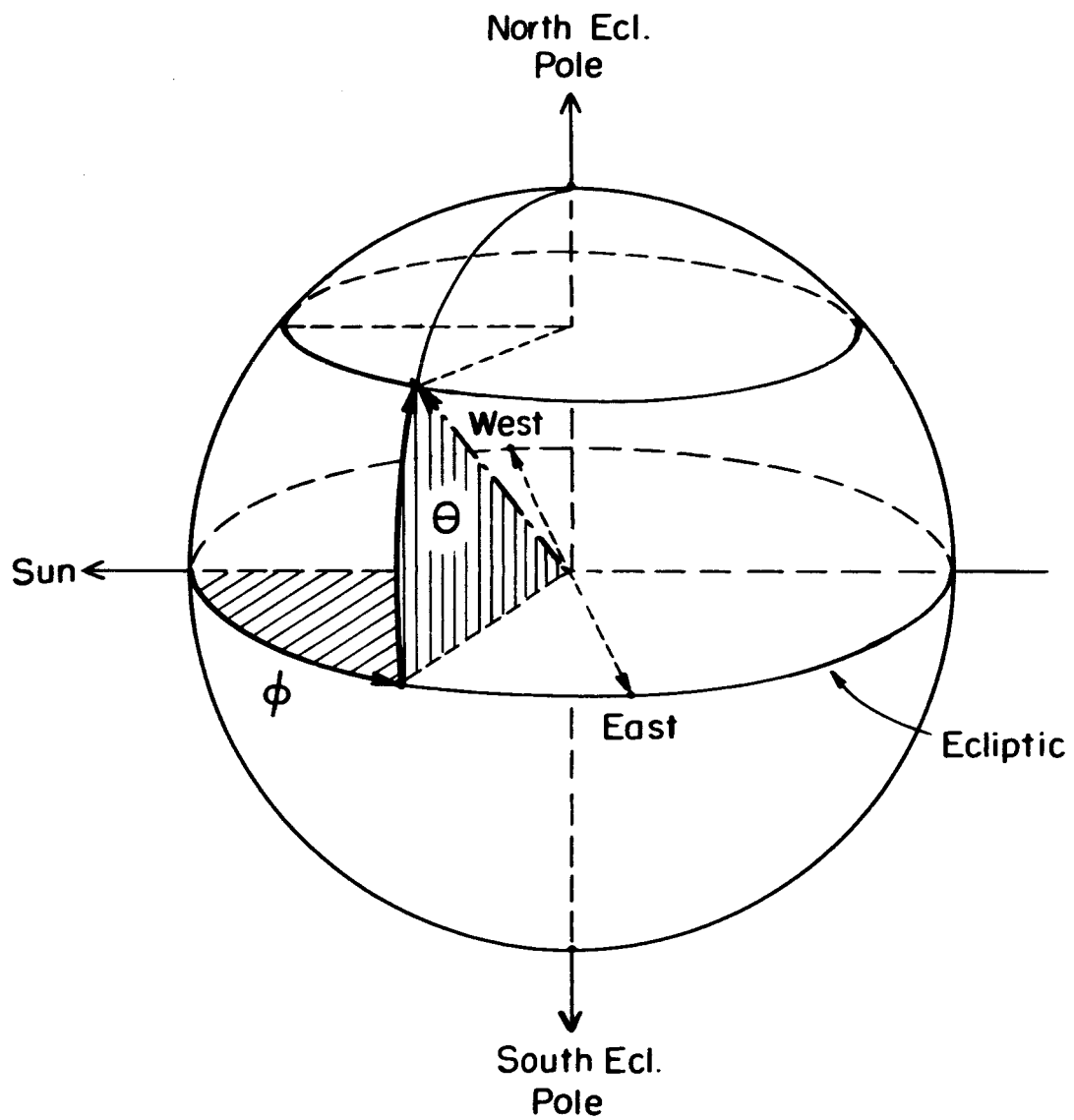


Fig. II

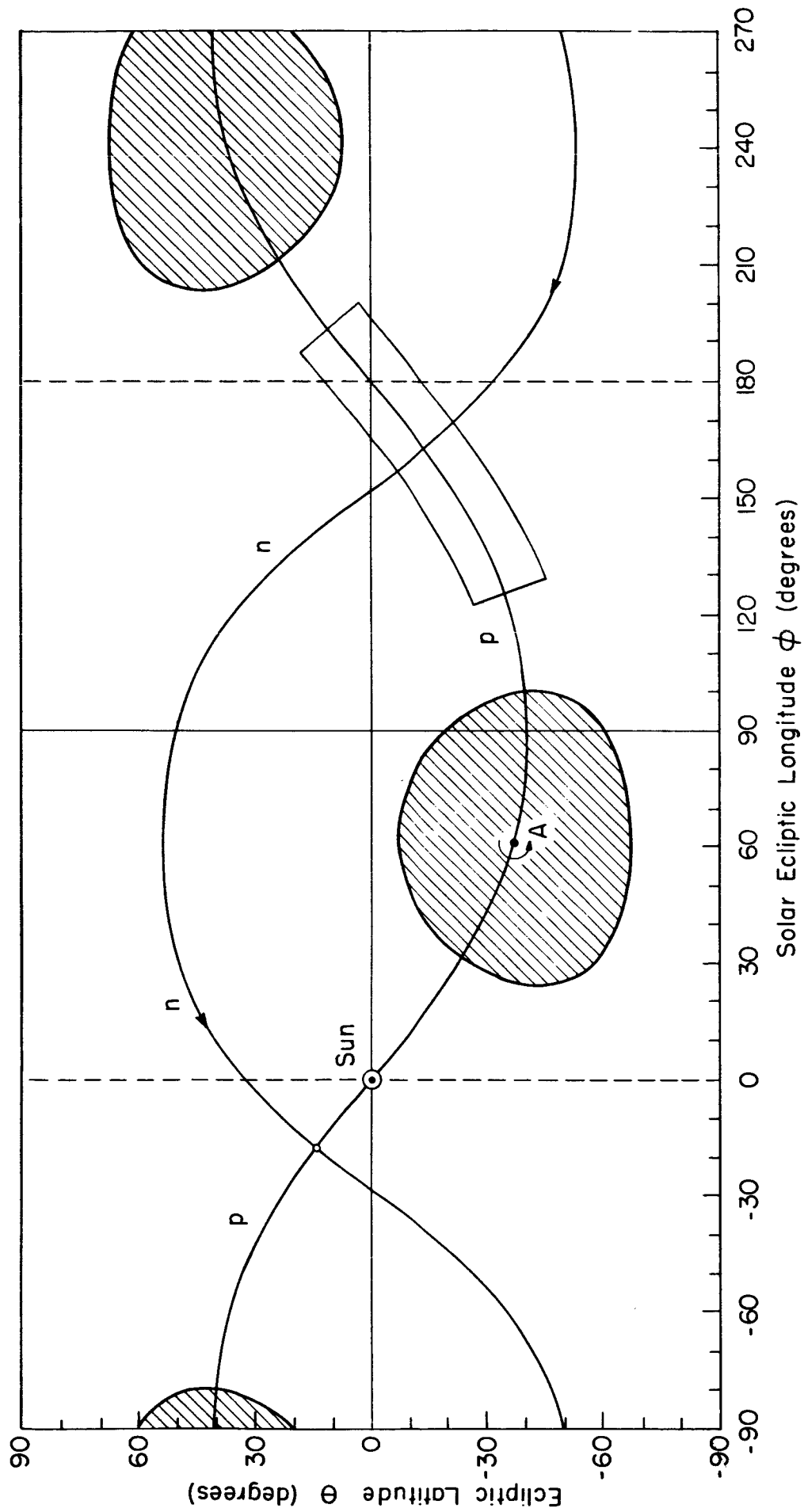


Fig. 12

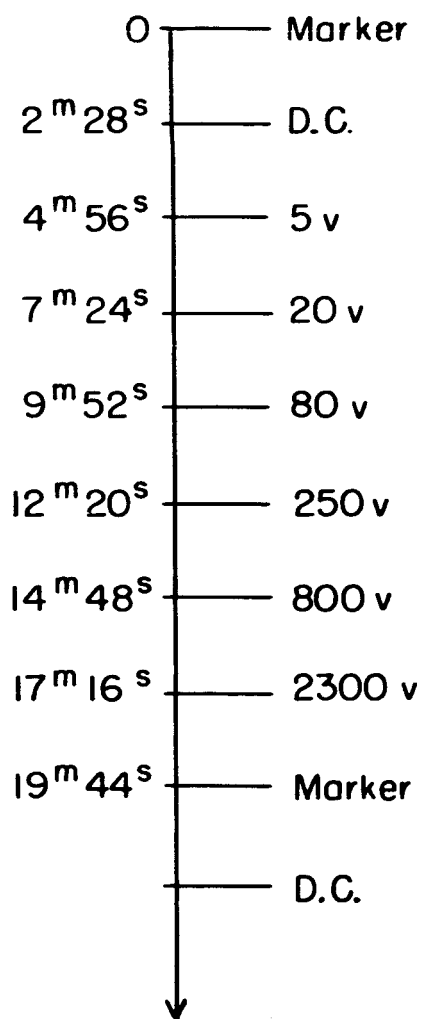
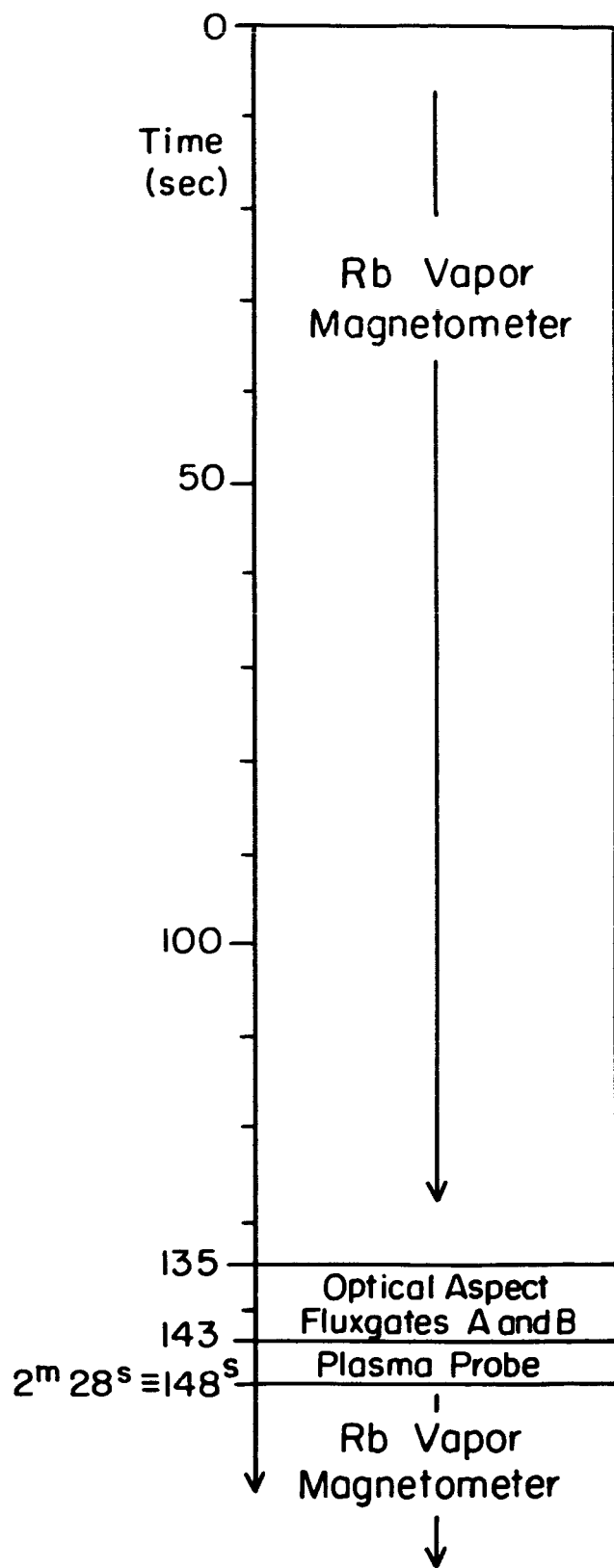


Fig. 13

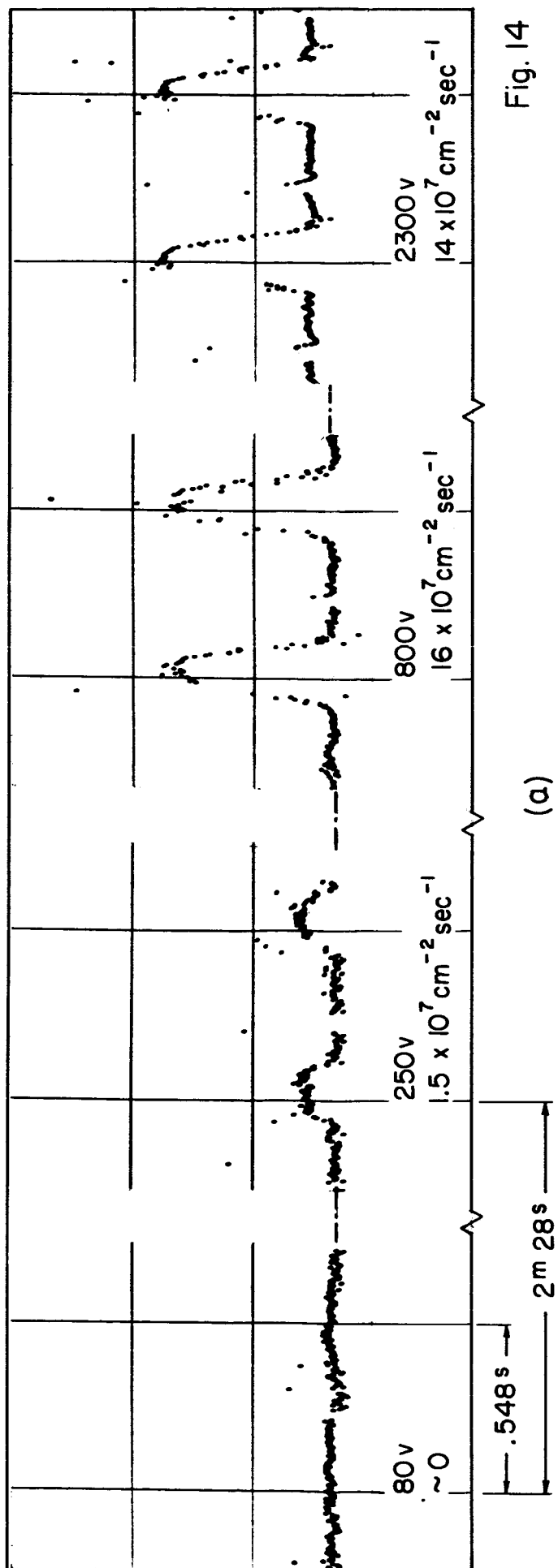


Fig. 14

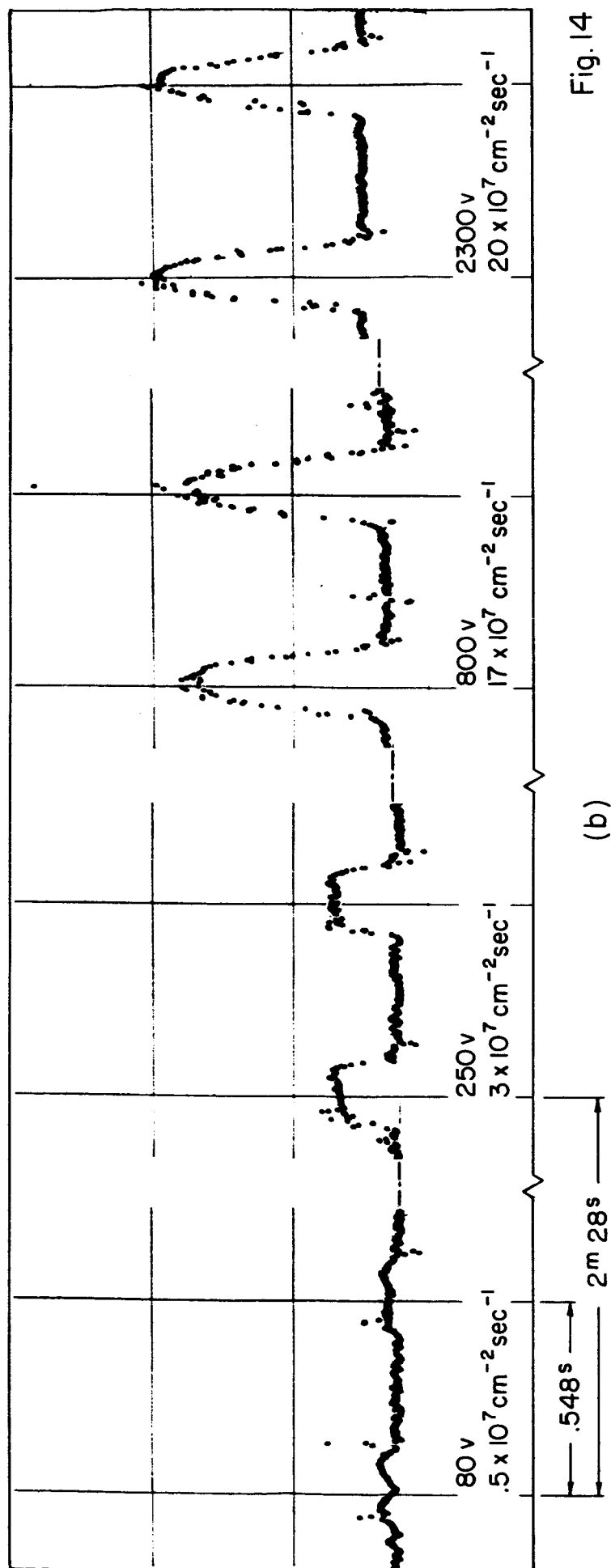


Fig. 14

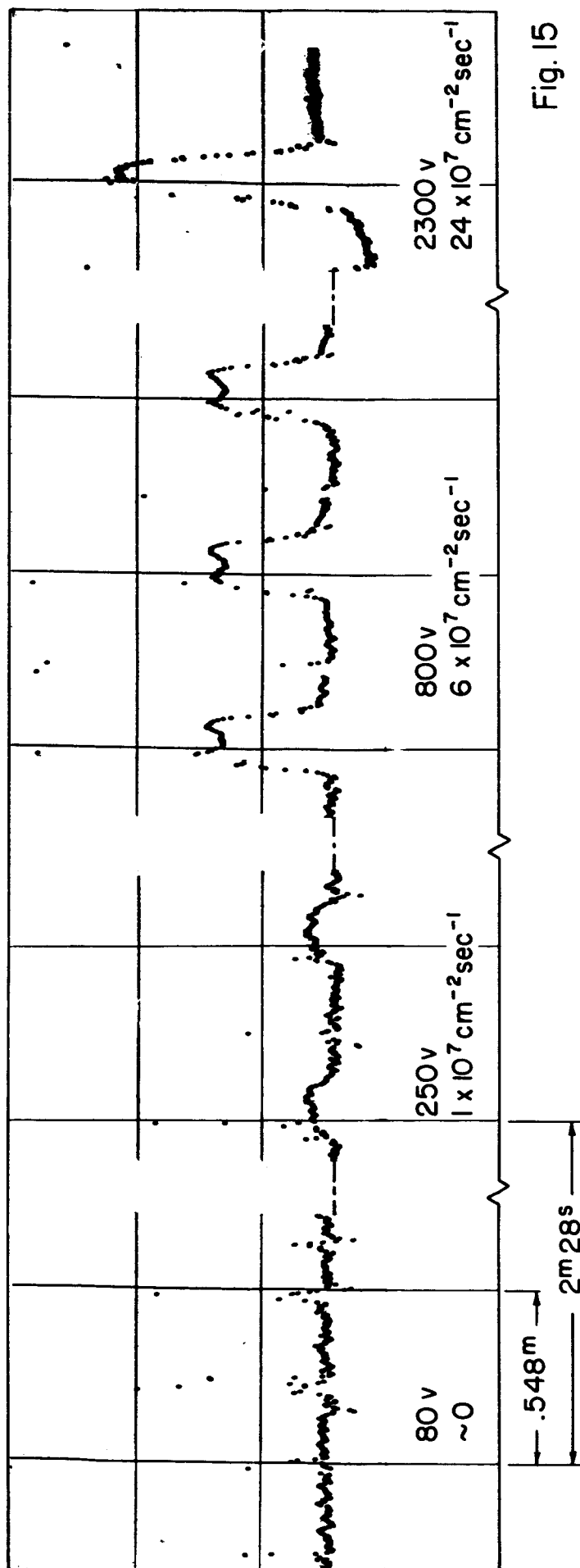
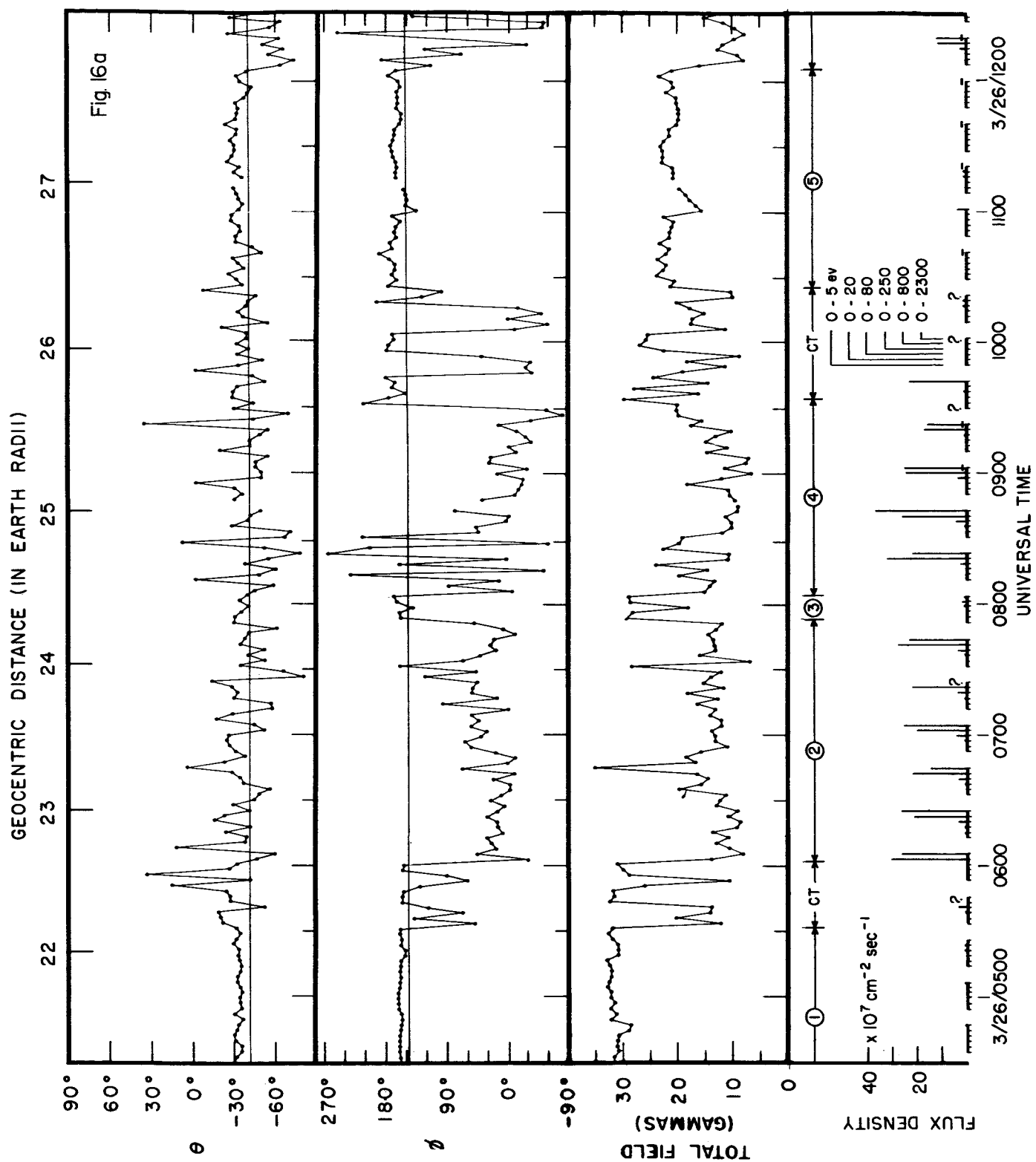
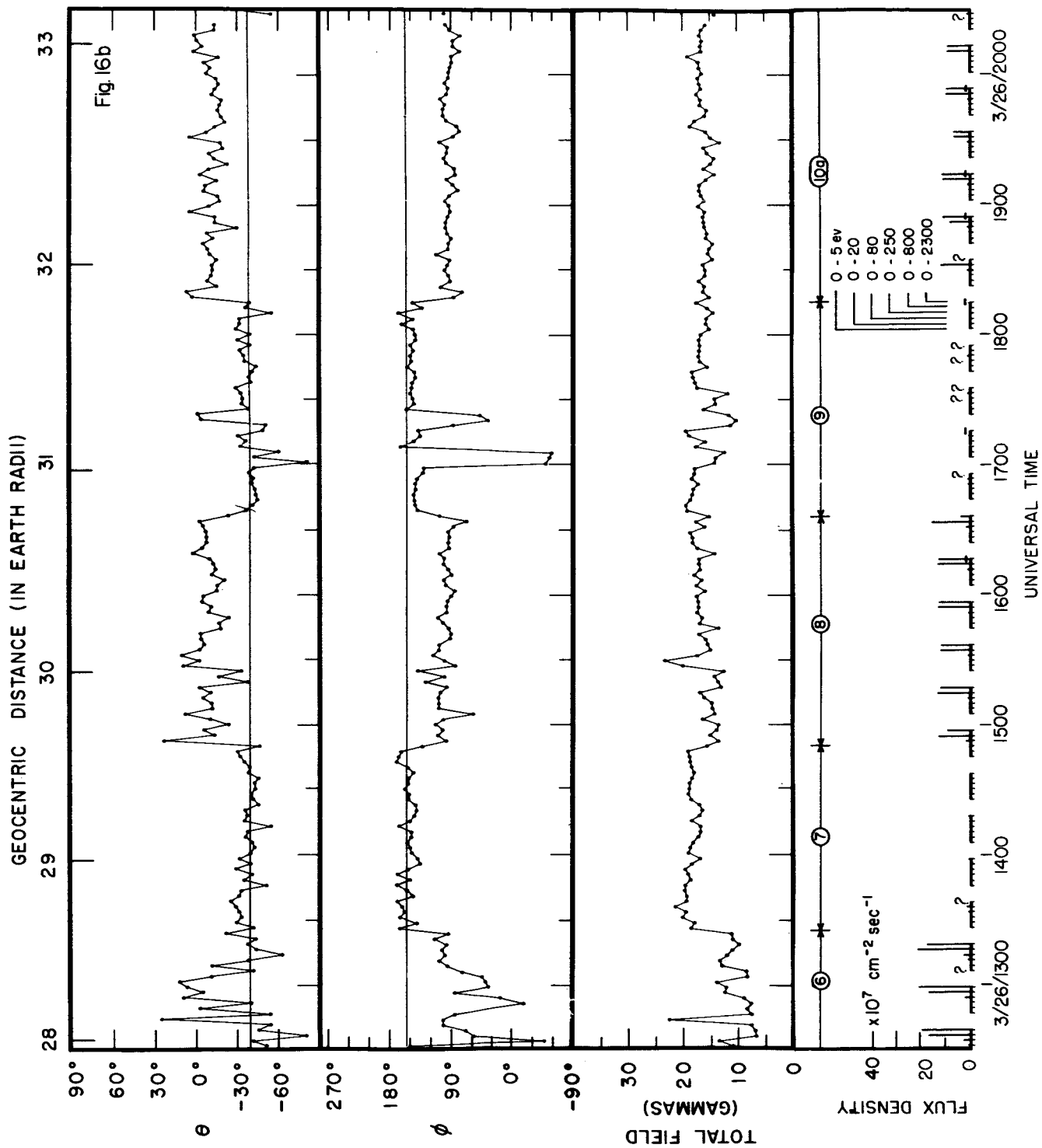
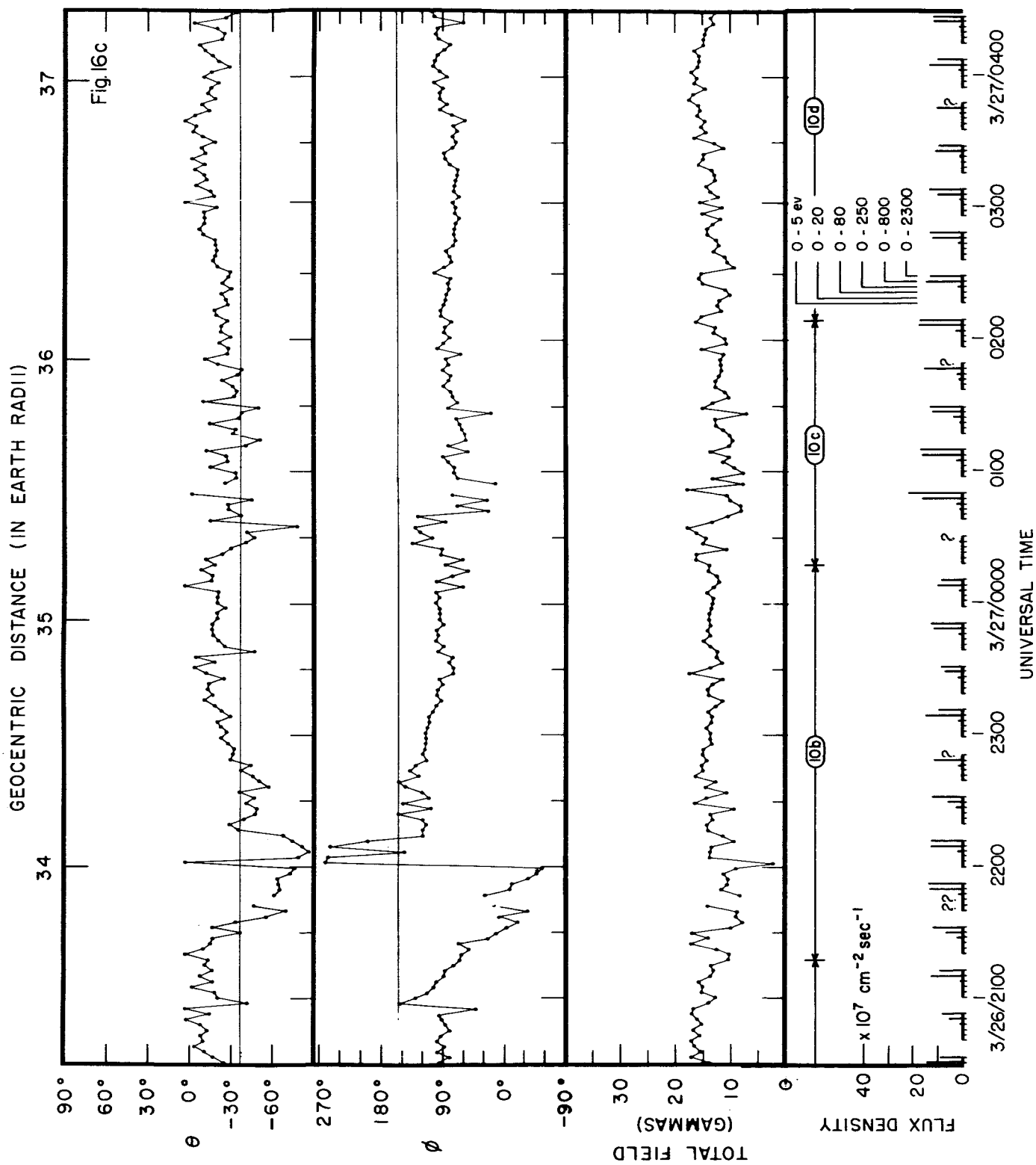


Fig. 15







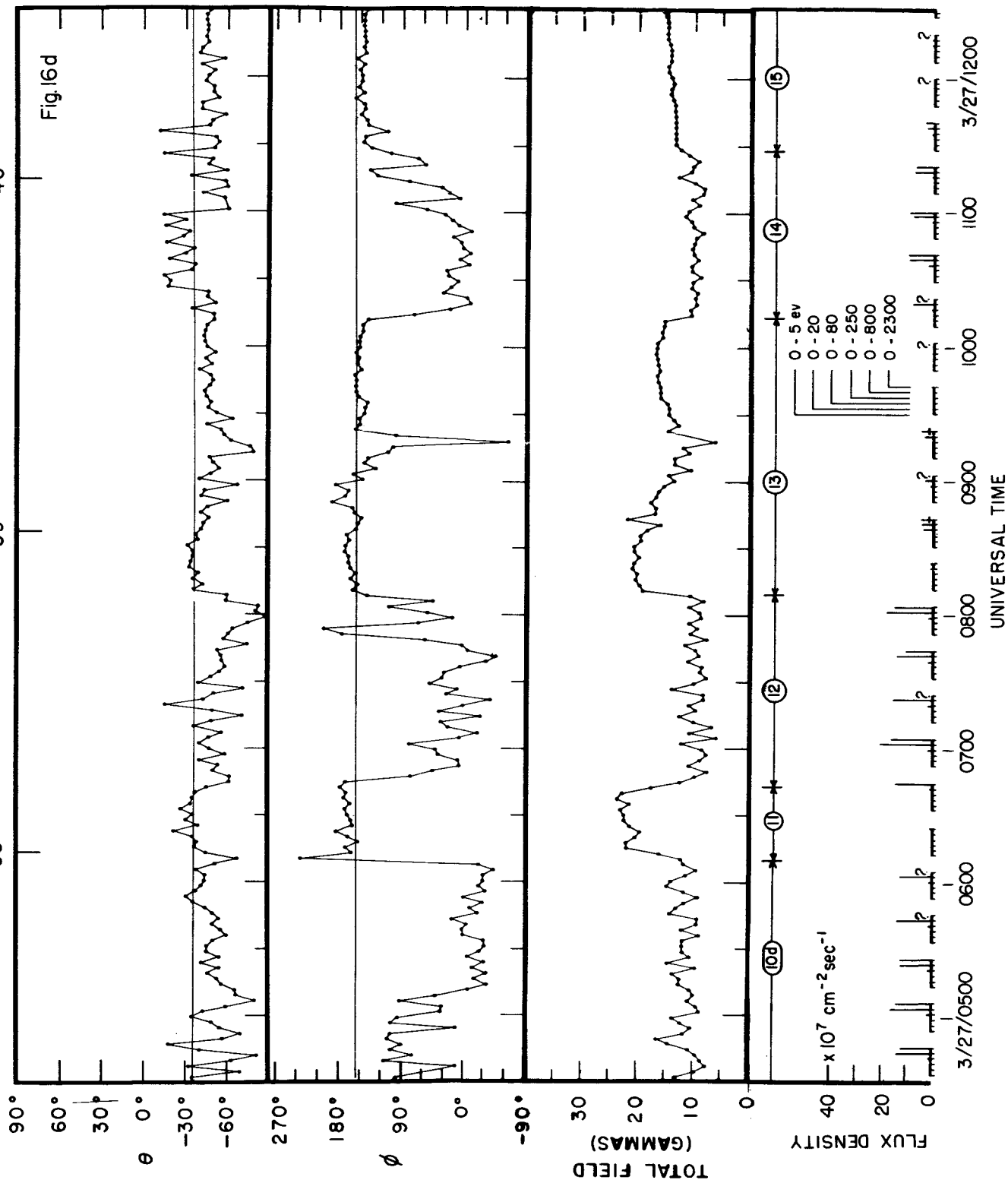
GEOCENTRIC DISTANCE (IN EARTH RADII)

38

39

40

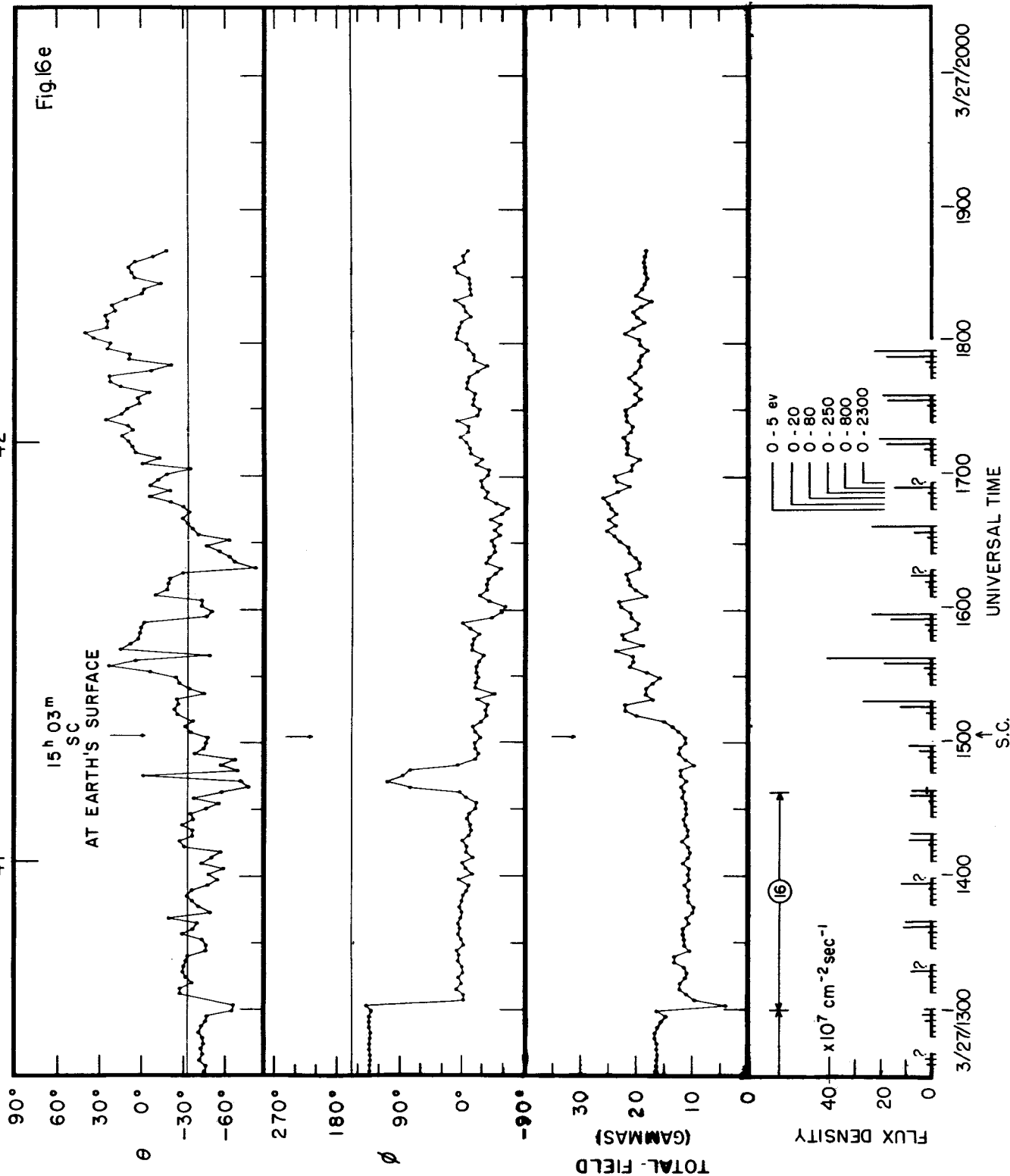
Fig. 16d



GEOCENTRIC DISTANCE (IN EARTH RADII)

41

42



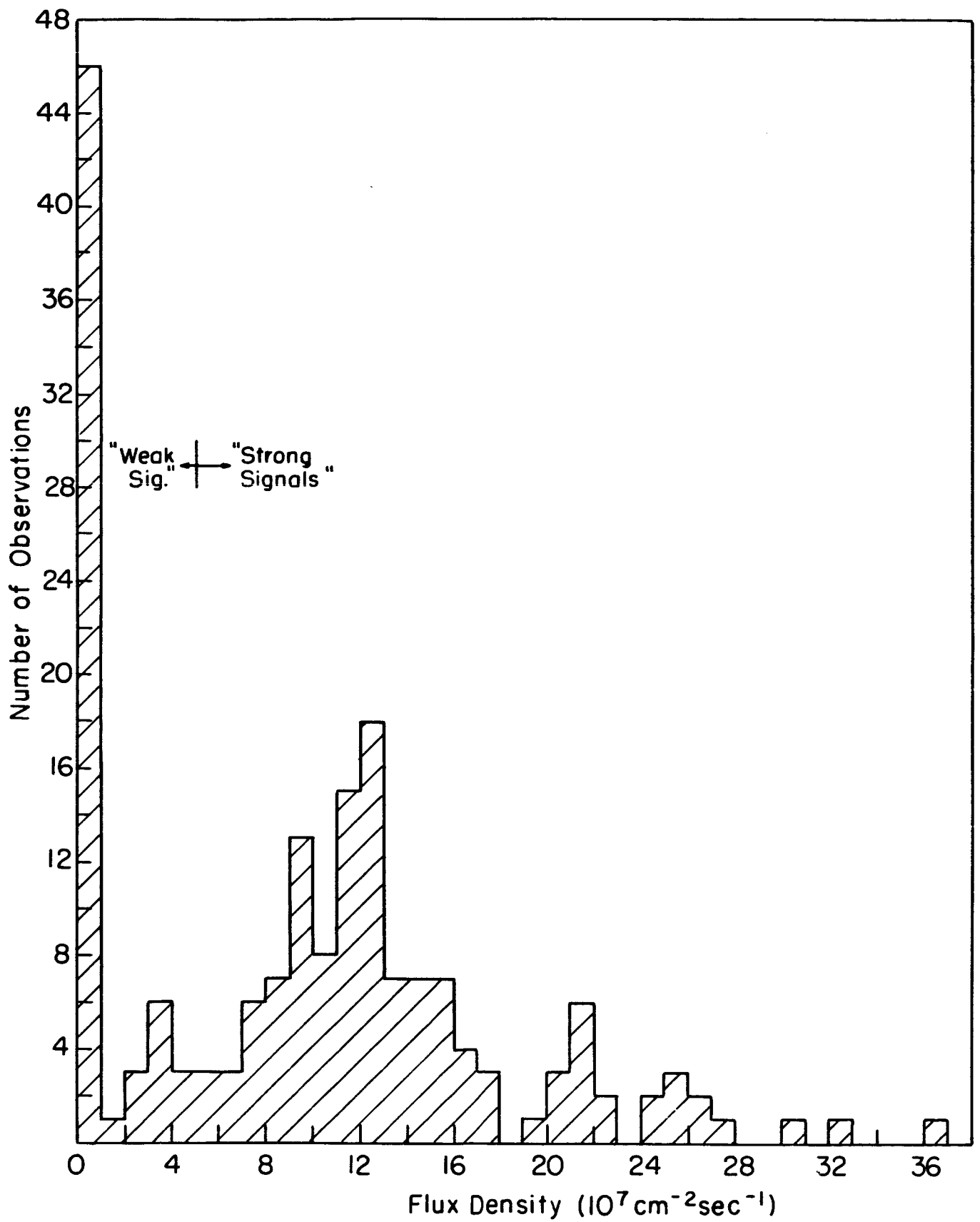


Fig. 17

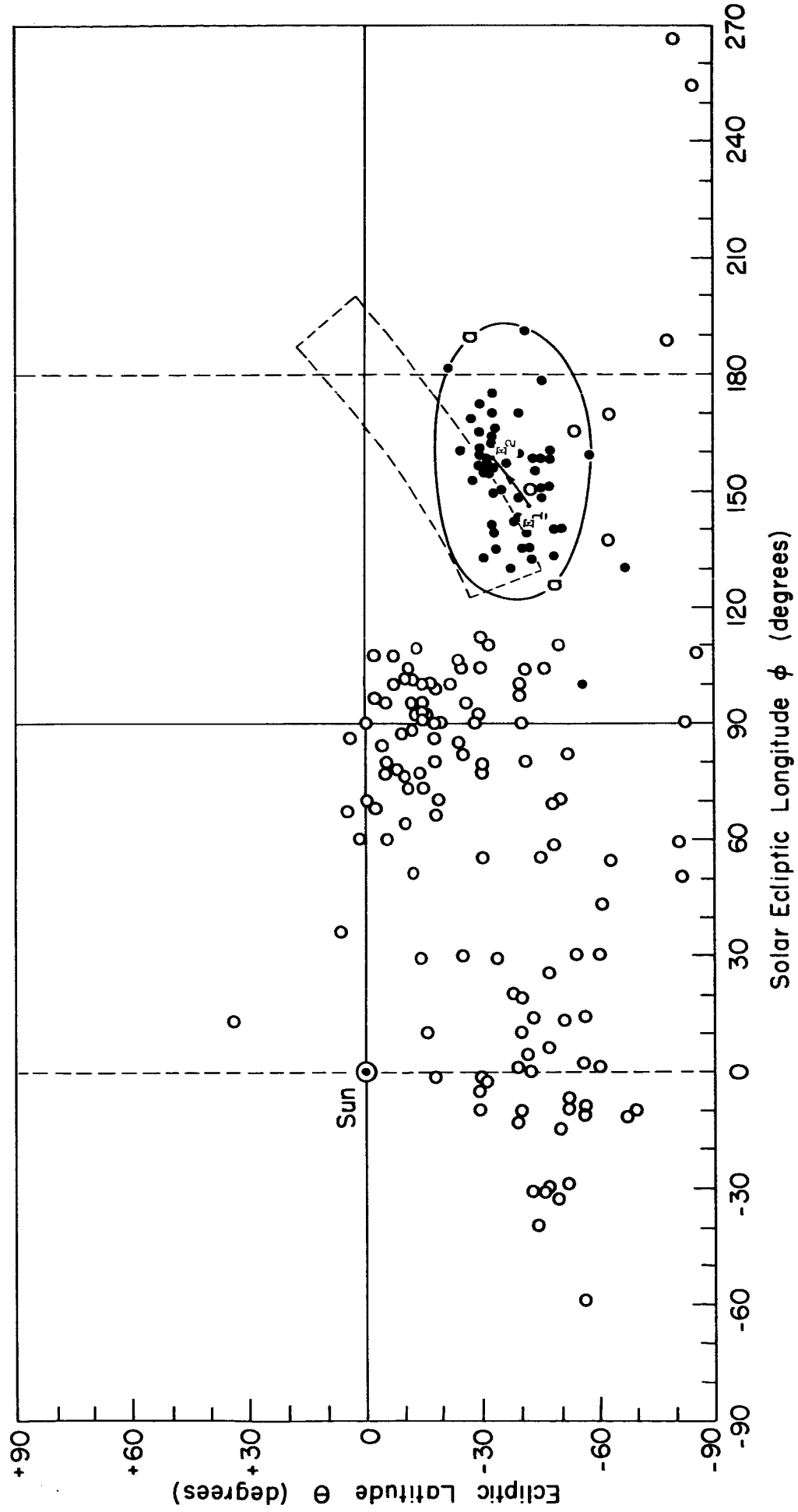


Fig. 18

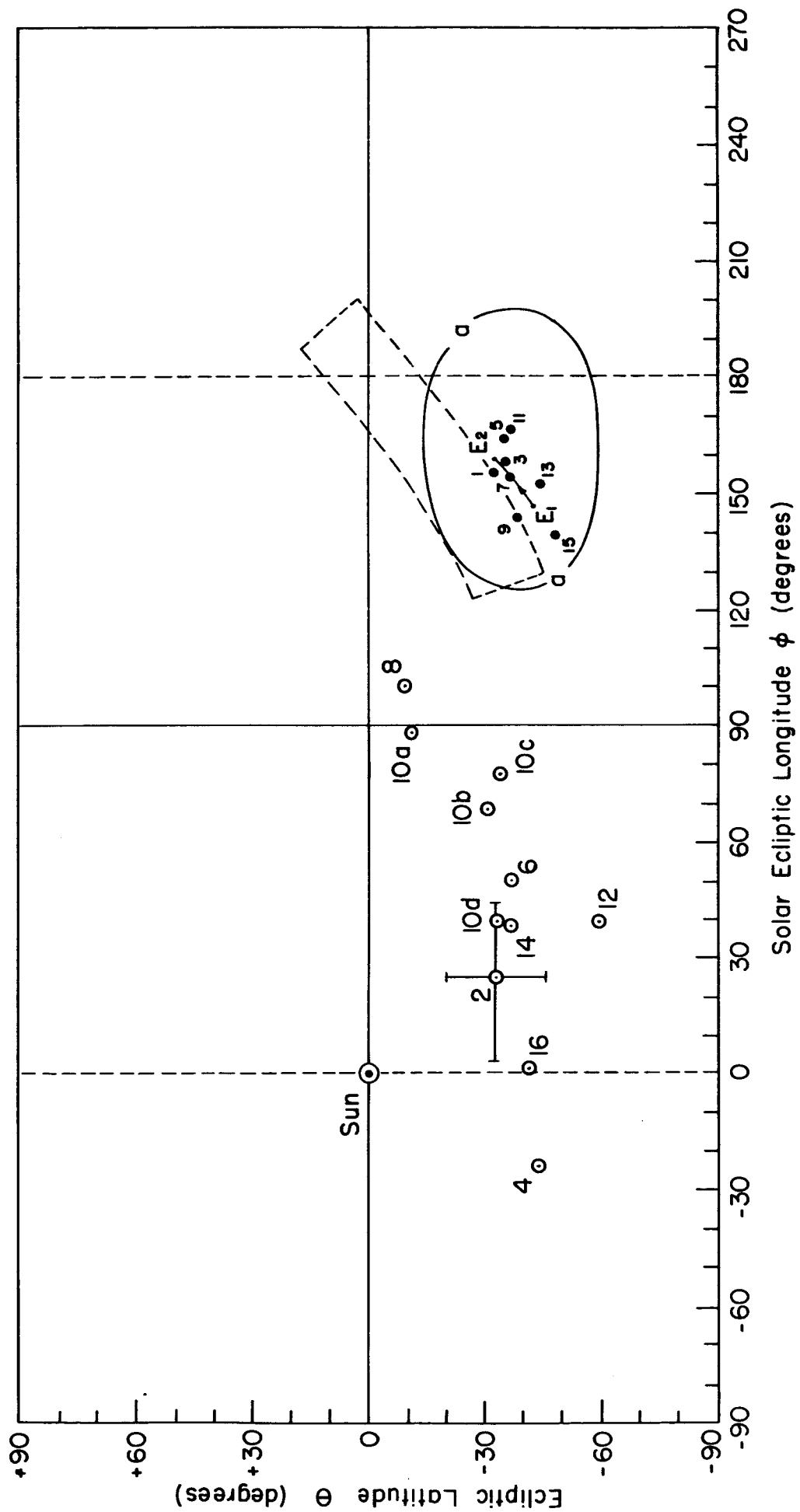


Fig. 19

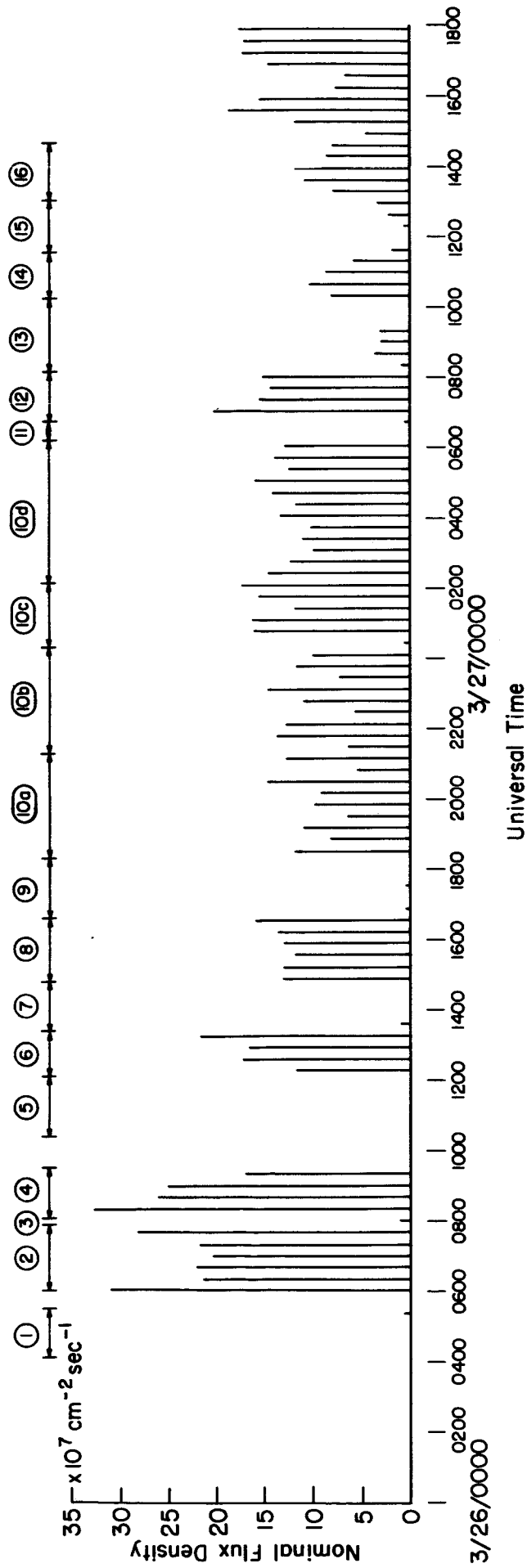


Fig. 20

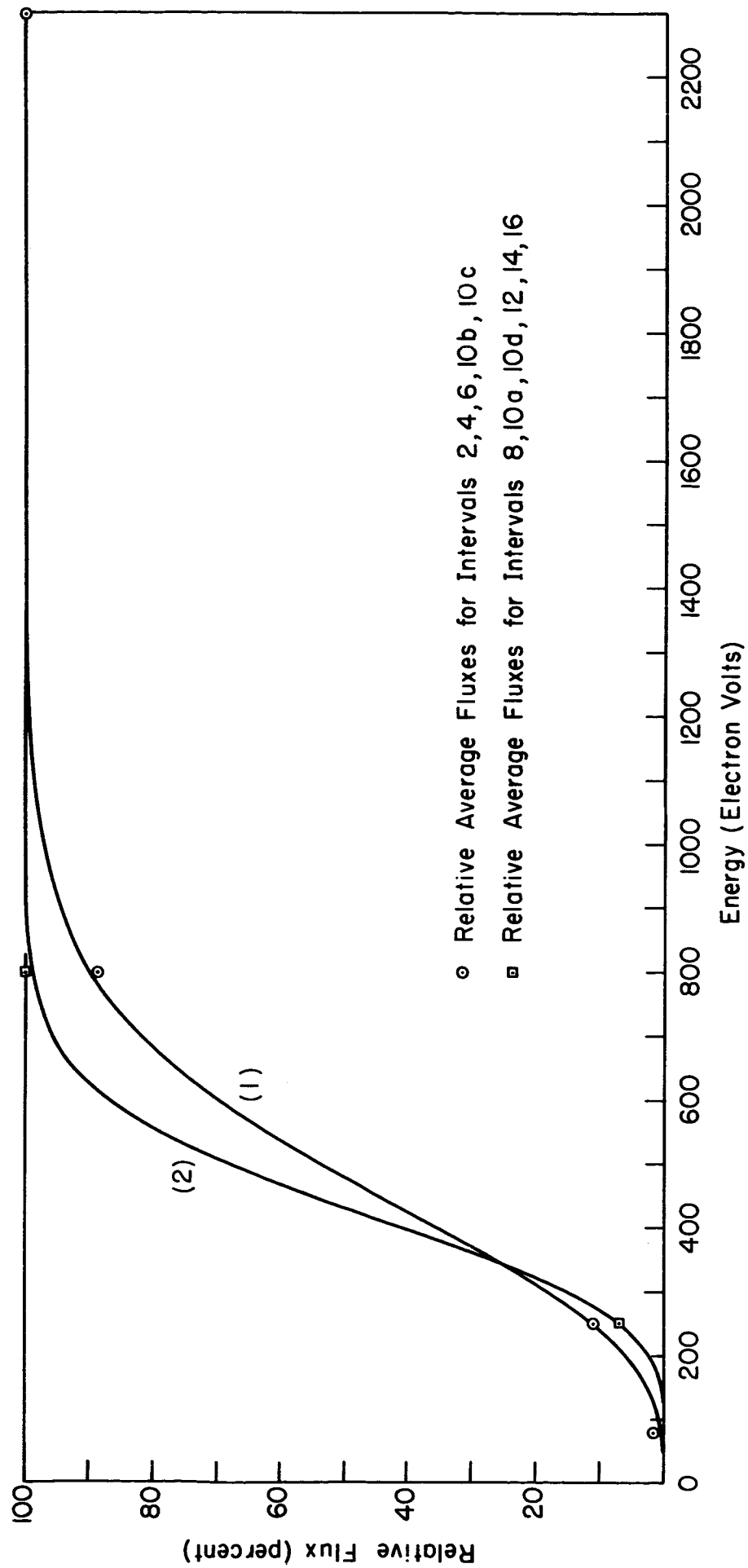


Fig. 21

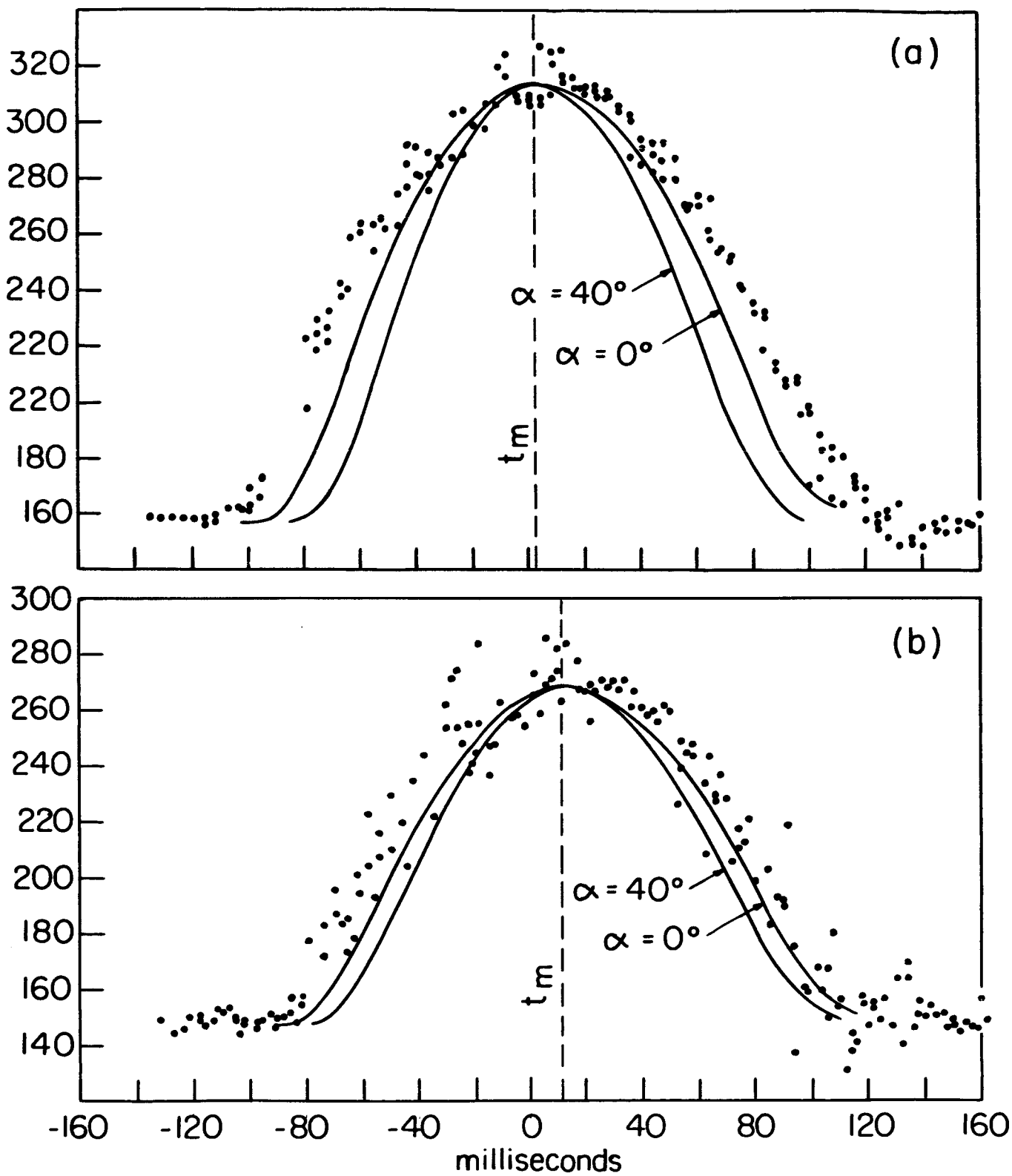


Fig. 22

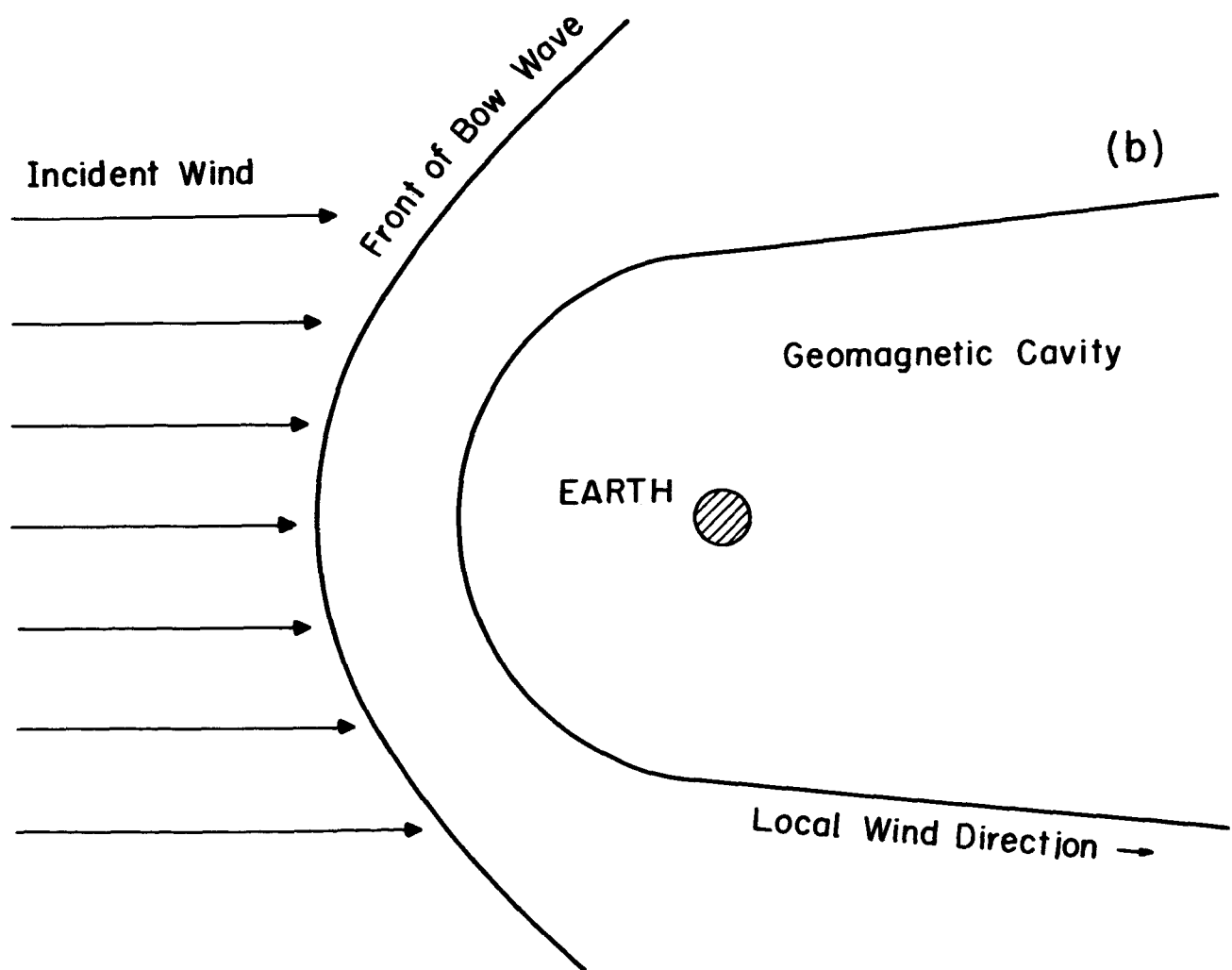
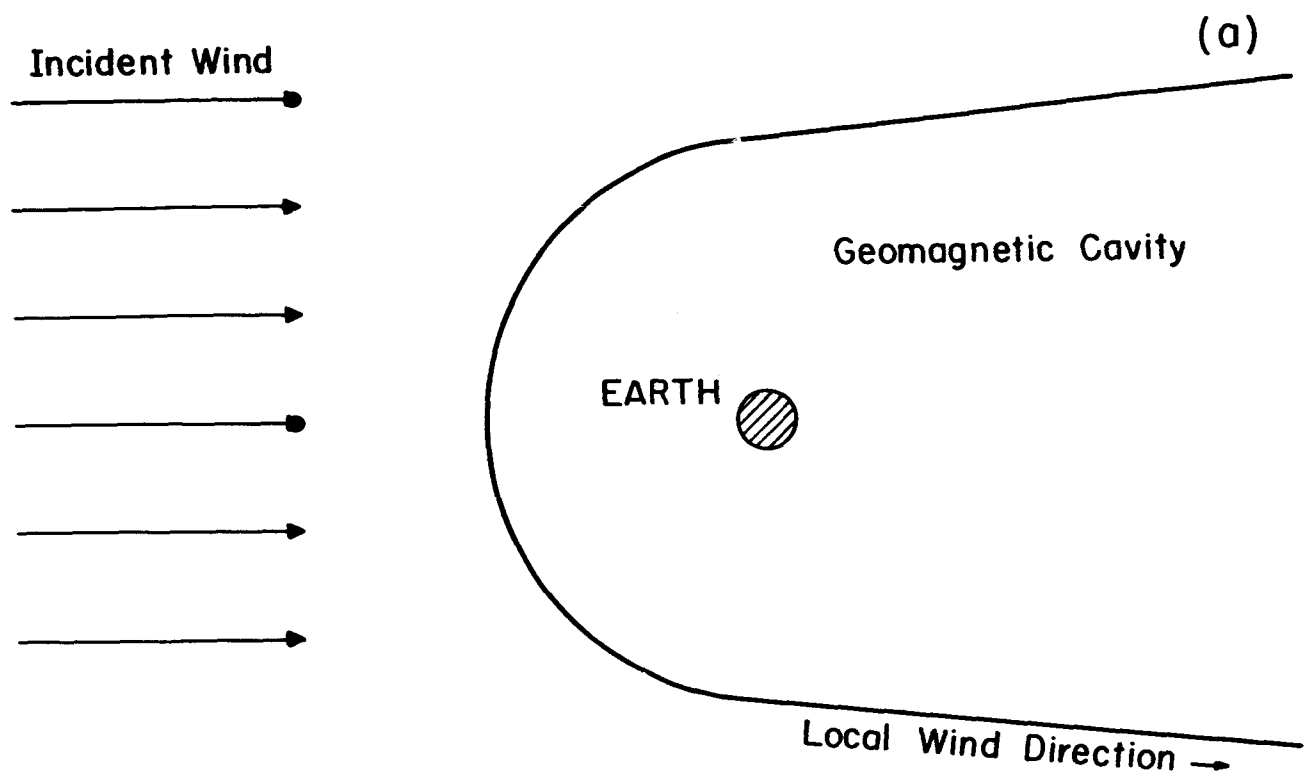


Fig. 23

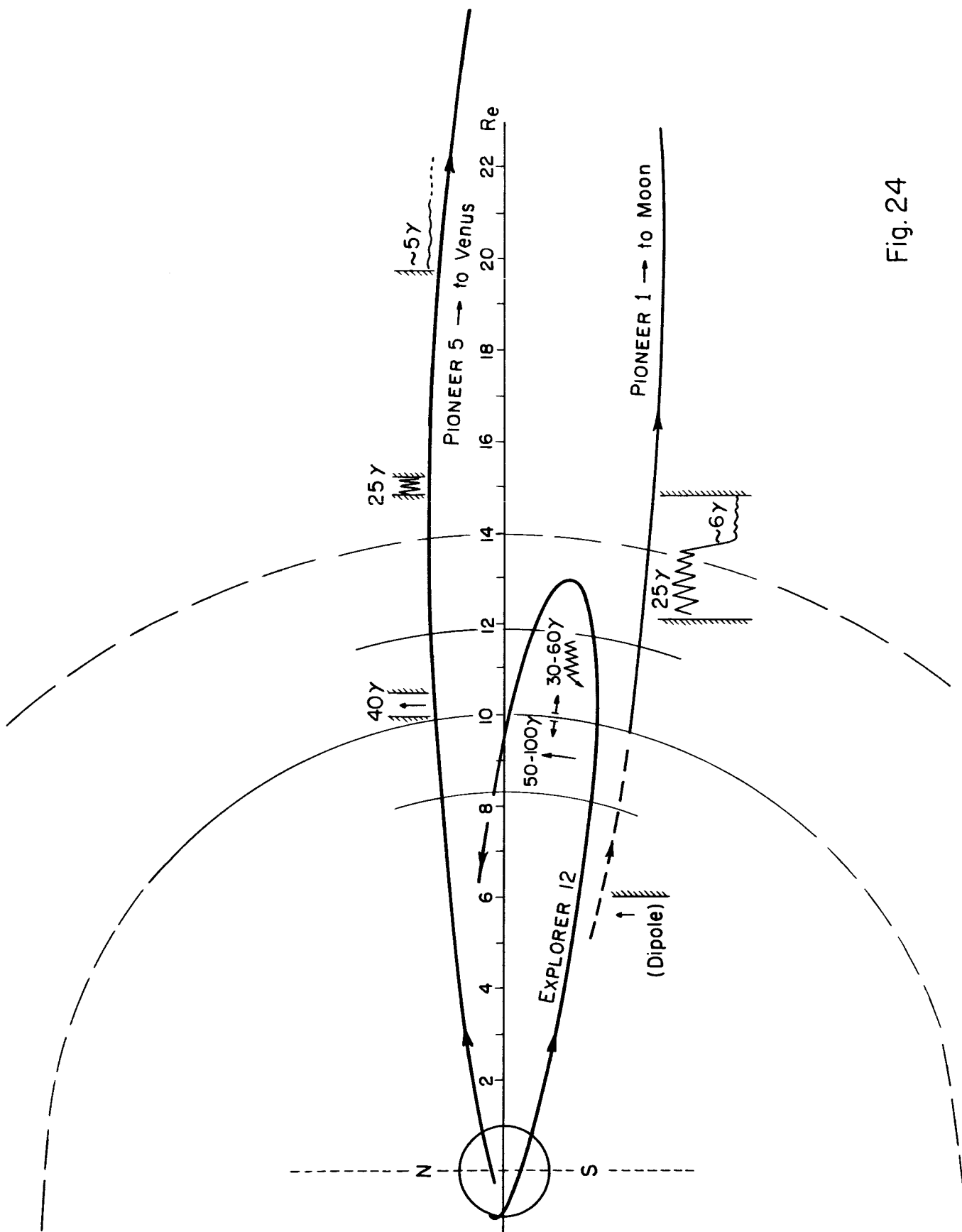


Fig. 24

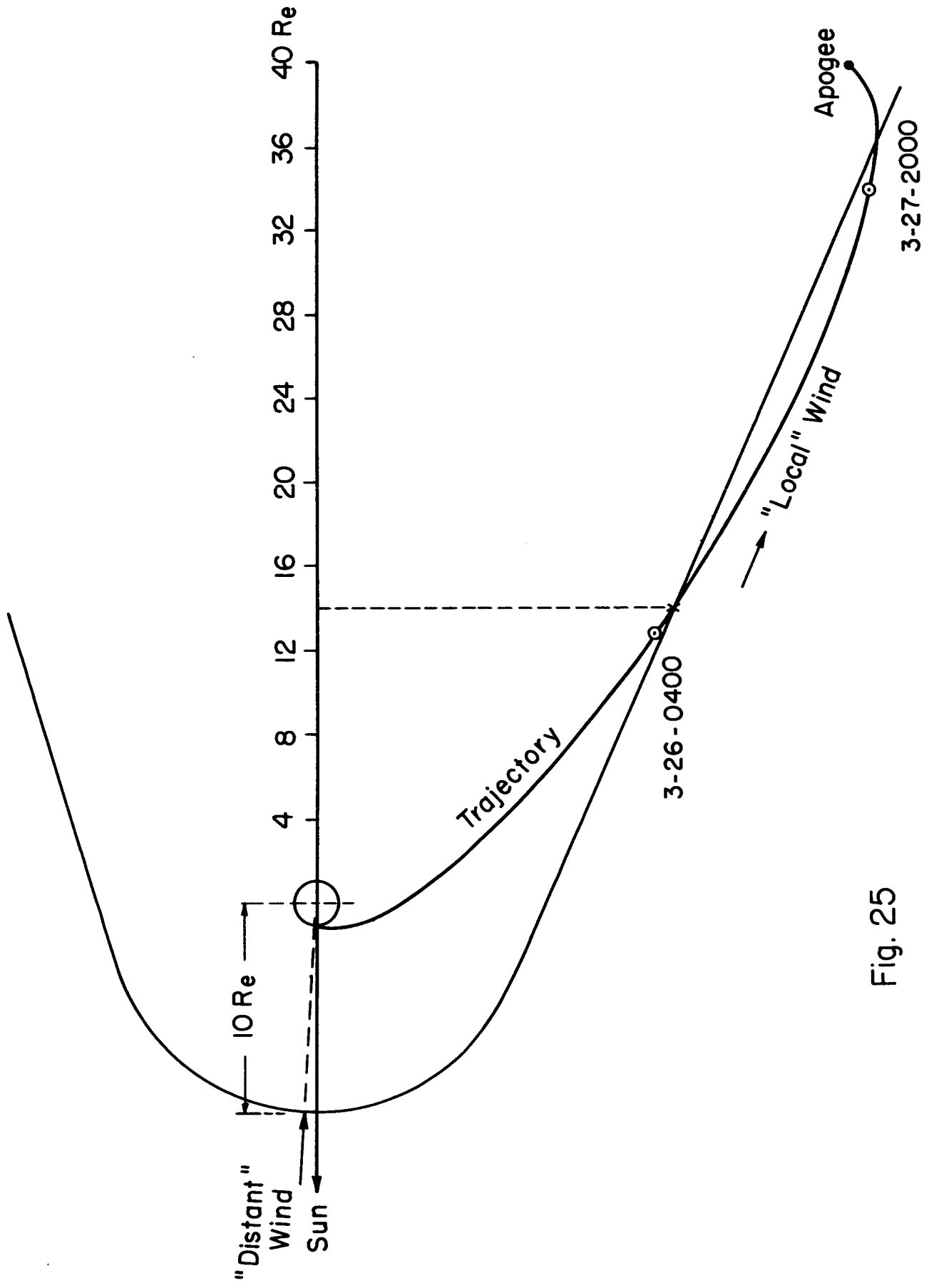
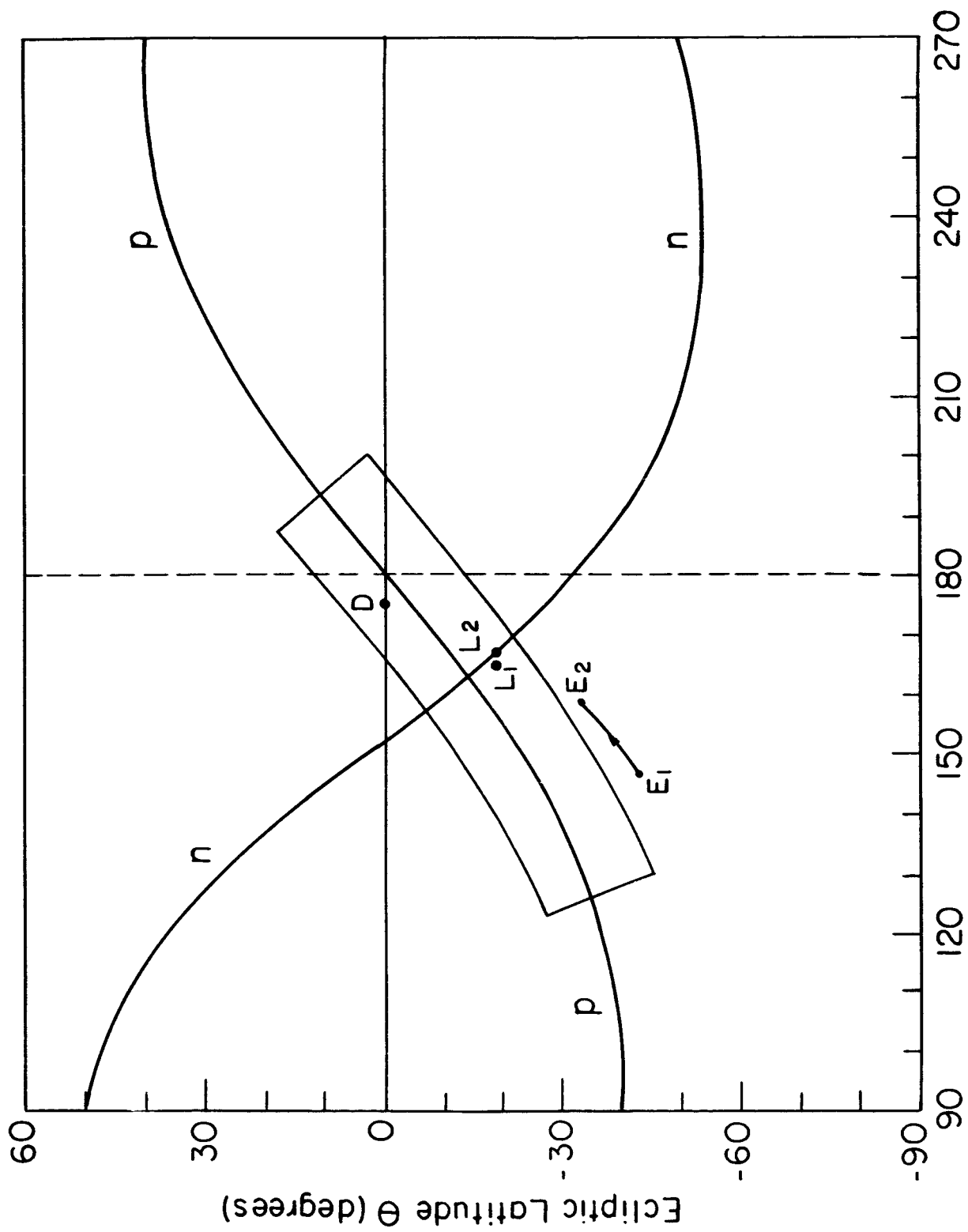


Fig. 25



Solar Ecliptic Longitude ϕ (degrees)

Fig. 26

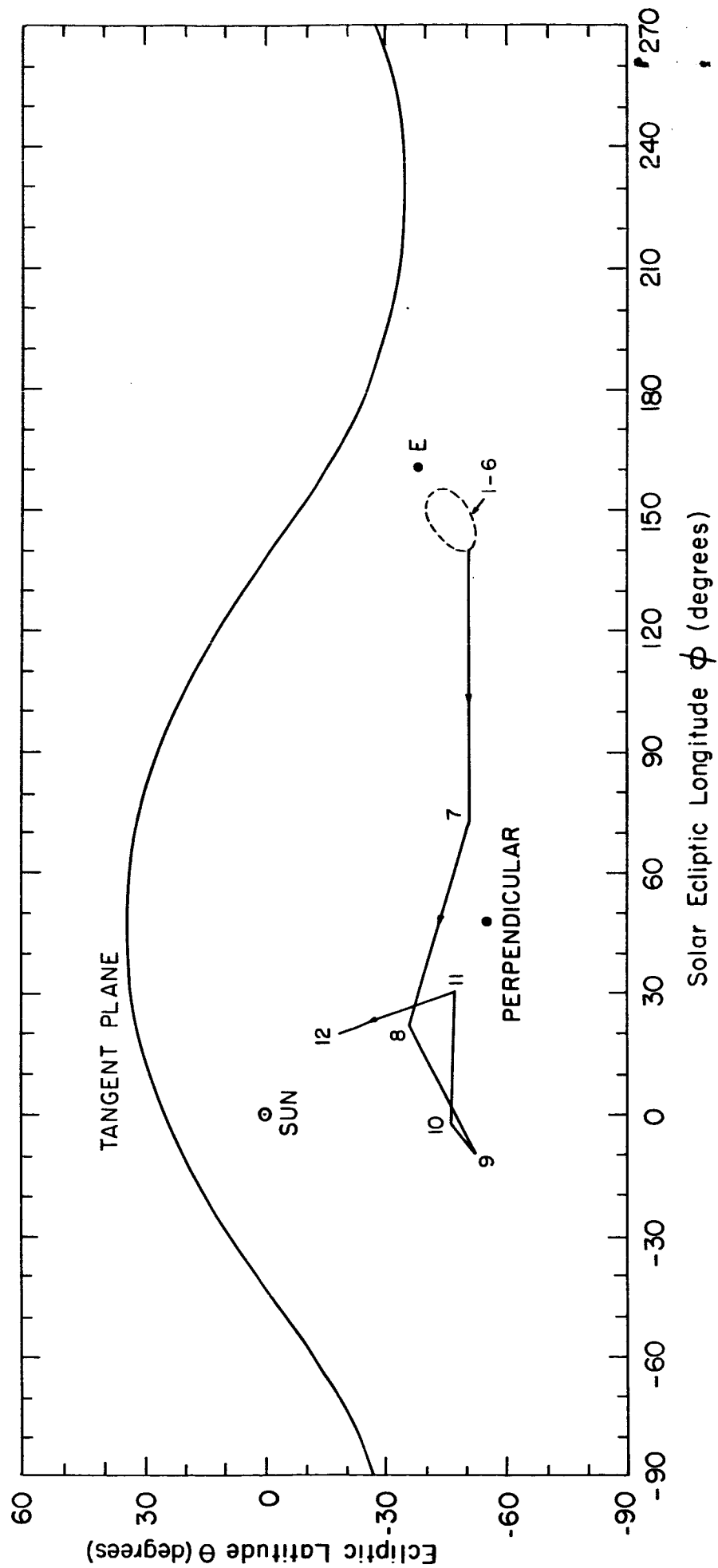


Fig. 27